This is to certify that the
dissertation entitled

# SUPRAMOLECULAR ASSEMBLY OF MESOPOROUS SILICAS WITH GEMINI SURFACTANTS AND MICROEMULSION TEMPLATING; SYNTHESIS, CHARACTERIZATION AND CATALYSIS

presented by

**Abhijeet Jayant Karkamkar**

has been accepted towards fulfillment
of the requirements for the

Ph.D. degree in Chemistry

Thomas J. Barnaveia
Major Professor's Signature

December 10, 2003
Date

# SUPRAMOLECULAR ASSEMBLY OF MESOPOROUS SILICAS WITH GEMINI SURFACTANTS AND MICROEMULSION TEMPLATING; SYNTHESIS, CHARACTERIZATION AND CATALYSIS

By

Abhijeet Jayant Karkamkar

A DISSERTATION

Submitted to
Michigan State University
In partial fulfillment of the requirements
for the degree of

DOCTOR OF PHILOSOPHY

Department of Chemistry

2003

# ABSTRACT

SUPRAMOLECULAR ASSEMBLY OF MESOPOROUS SILICAS WITH GEMINI SURFACTANTS AND MICROEMULSION TEMPLATING; SYNTHESIS, CHARACTERIZATION AND CATALYSIS

By

Abhijeet Jayant Karkamkar

In 1992 researchers from Mobil demonstrated the assembly of mesoporous silicate using organic cation surfactant assemblies[1]. These researchers were able to assemble mesoporous molecular sieves with pore sizes ranging from 2-10 nm and uniform pore size distributions from aluminosilicate and purely siliceous gels. Tanev and Pinnavaia assembled mesostructures using hydrogen bonding interactions between electrically neutral amine surfactant micelles ($S^0$) as the structure director and molecular silica species ($I^0$) as the source of silica[2].

Kim *et al* extended the ($S^0$ $I^0$) using a class of diamine based surfactants called Gemini surfactants to form ultrastable lamellar mesoporous silica[3]. The resulting mesostructures denoted as MSU-G silicas possessed unique structural characteristics such high cross-linking, exceptional thermal and hydrothermal stability, in addition to a vesicular structure. Presented here is a comprehensive study of the assembly of mesoporous silica molecular sieves using Gemini surfactants as the structure directors.

The hierarchical structures of mesostructured silicas assembed from electrically neutral Gemini surfactants of the type $C_nH_{2n+1}NH(CH_2)_mNH_2$ with n = 10, 12, 14 and m = 3, 4 are described in this study. Different hierarchical

structures are observed depending on a delicate balance between the hydrophilic interactions at the surfactant head group - silica interface and the hydrophobic interactions between the surfactant alkyl groups. Al-MSU-G derivatives prepared through *in situ* alumination reactions are far more efficient acid catalysts than 2%Al-MCM-41 for cumene cracking and the conversion of 2,4-di-*tert*-butylphenol and cinnamyl alcohol to a bulky flavan as the primary alkylation product.

A new family of mesostructured cellular foams (MSU-F) with microemulsion-templated structures has been synthesized using triblock copolymer P123 as structure-directing agents, 1,3,5-trimethylbenzene (TMB) as swelling agent and low-cost and water-soluble silicate precursors under near neutral conditions are described. The MSU-F foams consist of uniform spherical cells measuring 16 – 85 nm in diameter, windows with diameters of 5 – 40 nm and a narrow size distribution interconnecting the cells.

Mercaptopropyl-functionalized mesostructured catalysts assembled using direct assembly methods and ocatdecylamine as structure directors were converted to acidic catalysts by oxidation of thiol groups to sulfonic acid. These materials were tested for acid catalyzed esterification of glycerol with lauric acid. Conversions as high as 100 % in terms of lauric acid were observed with 66 % selectivity for the monoester.

(1) Beck, J. S.; Vartuli, J. C.; Roth, W. J.; Leonowicz, M. E.; Kresge, C. T.; Schmitt, K. D.; Chu, C. T. W.; Olson, D. H.; Sheppard, E. W.; et al. *J. Am. Chem. Soc.* **1992**, *114*, 10834-10843.

(2) Tanev, P. T.; Pinnavaia, T. J. *Science* **1995**, *267*, 865-867.

(3) Kim, S. S.; Zhang, W. Z.; Pinnavaia, T. J. *Science* **1998**, *282*, 1302-1305

*To aai and baba, for all your love and support!*

# ACKNOWLEDGEMENTS

*I want to thank my advisor Prof. Thomas J. Pinnavaia for his continuous support and guidance during my graduate studies. I cannot express my gratitude towards him in words for all the impact he is going to have on my thinking and ideologies. I hope to get inspired by his work ethic and sincerity. I also want to thank him for the intellectual freedom and flexibility he has allowed me so that I could complete my research successfully.*

*I am grateful to Dr. Aaron Odom, Dr. Dennis Miller, Dr. Simon Garrett and Dr. John Mccracken for serving on my guidance committee. I also wish to thank Dr. Xudong Fan at the Center for Advanced Microscopy for all his help with my electron microscopy needs.*

*I wish to extend my heartiest gratitude to Dr. Seong Su Kim for everything he has taught me over my years at MSU. Secondly I want to thank Dr. Yu Liu for offering his extensive help and discussing various ideas. I also want to express my thanks to current and former, group members Emily, Jainisha, Zhaorang, DK, In, ChyHyung, Siqi, Hui, Pete, Randy, Costas, Marc, Zhen and Tom for their friendship and help.*

*I also want to thank my friends RG, Pops, Padmesh, Vijay, Mahesh, Manish, Kiran and Tushar for the support and help.*

*Finally I want to thank my parents Jayant and Neelam, my brother Bittu and my fiancée Manasi for being patient and understanding over the years staying so far away from me.*

# TABLE OF CONTENTS

## LIST OF TABLES

## LIST OF FIGURES

Figur

Figur

Figur

Figu

Figu

Figu

Figu

Figure 4

Figure 4

Figure

Figure

Figure

Figure

Figure

Figure

Figure

Figure

Figure

Figure

Figure

LIST

Reac

Reac

Reac

Reac

## LIST OF REACTIONS

BE
BJ
Cn
CT
Ex
FC
g
H-
HK
HN
HR
I
I*
I-
IUF
$L_2$
$L_3$
LC
M
MA
MC
MC
MC
MC
MC
MC
mm
3-M
MS
MS

## LIST OF ABBREVIATIONS

| | |
|---|---|
| 2, 4-DTBP | -2, 4-di – *tert*- butylphenol |
| BET | Brunauer-Emmett-Teller |
| BJH | Barrett-Joyner-Halenda |
| Cmc | Critical micelle concentration |
| CTAB | Cetyltrimethylammonium Bromide, $C_{16}H_{33}N(CH_3)_3Br$ |
| EtOH | Ethanol |
| FCC | Fluid Catalytic Cracking |
| g | Packing parameter, based on the geometry of the surfactant |
| H-bonding | Hydrogen bonding |
| HK | Horvath and Kawazoe pore size distribution model |
| HMS | Hexagonal Mesoporous Silica |
| HRTEM | High resolution Transmission Electron Microscopy |
| $I^-$ | Anionic inorganic precursor |
| $I^+$ | Cationic inorganic precursor |
| $I^0$ | Neutral inorganic precursor |
| IUPAC | International Union of Pure and Applied Chemistry |
| $L_\alpha$ | Two dimensional lamellar phase |
| $L_3$ | Bi-continuous, three dimensional mesophase formed by bilayer structure |
| LCT | Liquid Crystal Templating |
| $M^+$ | Metal cation |
| MAS | Magic Angle Spinning |
| MCF | Mesostructured Cellular Foam |
| MCM-22 | Mobil composition of Matter 22, microporous zeolite synthesized using hexamethyleneimine |
| MCM-36 | Mobil composition of Matter 36, a pillared mesoporous MCM-22 |
| MCM-41 | Mobil composition of Matter 41, hexagonal mesophase |
| MCM-48 | Mobil composition of Matter 48, cubic mesophase |
| MCM-50 | Mobil composition of Matter 50, lamellar mesophase |
| mmol | Millimoles |
| 3-MPTMS | 3-Mercaptopropyltrimethoxysilane |
| MSU-F | Large pore mesostructured silicas synthesized with P123 surfactant, trimethylbenzene and water soluble silicates at near neutral assembly conditions |
| MSU-G | Ultra stable vesicular silica synthesized with amphiphilic Gemini diamine surfactant of the structure |

MS

MS

MS

MS

MS

MS

MP-

nm

N

N-

P/Po

PEO

PLS

ppm

PXR

$Q^2$

$Q^3$

$Q^4$

| | |
|---|---|
| | $C_{12}H_{25}NH(CH_2)_2NH_2$ under hydrothermal conditions |
| MSU-H | Hexagonal mesostructured silicas synthesized using PEO based surfactants and water soluble silicates at near neutral assembly conditions |
| MSU-S | Steam-stable mesoporous aluminosilicates synthesized using zeolitic precursors |
| $MSU\text{-}S_{(BEA)}$ | Steam-stable mesoporous aluminosilicates synthesized using beta zeolitic precursors |
| $MSU\text{-}S_{(MFI)}$ | Steam-stable mesoporous aluminosilicates synthesized using ZSM-5 (mobil 5) zeolitic precursors |
| MSU-V | Stable lamellar silica synthesized with hierarchical vesicular morphologies synthesized with α-ω diamine surfactants such as 1,12- dodecyldiamine |
| MSU-X | Wormhole mesostructured silicas synthesized with PEO based surfactants and TEOS under neutral ($N^0I^O$) assembly conditions |
| MP-MSU-X′ | Mercaptopropyl functionalized MSU-X′ mesostructured silicas |
| nm | Nanometer ($10^{-9}$ m) |
| NMR | Nuclear Magnetic Resonance |
| $N^0$ | Non-ionic amphiphilic PEO based surfactant |
| $N^0I^0$ | Neutral assembly pathway utilizing H-bonding between PEO based surfactant and inorganic precursor |
| P/Po | Relative pressure P = Pressure Po = Saturation pressure |
| PEO | Polyethylene oxide |
| PLS | Pillared-layered structures |
| ppm | Parts per million |
| PXRD | Powder X-ray diffraction |
| $Q^2$ | Incompletely condensed silica sites $Si(OSi)_2(OH)_2$ |
| $Q^3$ | Incompletely condensed silica sites $Si(OSi)_3(OH)$ |
| $Q^4$ | Completely condensed silica sites $Si(OSi)_4$ |

| | |
|---|---|
| $S^-$ | Anionic amphiphilic surfactant |
| $S^+$ | Cationic amphiphilic surfactant |
| $S^+I^-$ | Pathway 1 electrostatic assembly between cationic surfactant and anionic silica precursor |
| $S^+X^-I^+$ | Electrostatic assembly between cationic surfactant and cationic silica precursors halogen ions as mediating counter ions |
| SBA | Mesostructured silicas assembled under high acid low pH conditions with TEOS as the inorganic precursor |
| SBA-15 | Large pore hexagonal mesostructured silica assembled under high acid low pH conditions with TEOS as the inorganic precursor and triblock copolymer PEO based surfactant |
| $S_{BET}$ | Specific surface area in $m^2/g$ obtained from the linear part of the adsorption isotherm using Brunauer Emmett Teller equation |
| $SO_3H$-HMS | Sulfonic acid functionzalized HMS silica obtained by oxidation of thiol groups in MPHMS |
| $S^0$ | Neutral amphiphilic amine surfactant |
| $S^0I^0$ | Neutral assembly pathway between neutral amine surfactant and TEOS |
| TEM | Transmission Electron Microscopy |
| TEOS | Tetraethylorthosilicate |
| $T^2$ | Functionalized $Q^2$ site $RSi(OSi)_3OH$ |
| $T^3$ | Functionalized $Q^3$ site $RSi(OSi)_3$ |
| TMB | Trimethylbenzene |
| VPI-5 | Extra-large ring aluminophosphate microporous material consisting of 18 tetrahedral (18T) atoms |
| $X^-$ | Halogen or anionic counter ion |
| ZSM-5 | Zeolite Synthesized by Mobil using tetrapropyl ammonium bromide template having a 5 membered ring |

## 1.1 His

solids a
catalys
their m
cavities
sieves
are exe
the mic
synthet
within
A1P04-
range.
charact
Despite
the mar
of curre
had to

# Chapter 1

# Introduction and Objectives

## 1.1 Historical perspective

Microporous (pore diameter 5-20 Å) and mesoporous (20-500 Å) inorganic solids are two classes of materials that are used extensively as heterogeneous catalysts and adsorption media.[1] The utility of these materials is manifested in their microstructures that allow molecular access to large internal surfaces, cavities that enhance catalytic activity, and high adsorptive capacity. Molecular sieves represent a major sub-class of microporous materials. These materials are exemplified by a large family of aluminosilicates known as zeolites in which the micropores are regular arrays of uniformly sized channels. Considerable synthetic effort has been devoted to developing frameworks with pore diameters within the mesoporous range. The largest reported pore size till 1992 were A1P04-8[2], VPI-5[3] and cloverite[4-7], which have pore diameters within the 8-13 Å range. Cacoxenite[8], a natural ferroaluminophosphate, has been structurally characterized as having 14 Å channels, which approach the mesoporous range. Despite the outstanding progress made in producing large pore molecular sieves, the materials synthesized so far were still not suitable for use within the context of current catalytic processes. Largely for this reason alone another approach had to be undertaken in order to increase the mesoporosity of existing

microporous materials for the processing of large molecules such as the cracking and hydrocracking[9] of vacuum gas oil. This latter approach involved the generation of mesopores within the crystallites of the microporous zeolites.

## 1.2 Mesoporous materials

According to the definition provided by the International Union of Pure and Applied Chemistry, porous materials can be grouped into three classes based on their pore diameter ($d$): microporous, $d < 2.0$ nm; mesoporous, $2.0 \leq d \leq 50$ nm; macroporous, $d > 50$ nm[1]. In the case of zeolites, (for example, zeolite Y and CSZ-1[10,11],) it was shown that, during the dealumination of the zeolite by steam, mesopores in the range 10-20 nm were formed which could be characterized by different techniques, including gas adsorption, high-resolution electron microscopy, and analytical electron microscopy. When a large number of defects occur in a small area it can lead to coalescence of mesopores, with the formation of channels and cracks in the crystallite of the zeolite (Figure 1.1). The presence of the mesopores in crystallites of a zeolite should increase the accessibility of large molecules to the external openings of the pores[9].

In processes where catalyst regeneration occurs at high temperatures, the mesoporosity of the catalyst changes during regeneration. In cases such as Fluidized Catalytic Cracking (FCC), this occurs in an uncontrollable way. It appears, therefore that a procedure involving the formation of a secondary

mesc

speci

and

struct

struct

used

silicas

molec

comp

be of

sites

conta

instan

where

layere

high s

a plau

are cr

their s

new pi

compos

mesoporous system by steaming a microporous solid can only be useful for special applications. Therefore, more general solutions had to be explored.

Due to the difficulties in synthesizing zeolites having extra large channel and cavity sizes, a group of ultralarge pore materials consisting of layered structures with pillars in the interlamellar region, the so-called pillared-layered structures (PLS), have been synthesized.[12-14] The layered compounds typically used are smectite clays, metal (Zr, Ti, etc.) phosphates, double hydroxides, silicas, and metal oxides. Materials of this type, while they can be used as molecular sieves for adsorption as well as supports for catalytically active components, they have not found use as molecular sieve acid catalysts. It would be of interest to prepare such materials that possessed relatively strong acid sites in the layers. One can envisage one way to achieve similar materials, but containing layers of silica-alumina instead of silica. This could be achieved for instance, by starting with a layered compound such as lamellar MCM-50[15,16], wherein the amorphous layers are silica-alumina. One may attempt to pillar a layered material of this kind using TEOS and in this way generate an extremely high surface area silica-alumina with molecular sieve properties. If this is indeed a plausible solution, it can be improved if the layers instead of being amorphous are crystalline. Some zeolites go through a layered intermediate phase during their synthesis. Pillaring these intermediates would give rise to a whole series of new pillared compounds with controlled pore dimensions in which the (Si/Al) composition of the layers, as well as the nature of the pillars could be adapted to

Figure

zeolite$^{8+}$

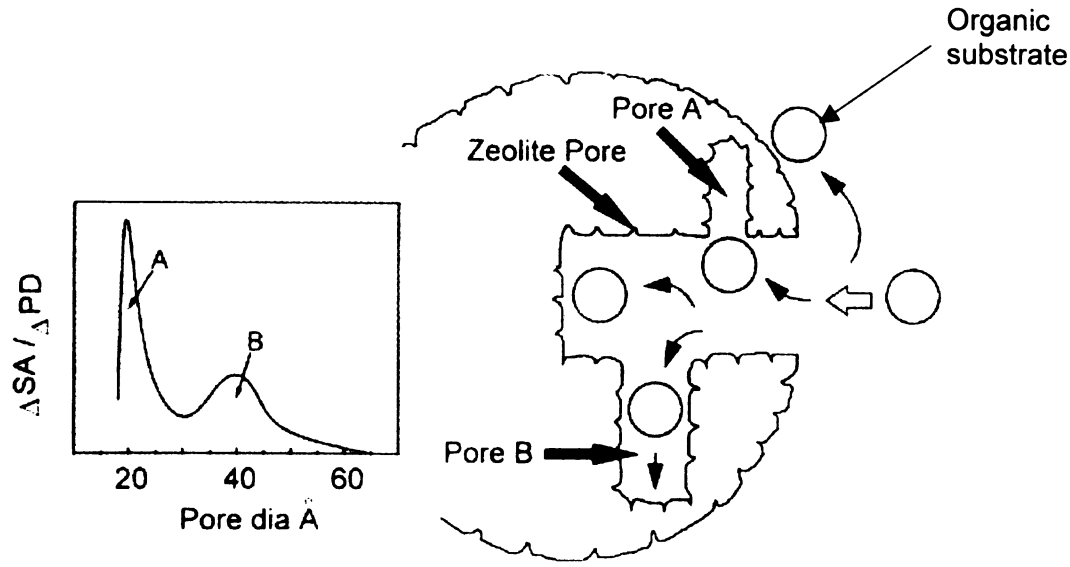


**Figure 1.1** Schematic representation of mesopores formed in a steamed zeolite[81].

suit a par

precursor

the MCM

layered

femente

both mic

higher th

pillar laye

the micro

fine cher

### 1.3 Meso

#### 1.3. 1 M

M

as in th

such as

irregular

efforts, a

available

In

mesopor

researche

suit a particular reaction to be catalyzed. This has been done with the lamellar precursor of MCM-22[17] zeolite, which has been pillared with TEOS, producing the MCM-36 molecular sieve. The procedure can also be applied to other layered zeolite precursors such as those formed during the preparation of ferrierite.[18] By this procedure one should obtain a pillared material combining both micro- and mesopores, and produce as a result crystalline layers, with higher thermal and hydrothermal stability. These new approaches to engineering pillar layered materials should allow the design of catalysts with regular pores in the micro- to mesoporosity range, for oil refining and petrochemistry, as well as fine chemicals production.

## 1.3 Mesoporous molecular sieves

### 1.3.1 MCM-41

Mesoporous materials are typically amorphous or paracrystalline solids, as in the case of transitional silicas, aluminas and modified layered materials such as pillared clays and silicates. The pores in these materials are generally irregularly spaced and broadly distributed in size. Despite the aforementioned efforts, a mesoporous material with narrow pore size distribution hasn't been available for catalytic cracking and refining reactions.

In 1992 researchers from Mobil demonstrated the assembly of mesoporous silicate using organic cation surfactant assemblies[15,16]. These researchers were able to assemble mesoporous molecular sieves with pore sizes

ranging f

and pur

($C_nH_{2n+1}N$

hydropho

of the m

micelles

2) Mob

sieves b

or c) pos

A

follows:

1. 0 SiO

$H_2O$

The pre

surfacta

product

The sur

in air at

N

prepare

to silica

phases

existing

ranging from 2-10 nm and uniform pore size distributions from aluminosilicate and purely siliceous gels. Long chain quaternary ammonium surfactants $(C_nH_{2n+1}N(CH_3)_3)^+$ in solution minimize their energy by forming micelles with their hydrophobic alkyl chain at the interior and the charged head group at the exterior of the micelle. Under certain conditions, these surfactants will form rod-like micelles that spontaneously order into hexagonal liquid crystals array. (Figure 1. 2) Mobil researchers were able to tailor the mesopore size of the molecular sieves by: a) varying surfactant chain length ($C_n$), b) addition of auxiliary agents, or c) post synthetic treatment to reduce pore size.

A typical reaction mixture composition for the preparation of MCM-41 is as follows:

1. 0 $SiO_2$: 0. 03 $Al_2O_3$: 0. 007 $Na_2O$: 0. 183 $(CTMA)_2O$: 0. 156 $(TMA)_2O$: 23. 5 $H_2O$

The preparation consisted of mixing the above inorganic precursors with the surfactant solution and autoclaving the mixture at 100-150 °C for 4-144 h. The product was then recovered by filtration and washed with water and air-dried. The surfactant was removed by calcination at 550 °C for 1 h in flowing $N_2$ and 6 h in air at the same temperature.

MCM-41 identifies the hexagonal subclass of these mesoporous materials prepared with surfactant to silica ratios less than 1. Cubic (MCM-48, surfactant to silica >1) and lamellar (MCM-50, surfactant to silica much greater than 1) phases have also been identified and are consistent with liquid crystal phases existing in surfactant /water mixtures.

A

crystal s

formatior

number

are depc

as, for

different

inorganic

structure

but mim

P

show at

unit cell

characte

indicate

sharp s

within th

step o c

pressur

be appr

The por

Horvath

hexagon

A liquid crystal templating mechanism (LCT) in which surfactant liquid crystal structures serve as organic templates has been proposed for the formation of these materials. Related mechanisms have been proposed for a number of systems in which inorganic structures of widely varying morphologies are deposited in the presence of preformed micellar arrays or micellar structures, as, for example, in the biochemical formation of bones and shells from 40 different materials.[19] However, in the biological system, the deposition of inorganic species is dynamically controlled, and the products are dense structures whose ultimate morphology do not mimic the vesicle structures per se but mimics the biologically controlled "shape" of the vesicle array.

Powder X-ray diffraction pattern (Figure 1.3) of MCM-41 characteristically show at least 3 peaks ($d_{100}$, $d_{110}$, and $d_{200}$) that can be indexed to the hexagonal unit cell with a unit cell parameter $a_o=2d_{100}/\sqrt{3}$. MCM-48 and MCM-50 also show characteristic X-ray patterns. Adsorption studies on these materials (Figure 1.4) indicate Type IV isotherms typical of mesoporous materials, with a characteristic sharp step showing significant adsorption uptake due to capillary condensation within the framework-confined mesopores. The relative pressure at which this step occurs is determined by the size of the pore and shifts to higher relative pressures as the pore diameter increases. BET surface areas are estimated to be approximately 1000 $m^2/g$. Mesopore volumes range from 0.7 to 1.2 $cm^3/g$. The pore size distribution is calculated from the adsorption branch with the Horvath and Kawazoe model.[20] Figure 1.5 (a-d) clearly shows the presence of a hexagonally ordered pore structure. MCM-41 primarily has a monolithic

morphol

figure 1

(100) pl

at a ver

MCM-4

emphas

(figure

41. wh

paramo

channe

limitatio

pores.

produc

autocla

homog

of MC

stabilit

less.

homog

fast ar

synthe

therma

morphology, as is clearly evident from the TEM image shown in figure 1.5 a, figure 1.5 c shows a lamellar pattern which is oriented cylinders seen from the (100) plane. Figure 1.5 d is a HRTEM image showing the uniformity of the pores at a very high magnification. Figure 1.5 e is an electron diffraction pattern for MCM-41 materials showing the hexagonal ordering of pores. It is important emphasize the fact that the electron diffraction pattern and X-ray diffraction (figure 1.3) arise from the orientation of the pores and not from the walls of MCM-41, which are amorphous in nature. The control of crystal size can be of paramount importance when mesoporous molecular sieves with unidirectional channels, such as MCM-41, are to be used in catalytic processes. Diffusion limitations exists, one should decrease as much as possible the length of the pores. This can be achieved synthetically by decreasing the crystal size of the product. Various techniques such as microwave heating instead of traditional autoclaves were explored to shorten crystallization times and achieve homogeneous nucleation. When microwave heating was applied to the synthesis of MCM-41, high-quality hexagonal mesoporous materials of good thermal stability were obtained by heating precursor gels to about 150 °C for 1 h or even less. Calcined samples had a uniform size of about 100 nm. The homogeneousness and small crystal sizes obtained are probably the result of the fast and homogeneous condensation reactions occurring during the microwave synthesis.[21] This fast condensation should also be responsible for the high thermal stability of the resultant materials.

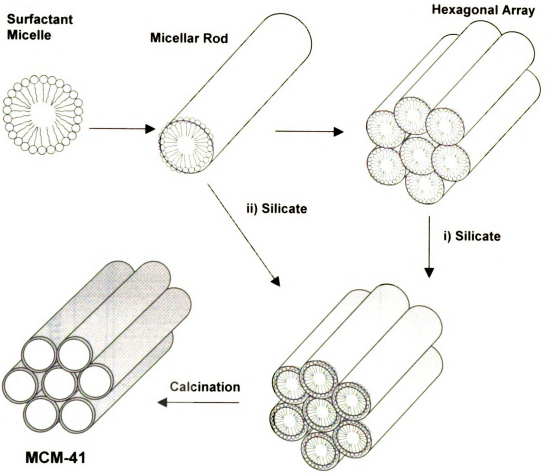


**Figure 1.2** Proposed mechanistic pathways for the formation of MCM-41: (1) liquid crystal initiated and (2) silicate anion initiated.[15]

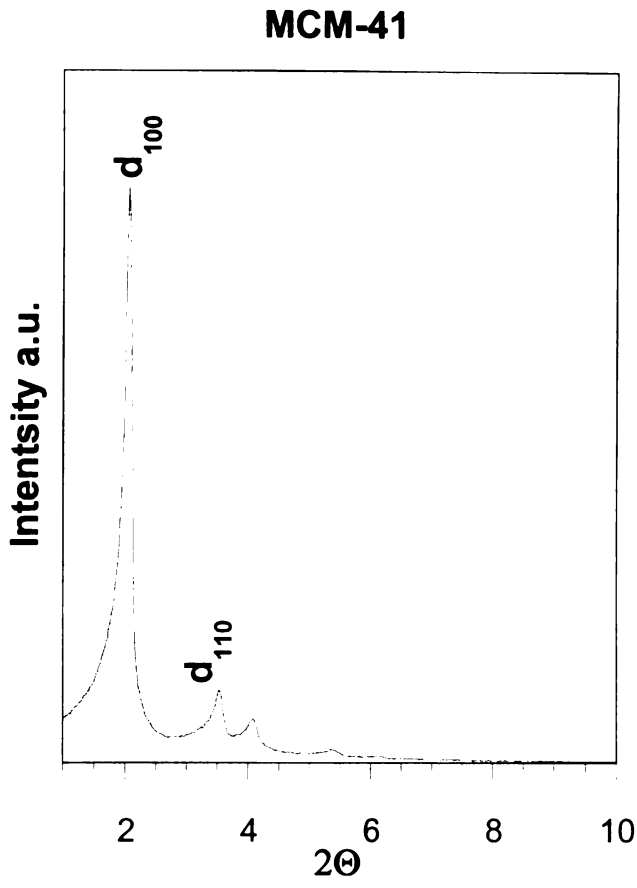


**Figure1.3** Powder X-ray diffraction pattern of MCM-41 with at least 3 peaks ($d_{100}$, $d_{110}$, and $d_{200}$) that can be indexed to the hexagonal unit cell with a unit cell parameter $a_o=2d_{100}/\sqrt{3}$. (Adapted from ref. 15)

Volume adsorbed $cm^3/g$, STP

Figur

sieves

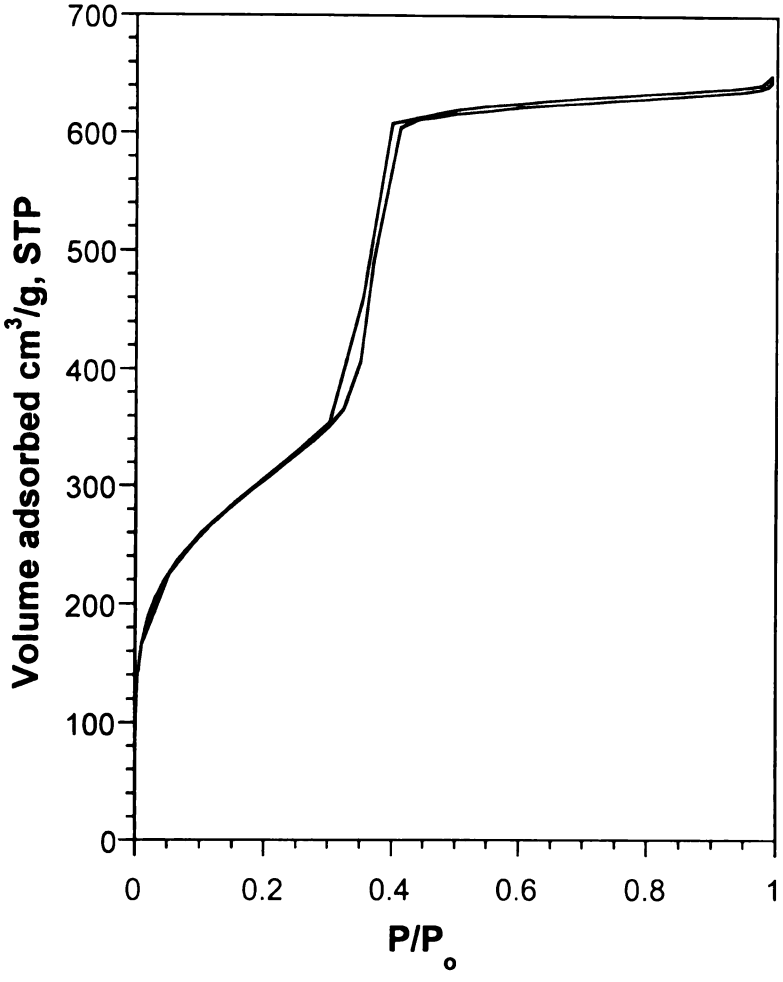


**Figure1.4** $N_2$ adsorption-desorption isotherms of calcined MCM-41 molecular sieves prepared as described in the text. (Adapted from ref. 15)

**Figure 1.5**

sieves. sh

a) Lo

por

b) Hig

alo

c) Hig

the

d) Ultr

3.3

e) Ele

pa

**Figure 1.5** Transmission electron micrographs (TEM) of MCM-41 silica molecular sieves. showing the following[15]

a) Low magnification TEM image showing long range hexagonal ordering of pores along the 001 axis
b) High magnification TEM image showing hexagonal ordering of pores along the 001 axis
c) High magnification TEM image showing lamellar orienation of pores along the 100 axis
d) Ultrahigh magnification image of hexagonal pores in MCM-41 showing a 3.3 nm pore
e) Electron diffraction of hexagonally ordered MCM-41 showing diffraction pattern from orientation of pores.

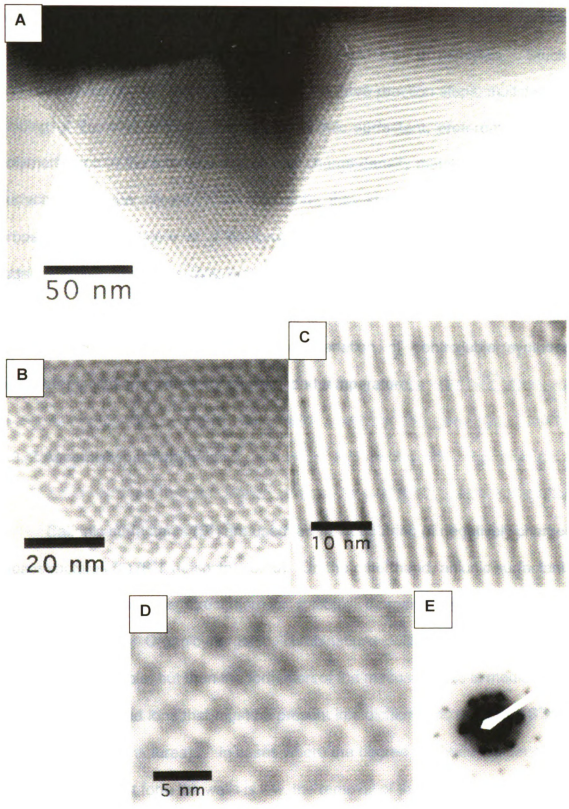
A
50 nm
B
20 nm
C
10 nm
D
5 nm
E

Similarly various attempts were explored to obtained better access by building three dimensional structured arrays out of MCM-41 type of materials. Stucky and co-workers divided the global process into three reaction steps: multidentate binding of the silicate oligomers to the cationic surfactant, preferential silicate polymerization in the interface region, and charge density matching between the surfactant and the silicate.[22-25] Furthermore, they state that in this model, the properties and structure of a particular system were not determined by the organic arrays that have long-range preorganized order, but by the dynamic interplay among ion-pair inorganic and organic species, so that different phases can be readily obtained through small variation of controllable synthesis parameter including mixture composition and temperature.

### 1.3. 2 Assembly pathways

Cationic surfactants ($S^+$) are used for the structuring of negatively charged mesostructures ($I^-$) ($S^+I^-$ mesostructures). On the other hand, anionic surfactants ($S^-$) are employed for structuring of cationic inorganic species ($I^+$) ($S^-I^+$ mesostructures). Organic-inorganic combinations with identically charged partners are possible, but then the formation of the mesostructure is mediated by the counter-charged ions that must be present in stoichiometric amounts ($S^+X^-I^+$, and $S^-M^+I^-$ mesostructures).[25] In cases where the degree of condensation of the oligomeric ions that form the walls is low, the removal of the template leads to the collapse of the ordered mesostructure. It would then be of both fundamental and

practical interest to develop new synthetic routes, which allow the template to be more easily removed.

Pinnavaia and Tanev[26-28] developed novel synthetic strategies to synthesize materials that would be more robust, having shorter channel path lengths for better access to catalytic sites. Moreover, these materials would be suitable for the extraction of the surfactant and reuse of the extracted surfactant for mesostructure synthesis. This approach involved the use of a neutral amine surfactant ($S^0$) and an electrically neutral inorganic precursor ($I^0$) typically TEOS for silicate systems. This approach was denoted as the ($S^0I^0$) method. This method arguably is the most innovative approach to deal with many limiting issues arising from conventional MCM-41 type synthesis. The $S^0I^0$ approach solves the problem of highly monolithic structures by generating smaller crystallite sizes and intrinsically accessible 3-D framework. By tuning the synthesis conditions it is possible to control the degree of condensation and hence the cross-linking of the silicate structure resulting in more rigid and robust structures.[29]

As the first examples of ultrastable mesoporous lamellar silicas with a vesicular hierarchical structure, MSU-G silicas were successfully synthesized using Gemini amine surfactants.[30] In contrast to MCM-41, which was assembled through an electrostatic pathway involving a cationic surfactant and an anionic precursor, MSU-G was prepared *via* an electrically neutral, H-bonded pathway.

**Table**

inorg

**Surfa**

Catio

Anio

Catio

Neut

Non

Non

Non

**Table 1.1** Summary for the self-assembly reaction of different surfactant and inorganic species

| **Surfactant** | **Inorganic Precursor** | **Pathway** | **Examples** |
|---|---|---|---|
| Cationic | Anionic | $S^+ I^-$ | MCM-41, metal oxides, MCM-48 |
| Anionic | Cationic | $S^- I^+$ | Alumina, Iron oxide |
| Cationic | Cationic | $S^+ X^- I^+$ | $Zn_2(PO_4)$, $SiO_2$ (strongly acidic) |
| Neutral | Neutral | $S^0 I^0$ | HMS, MSU-V, MSU-G, |
| Non Ionic (neutral) | Neutral | $N^0 I^0$ | MSU-X |
| Non Ionic (neutral) | Neutral | $(N^0 H^+)(X^- I^+)$ | SBA-15, MCF |
| Non Ionic (neutral) | Anionic | $(N^0 H^+)(I^-)$ | MSU-H, MSU-F |

U

volume

treatme

porosit

compa

SBA-3

hydrot

sacrific

show a

relative

capilla

mespo

howev

corres

This is

textura

showi

Pinna

surfac

glycol

conce

templa

Upon calcination at 1000 °C for 4 h, MSU-G retained 75% of its initial pore volume and pore size, as well as 90% of its surface area. Hydrothermal treatment in boiling water for 56 h had a negligible effect on the framework porosity of MSU-G, as confirmed by XRD and $N_2$ sorption isotherms. In comparison to MSU-G[30,31], as well as SBA-15[32], previously reported KIT-1[33], SBA-3[34], and MCM-41 mesostructured silicas exhibited comparatively poor hydrothermal stability. The framework structures were almost completely sacrificed in boiling water after 56 h. Nitrogen adsorption-desorbtion isotherms show a typical type IV isotherm for mesoporous materials with uptake of $N_2$ at relative pressures of ~0. 3-0. 4. The uptake at these relative pressures is due to capillary condensation of the gas within the confined space of the framework mespores.[31] An important difference between MCM-41 (figure1.3) and MSU-G, however is the significant uptake of $N_2$ at higher partial pressures. This uptake corresponds to the capillary condensation of $N_2$ with interparticulate mesopores. This is similar to the uptake observed in a HMS type silica and is indicative of the textural mesoporosity. Figure1.7 is a TEM image of MSU-G vesicular structures showing a multilamellar pattern.

Another contribution of mesostructured chemistry in its infancy from Pinnavaia and co-workers was the use of nonionic polyethylene oxide surfactants.[35,36] Attard and co-workers[37] extended this approach to ethylene glycol hexadecyl ether at high concentrations as structure directors, which was conceived as $N^0\ I^0$ assembly pathway. When one considers these neutral templating routes the interaction at the $S^0\ I^0$ and $N^0\ I^0$ interface probably occurs

through hydrogen bonds which, by being weaker than electrostatic interactions, allow the extraction of the neutral template molecules by washing with ethanol.[38] Stucky and co-workers proposed a new procedure for synthesizing silica and silica-alumina MCM-41 materials,[23] which involves highly acidic synthesis conditions instead of the basic or mildly acid conditions commonly used. Maintaining consistencies with the charge density matching principle, it has been proposed that the templating mechanism during the acid synthesis of MCM-41 follows a path in which $S^+X^-I^+$ mesostructures are involved, where $I^+$ is a positively charged silica precursor, $S^+$ is the alkyltrimethylammonium cation, and $X^-$ is the compensating anion of the surfactant. If this were true it would be expected that samples prepared using different acids will give MCM-41 mesostructures with different final chemical composition, d spacings, and pore diameters. There is considerable discussion concerning whether the pathway indicated as $S^+X^-I^+$ is truly $S^+X^-I^+$ or more correctly $I^+X^-S^+$.[39]

### 1.3. 3 Large pore mesoporous materials

A variety of nonionic surfactants were found to assemble mesostructured morphologies using hydrogen bonding pathways.[40] In addition to alkyl-PEO surfactants, alkyl-phenyl surfactants with the basic formula $R_n$-Ph-O$(EO)_m$H, such as IGEPAL-RC™ and TRITON-X™, triblock co-polymer surfactants such as PLURONIC™ having basic the formula $(EO)_n(PO)_m(EO)_n$. Similarly Pluronic-R™ where the hydrophobic polypropylene oxide segments can be reversed to have the basic formula $(PO)_m(EO)_n(PO)_m$.Stucky and co-workers extended the $S^+X^-I^+$

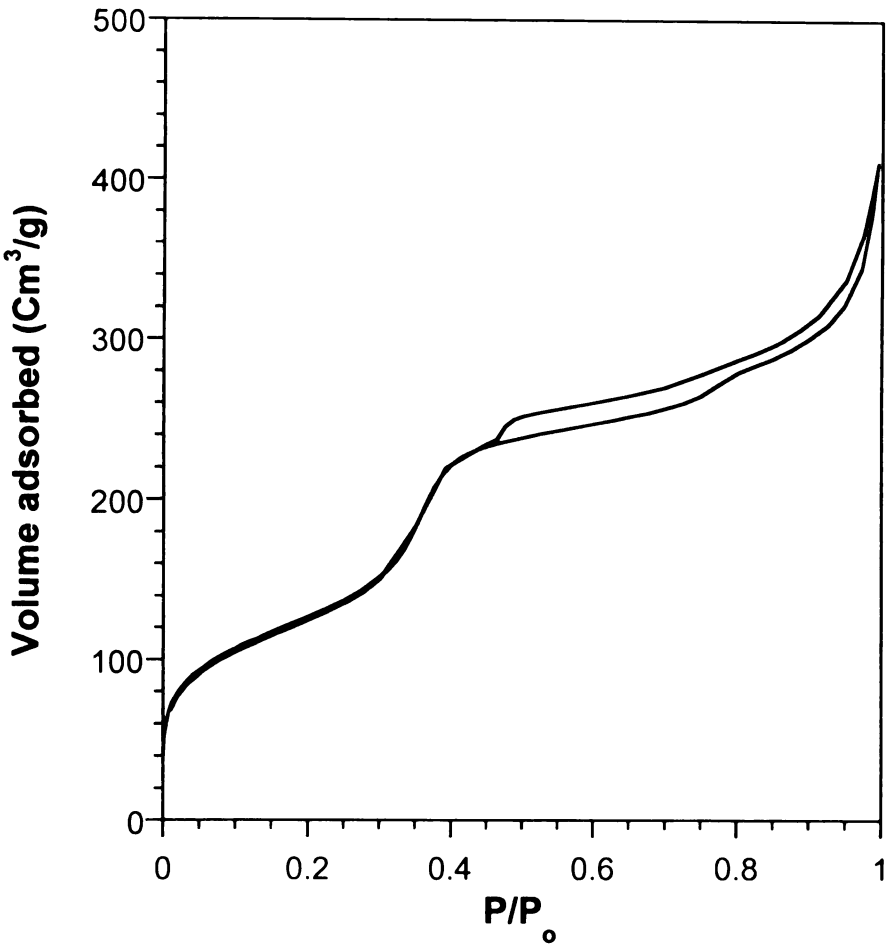


**Figure1.6** $N_2$ adsorption-desorption isotherms of calcined MSU-G silica molecular sieves showing a $N_2$ uptake at higher partial pressures.

**Figure1.7** Representative TEM micrographs of calcined MSU-G silica prepared by u sing $C_{12}H_{25}NH(CH_2)_2NH_2$ as the structure director and TEOS as the silica source (A) vesicle-like and (B) fractured vesicle morphology.

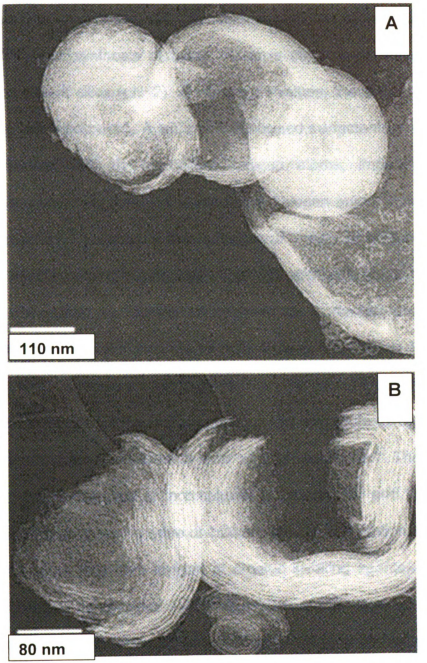
A
110 nm
B
80 nm

pathw

meso

pathv

isoele

hydro

ions

Coul

pathv

relate

mate

PLUR

of SE

earlie

silica

cond

cons

silica

Meso

highl

meso

silica

discu

pathway using PEO surfactants for the assembly of periodically ordered mesoporous silicas under strongly acid conditions called the $(N^oH^+)(X^-I^+)$ pathway.[32,41] The synthesis of these silicas is done at pH values below the isoelectric point of silica (pH~2). At these pH values, the silica source (TEOS) hydrolyzes into silicic acid. Also, the PEO based surfactants have hydronium ions associated with the methylene oxygen atoms, imparting long-range Coulombic interactions through the mediating halogen anion. This electrostatic pathway $(N^oH^+)(X^-I^+)$ results in the formation of variety of mesophases closely related to the choice of the surfactant. This high acidity assembly route results in materials designated as SBA-15 silicas when the surfactant used is P123, a PLURONIC™ surfactant having the formula $(EO)_{20}(PO)_{70}(EO)_{20}$. The pore sizes of SBA-15 type materials are much larger than the mesoporous silicas reported earlier. Pinnavaia and co-workers reported a low-cost route using water soluble silicates denoted as MSU-H under near neutral conditions.[42] The ratio of fully condensed ($Q^4$) silica sites to incompletely condensed $Q^3$ and $Q^2$ sites is 4.5, considerably higher than the value of 1.28 reported for conventional SBA-15.

Futhermore, with the addition of organic swelling agents and modifiers, silicas can be synthesized with spherical pores and designated as Mesostructured Cellular Foams[43] (MCF). The synthesis is normally carried out in highly acidic media with TEOS as the silica source. Related MSU-F[42] mesostructures are prepared under near neutral conditions using water-soluble silicates, such as sodium silicate as the silica source. These materials are discussed in significant detail in Chapter 4.

1. 3. 4

regula

cataly

utility

hetero

compa

the p

molec

applic

in co

mesc

appli

thinn

mesc

these

decr

-OH

the s

prima

of al

gels a

### 1. 3. 4 Hydrothermal and steam stability

Mesoporous molecular sieves present very high surface areas with very regular pore size dimensions. These properties alone, even if no intrinsic catalytically active sites can be generated in the structure, are already of great utility as carriers for supporting catalytically active phases such as heteropolyacids, amines, transition metal complexes, and oxides.[44] In comparison to microporous zeolites, ordered mesoporous materials overcome the pore size constraint of zeolites and allow the more facile diffusion of bulky molecules. These are properties that are highly desirable for potential applications in FCC (fluid catalytic cracking) processes and chemical conversions in condensed media. However, the acidity and hydrothermal stability of mesostructured aluminosilicates are less than required for many catalytic applications. The instability of these structures has been attributed in part to the thinness and incomplete crosslinking of the pore walls.[45]

Since hydrothermal stability and acidity are essential for the application of mesoporous materials in catalysis, several approaches have aimed at improving these properties. The strategies that have been investigated include (i) decreasing the silanol group content of the framework by silylation of the surface –OH groups in order to make the surface more hydrophobic and thereby improve the stability in water,[46,47] (ii) thickening the walls of MCM-41 by post-treatment of primary MCM-41 to improve the hydrothermal stability, and subsequently grafting of aluminum centers into the framework walls[48-50](iii) adding salts to synthesize gels and facilitate the condensation of silanol groups during the formation of the

framework, thereby improving framework crosslinking,[51] (iv) partially transforming the walls into a pentasil zeolite phase by post-synthesis treatment of the original mesoporous aluminosilicate with zeolite structure-directing agents, such as tetrapropylammonium salts[52,53], (v) generating microporous zeolite–mesostructure composite mixtures to improve both hydrothermal stability and acidity[54,55], (vi) using triblock copolymer surfactants to make thick wall mesoporous structures such as SBA-15[41], and (vii) using neutral Gemini amine surfactants to make thick-walled, vesicle-like lamellar frameworks with improved hydrothermal stability.[30,31]

The improved hydrothermal stability of MSU-G, like SBA-15, is attributable in large part to the thicker framework walls (2. 5 nm) in comparison to MCM-41, KIT-1, and SBA-3. This same structural feature is expected to contribute to the stability of aluminum-substituted derivatives. Another notable feature associated with the higher hydrothermal stability of MSU-G was the higher $Q^4/Q^3$ ratio (6. 2) for the framework $SiO_4$ units.[31] Normally, as-synthesized mesoporous silicates have $Q^4/Q^3$ ratios less than 2.0 and calcined forms have ratios less than 3.0. The higher $Q^4/Q^3$ value for MSU-G means that the framework walls are more completely crosslinked and probably more hydrophobic than other mesostructured silicates. These features contribute substantially to the improved hydrothermal stability. In general, as-prepared silica mesostructures assembled through electrically neutral assembly pathways are more highly crosslinked than mesostructures prepared *via* an electrostatic charge matching mechanism. In an effort to increase the wall thickness and crosslinking of MCM-41, Mokaya

employed calcined MCM-41 as the silica source for the secondary synthesis of the same mesostructure.[48-50] He also prolonged the synthesis time of MCM-41. Upon secondary synthesis, the restructured MCM-41 silica exhibited improved long-range structural ordering and a marked increase in hydrothermal stability. Basically, the improved hydrothermal stability was attributed to the increased pore wall thickness by secondary synthesis. Moreover, after post-synthesis grafting of aluminum centers onto the framework walls of the secondary silica MCM-41, both the hydrothermal stability and acidity were significantly improved.

In comparison to crystalline microporous zeolites, mesoporous aluminosilicates lack hydrothermal stability and strong acidity due to their non-crystalline framework walls. Thus, several efforts to crystallize the walls of mesoporous aluminosilicate have been reported. In 1997, van Bekkum *et al* first used the zeolite structure-directing agent tetrapropylammonium cation to treat Al-MCM-41 and Al-HMS mesostructures. The strategy was to improve the acidity of Al-MCM-41 and Al-HMS by partially recrystallizing the pore walls into nanosized ZSM-5.[56]

It is unlikely that the framework wall of MCM-41 can be transformed to a crystalline zeolite phase while still maintaining the hexagonal MCM-41 mesostructure. The unit cell of ZSM-5 is around 2.5 nm, which is larger than the wall thickness of MCM-41. Clearly, once a zeolite phase is formed from MCM-41, it is likely to appear as a separated zeolite phase. This expectation was confirmed by more recent results from van Beckkum *et al*.[57] In the best case, the wall of MCM-41 was transformed into 3 nm ZSM-5 crystallites.

Following-up on van Beckkum's approach, Kaliaguine and co-workers investigated the possibility of transforming a thicker wall MCF aluminosilicate into a crystalline zeolitic framework. A ZSM-5 phase with 42% crystallinity was formed after hydrothermal treatment with tetrapropylammonium hydroxide. The $N_2$ isotherms for this material (denoted UL-ZSM-5), exhibited a typical type IV shape and a steep rise at low relative $P/P_o$, indicating the presence of both micropore and mesopore structures.[53]

Liu *et al* reported the first steam-stable hexagonal mesoporous aluminosilicates were successfully assembled from faujasitic-type Y zeolite seeds.[58] Nanoclustered zeolite Y seeds were prepared by reacting sodium hydroxide, sodium aluminate, and sodium silicate under vigorous stirring at 100 °C overnight. The assembly of a hexagonal mesostructure was achieved by lowering the pH of the seed solution to a value of about 9.0 and introducing cetyltrimethylammonium bromide (CTAB) as the structure director. The aluminum loading in the final mesostructures was controlled by the composition of the original seed solution (10–35 mol% Al). The steam-stable mesoporous aluminosilicate (denoted MSU-S) was obtained by exchanging the as-synthesized structure with $NH_4NO_3$ and then calcining at 540 °C for 7 h. In further developing the concept of using protozeolitic nanoclusters for mesostructure assembly, Liu *et al* prepared hydrothermally stable and strongly acidic MCM-41 analogs from zeolite ZSM-5 and Beta seeds, which are nucleated by tetrapropylammonium and tetraethylammonium cations, respectively.[58] The resulting aluminosilicate mesostructures were denoted MSU-$S_{(MFI)}$ and MSU-

by

lat

pr

wa

tet

(de

MA

or

tha

MA

but

Bet

The

of

zeo

whi

larg

mat

$^{27}$Al

$S_{(BEA)}$. Significant improvement in cumene cracking activities of MSU-$S_{(MFI)}$ and MSU-$S_{(BEA)}$ was observed as compared to 1.5% Al-MCM-41, which was prepared by the direct assembly of conventional aluminate and silicate anions. For this latter sample the aluminum and silica sources were the same as those used to prepare MSU-$S_{(MFI)}$ and MSU-$S_{(BEA)}$, except that tetramethylammonium hydroxide was used in place of structure-directing tetrapropylammonium or tetraethylammonium hydroxide.

Zhang *et al.* have also reported a hydrothermally stable MCM-41 analog (denoted MAS-5) which was assembled from zeolite Beta seeds.[59,60] Apparently, MAS-5 still retained well-ordered hexagonal arrays after boiling in water for 300 h or steaming at 800 °C for 2 h. The MAS-5 material also exhibited stronger acidity than conventional Al-MCM-41 for 1,3,5-triisopropylbenzene cracking. In addition, MAS-5 showed higher catalytic activity than Beta zeolite for the alkylation of 2-butene with isobutene. The acidity of MAS-5 was reported to be very similar to Beta zeolite, as judged by temperature programmed desorption of ammonia. The higher catalytic activity for the alkylation was attributed to the easier diffusion of products in the mesoporous channels of MAS-5 than in microporous Beta zeolite. Five-membered ring vibrations also were observed in MAS-5 by IR, which indicated the incorporation of Beta zeolite subunits in the framework.

Liu and Pinnavaia further extended the protozeolitic seed approach to large pore mesostructured materials such as SBA-15, MSU-H, MCF and MSU-F materials.[61] They further proposed backed by evidence from FTIR, $^{29}Si$ NMR and $^{27}Al$ NMR, that the hydrothermal stability and catalytic activity of MSU-$S_{(MFI)}$ and

MSU-$S_{(BEA)}$ arise form the presence of zeolitic subunits of $AlO_4$ and $SiO_4$ tetrahedra in the framework walls of the mesostructures. There is probably little risk in predicting that a mesostructured aluminosilicate with fully crystalline walls and superior stability will be developed in the future.

**1. 3. 5 Organofunctional mesoporous materials**

Solid catalysts provide numerous opportunities for recovering and recycling catalysts from reaction environments. These features can lead to improved processing steps, better process economics, and environmentally friendly industrial manufacturing. Thus, the motivating factors for creating recoverable catalysts are large.

Traditional heterogeneous catalysts are rather limited in the nature of their active sites and thus the scope of reactions that they can accomplish. Soluble organic catalysts can catalyze a much larger variety of reaction types than traditional solid catalysts but suffer from their inability (or high degree of difficulty) to be recycled. Since much is known about organic catalysts, the immobilization of these entities onto solids to create organic-inorganic hybrid catalysts can be accomplished with some aspects of design. The goal is to utilize the organic moiety as the active site and the solid to provide avenues to recovery and possibly recyclability of the organic active site. [62]

These hybrids can be synthesized by a number of methods: (i) adsorption of the organic species into the pores of the support; (ii) construction of the organic molecule piece by piece within the confines of cavities of the support (the "ship-in a-bottle" technique); (iii) attachment of the desired functionality to the

support by covalent bond formation; (iv) direct synthesis into the final composite material. The types of solids used can be organic, e.g. polymers, or inorganic, e.g. silica and alumina.[62-64]

Acid functional groups have also been used as organic modifiers to silica surfaces. Harmer and co-workers have attached a perfluorosulfonic moiety onto silica for use in acid catalysis applications.[65] The perfluorosulfonic group is a strong acid and has excellent chemical and thermal stability. The perfluorosulfonyl fluoride silane was synthesized in a hydrosilylation procedure, using the corresponding olefin. The acid sites were generated by hydrolysis of the perfluorosulfonyl fluoride functionality. Harmer also reported the use of the perfluorosulfonic acid silane in the co-condensation of silica, using traditional sol-gel techniques[66]. Activities of both the grafted and co-condensed silica hybrids were reported as similar. The grafted acid catalyst was tested in several acid-catalyzed reactions, such as aromatic alkylation, alkene isomerization, and Friedel-Crafts acylation, and the respective conversions were 99, 95, and 89%. In the alkylation and isomerization reactions, the hybrid catalyst significantly outperformed some of the alternative solid resin catalysts currently used, e. g., Nafion resin NR 50 and Amberlyst-15. The hybrid catalyst achieved a conversion of 43% for the alkylation of benzene with dodec-1-ene at 80 °C for 1 h, conditions where the traditional acid resins gave 3-5%. It is interesting to note that the acid loadings of the solid catalysts are 0.2, 0.9, and 4.6 mequiv of $H^+$/g of catalyst for the hybrid silica, Nafion NR 50, and Amberlyst-15 resins, respectively. Despite a lower number density of acid sites, the hybrid silica

cata

orga

elec

con

diel

dev

org

inve

wat

con

with

high

mat

of t

disc

esta

syn

hex

por

cha

hyd

catalyst still outperformed the resins in the reactions reported. Similarly many organofunctional derivatives of mesoporous silica were prepared for catalytic and electronic applications. Miller *et al* at IBM reported the use of thin films containing nanometer sized pores for their potential use as optical elements, low-dielectric constant (low-k) materials. Extensive research is being conducted to develop high strength low dielectric materials that have a $k<2$ using organosilicates with a polymeric sacrificial porogen.[67-69]

Mercaptopropyl functionalized mesoporous materials have been investigated in great detail due to their high mercury trapping potential for ground water remediation.[70-72] Pinnvaia and Liu[73-76] have independently developed considerable methodologies to synthesize mercaptopropyl functionalized silicas with high affinity for mercury[77]. Yutaka and Pinnavaia synthesized silicas with as high as 60% of the silicon centers functionalized with mercapto groups. These materials are precursors to sulfonic acid functionalized silicas by simple oxidation of the thiol group to sulfonic acid by oxidizing agents[78]. These materials are discussed more in detail in chapter 5 with respect to their catalytic evaluation in esterification of lauric acid by glycerol.

In a novel synthetic method Inagaki *et al* reported the surfactant-mediated synthesis of an ordered benzene-silica hybrid material; this material has an hexagonal array of mesopores with a lattice constant of 52.5 Å, and crystal-like pore walls that exhibit structural periodicity with a spacing of 7.6 Å along the channel direction.[79] The periodic pore surface structure results from alternating hydrophilic and hydrophobic layers, composed of silica and benzene,

res

dire

bet

eie

pat

wit

cor

pre

of

rig

wit

mo

"de

ma

1.

alu

the

The

199

pos

firs

respectively. They believe that this material is formed as a result of structure-directing interactions between the benzene-silica precursor molecules, and between the precursor molecules and the surfactants. Both the transmission electron microscope (TEM) images and corresponding electron diffraction patterns revealed a clear hexagonal arrangement of one-dimensional channels with uniform size (Figure 1.8 A and inset). Nitrogen adsorption isotherms also confirmed the existence of uniform mesopores

There are numerous organic-inorganic hybrid materials that have been prepared and characterized but not yet tested as catalysts. Additionally, very few of the materials that have been exposed to reaction conditions have been rigorously tested for reuse. Thus, there are many opportunities for investigation with currently available materials. Since much is known about how organic moieties can serve as catalysts for homogeneous reactions, many elements of "design" can be used in future developments of organic-inorganic hybrid materials for use as recyclable catalysts.

### 1. 3. 6 Nonsiliceous Mesoporous materials and nanocasting

Since the discovery of FSM-16[80] and MCM-41[16], both silica and aluminumsilicate ordered mesoporous materials; much work has been devoted to the study of the synthesis, properties, and possible uses of such materials. These topics are covered in several comprehensive recent reviews.[81] Already in 1993 it was suggested, on the basis of mechanistic ideas, that it should be possible to synthesize non-siliceous materials following similar pathways.[82] The first examples were reported in 1994[39]. However, it had not been possible to

rem

mes

silic

dev

mat

mes

ma

rec

syn

stru

wit

an

line

for

su

a s

pu

fu

of

int

remove the template in these materials. Thus, no mesoporous materials, but only mesostructured materials, could be obtained. The first mesoporous non-siliceous frameworks were reported in 1995/1996[83], from which rapid development started. However, the field of non-siliceous ordered mesoporous materials has found considerably less attention compared to that of mesostructured silica.

The possibility of using ordered mesoporous silica as molds for other materials, especially polymers, was realized relatively early. However, only recently have ordered mesoporous carbons and metallic materials been synthesized by "nanocasting" in mesoporous silica molds. Because a 3-D structure is necessary in the mold to maintain a stable replica, only experiments with MCM-48, MSU-1, and SBA-15 were successful.[84,85] SBA-15 in principle has an unidimensional channel system. However, micropores seem to connect the linear hexagonally packed mesopores, thus providing the cross-linking necessary for obtaining a stable replica. MCM-41, on the other hand, proved to be less suitable for the production of porous carbons or metals.[86]

The mesoporous carbons are prepared by infiltrating the pore system with a suitable carbon precursor and subsequent pyrolysis of the precursor to give pure carbon. Suitable precursors were sucrose in the presence of sulfuric acid, furfuryl alcohol, or a phenol-formaldehyde resin, dependent on the exact nature of the system. Metal containing materials are prepared by chemical vapor infiltration with volatile metal precursor complexes and subsequent pyrolysis.

Bo

fro

hav

sui

dis

cas

by

car

pre

mig

uni

dia

alu

car

dev

por

bro

opt

syn

mat

Both carbons and metal containing materials in silica frameworks can then freed from the silica template either by NaOH solution or with HF.

It is at present not clear how general these pathways are because they have only recently been discovered. It is clear, though, that they will only be suitable for framework compositions that are stable under the conditions used to dissolve the mold, that is, stable in relatively concentrated NaOH or HF in the case of silica. One might, however, go one step further and use the carbons cast by this technique again as a mold for yet another framework and then remove the carbon by calcination to increase the flexibility[87,88]. It is to be expected that the precision of the nanocasting will decrease with every additional step, but this might be tolerable, depending on the system envisaged. A periodic array of uniform ordered nanoporous carbon can easily be synthesized with tunable pore diameters and rigid structural order as shown in Figure1.9, using the mesoporous aluminosilicate molecular sieves SBA-15 as templates.[85] These nanostructured carbon materials are potentially of great technological interest for the development of electronic, catalytic, and hydrogen-storage systems.

Kanatizidis *et al* reported open framework metal chalcogenide solids, with pore sizes on the nano- and mesoscale.[89] These materials are of potentially broad technological and fundamental interest in research areas ranging from optoelectronics to the physics of quantum confinement. They further describe a synthetic strategy that allows the preparation of a large class of mesoporous materials based on supramolecular assembly of tetrahedral Zintl anions $[SnSe_4]^{4-}$

Fig

pa

im

the

A.

Un

B.

Ma

wa

À

À

de

co

sp

the

Sc

**Figure1.8** Tranmission electron micrographs (TEM) images, electron diffraction patterns and the resulting structural model of mesoporous benzene–silica. The images and the patterns are arranged in the correct orientation relation—that is, the diffraction spots and corresponding lattice planes are normal to each other. A. Image and pattern taken with [001] incidence, parallel to the channels. Uniform mesopores with a diameter of 38 Å are arranged in a hexagonal manner. B. Image and pattern taken with [100] incidence, perpendicular to the channels. Many lattice fringes with a spacing of 7.6 Å are observed in the pore walls. The wavy contrast, which is perpendicular to the lattice fringes, with a spacing of 45.5 Å (d = 3a/2) is also discernible. Note that we cannot observe the contrast of 7.6-Å and 45.5-Å spacings at the best condition simultaneously for both, because the dependence of the contrast transfer function of the objective lens on focus condition is different for both. The electron diffraction pattern also shows diffused spots due to the 7.6-Å periodicity (large arrow) in the perpendicular direction to the spots due to channel arrangement with d = 45.5 Å (small arrow). C, Schematic model of mesoporous benzene–silica derived from the results of the TEM images and electron diffraction patterns.[79]

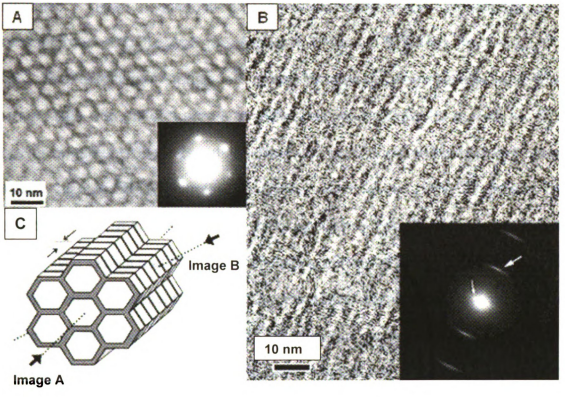
A
10 nm
C
Image B
Image A
B
10 nm

with transition metals in the presence of cetylpyridinium (CP) surfactant molecules.[90] These mesostructured semiconducting selenide materials are of the general formulae $(CP)_{4-2x}M_xSnSe_4$ (where 1. 0 < $x$ < 1. 3; M=Mn, Fe, Co, Zn, Cd, Hg). The resulting materials are open framework chalcogenides and form mesophases with uniform pore size (with spacings between 35 and 40 Å). The pore arrangement depends on the synthetic conditions and metal used, and include disordered wormhole, hexagonal, and even cubic phases. All compounds are medium bandgap semiconductors (varying between 1.4 and 2.5 eV). We expect that such semiconducting porous networks could be used for optoelectronic, photosynthetic and photocatalytic applications. This chapter makes an attempt to touch briefly on the various aspects of mesoporous materials from the past, present, and future perspectives. As can be seen from the trend over the last few years, the focus of research keeps changing drastically over very short time spans. In the mid to late 90's the focus primarily was on development of new structures and morphologies of oxidic frameworks. However, as it becomes more and more difficult to synthesize new materials and frameworks, novel ideas such as mesoporous carbon, are receiving a lot of attention. Despite significant development, a truly crystalline, extremely stable mesoporous catalyst still remains an elusive dream hopefully to be achieved in the near future.

**Figure1.9** Ordered nanoporous carbon obtained by template synthesis using ordered mesoporous silica SBA-15[85].

**A**, TEM image viewed along the direction of the ordered nanoporous carbon and the corresponding Fourier diffractogram.

**B**, Schematic model for the carbon structure. The structural model is provided to indicate that the carbon nanopores are rigidly interconnected into a highly ordered hexagonal array by carbon spacers. The outside diameter of the carbon structures is controllable by the choice of a template SBA-15 aluminosilicate with suitable diameter; the inside diameter is controllable by the amount of the carbon source

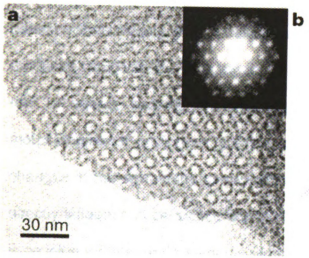
a
b
30 nm

1.

be

pa

MS

dia

be

pro

rol

mo

cha

dire

is d

tribi

solu

1.4.

has

atten

meso

exten

## 1. 4 Research Objectives

There are three basic research objectives for which the current work has been undertaken. The first and foremost being the understanding of various parameters that affect the self-assembly of vesicular mesostructures denoted as MSU-G formed by a $S^oI^o$ methodologies involving a monosubstituted alkylene diamine structure director and TEOS as the silica source. The correlation between the surfactant compositions with the morphology of hierarchical silica produced needs to be understood. The second objective is to understand the role of shape, and its chemical significance in catalytic activity. Diverse morphologies of mesoporous silica are obtained by inducing relatively minor changes in the surfactant composition. Mesostructured silica thus obtained will directly influence accessibility and resulting catalytic activity. The third objective is develop a better understanding of the microemulsion templating pathway using triblock PLURONIC$^{TM}$ surfactants with sodium silicate as the low-cost water-soluble silicate with trimethylbenzene as an emulsifier.

### 1.4.1 MSU-G mesostructures

The assembly of mesotructures using neutral amine surfactants (HMS) has been studied extensively and is receiving a significant amount of attention.[26,91,92] To date, however, there has been no investigation of mesostructures synthesized using diamine-based surfactants. The ability to extend the $S^oI^0$ approach from primary alkylamine surfactants to monosubstituted

all

is

sil

he

ch

si

su

Ou

1-4

and

wea

hea

incr

that

mes

inhe

Com

Gem

only

silica

inhor

alkylenediamine surfactants to generate ultrastable vesicular mesoporous silicas is a step forward in explain hydrogen-bonded assembly of mesostructured silicas. However, there is little understanding of the effect of surfactant headgroup on mesostructured silica morphology. We plan to study the effect of changing headgroup and hydrophobe chain length on the morphology of MSU-G silicas.

The original work reported by Kim *et al* used ethylene diamine-based surfactants with the hydrophobe chain length of 10, 12, and 14 carbon atoms.[30] Our approach is to modify the surfactant headgroups to 1-3 diaminopropane and 1-4 diaminobutane based surfactants with hydrophobic chain lengths of 10, 12, and 14. The temperature at which HMS silicas are synthesized is limited due to weak hydrogen bonding interactions. However, with the use of diamine headgroups the hydrogen bonding and the chelation effect could be combined to increase the syntheis temperature to 100 $^{0}$C. This allows for better crosslinking that makes the MSU-G structures ultrastable. Another key feature of the MSU-G mesoporous silicas is that they are the only mesoporous structures to have inherent thermal and hydrothermal stability with any post-synthetic processing. Commercial tallow diamine surfactants having chemical compositions similar to Gemini surfactants were studied extensively by Pauly.[29] However, he observed only a wormhole morphology similar to that reported for HMS mesostructured silica. The probable reason for not obtaining a vesicular morphology was the inhomogeneity of the hydrophobic chain length in the tallow diamine surfactants.

int

su

wa

rou

D-

me

ne

1.4

con

Ger

mat

acti

has

mes

comp

activi

that,

shoul

these

due to

A secondary objective was to minimize the amount of cost and process intensive Gemini surfactant needed for vesicle assembly by replacing the surfactant with a commercially available co-surfactant. The co-surfactant choice was Jeffamine D-400 a polyoxopropylene α-ω diamine based curing agent routinely used in curing of epoxy polymers. The structural motif of the Jeffamine D-400 is similar to that of the diamine surfactant used in the synthesis of MSU-G mesoporous materials. The present work also explores the possibility of forming new hierarchical structures by increasing the amount of the co-surfactant.

### 1.4.2 Significance of shape on catalytic activity

A myriad of morphologies can be obtained by tuning the surfactant composition of Gemini surfactants. The headgroup and chain length of the Gemini surfactants play a key role in the type of morphology obtained. These materials can be modified *in situ* or by post assembly treatment with catalytically active metals such as aluminum and tested for catalytic probe reactions. There has been a significant amount of research carried out on the cracking activity of mesoporous catalysts using MCM-41, HMS, and other aluminosilicates compositions.[92-94] However, there is little data correlating structure and cracking activity especially for MSU-G type vesicular morphology. Researchers agree that, to obtain the highest catalytic cracking activity, the diffusional limitations should be minimized. One approach would be to minimize the channel length of these structures. MSU-G hierarchical structures have inherent short pore lengths due to the orientation of pores orthogonal to the wall of silicates. This will

facilitate access of the hydrocarbon moiety to the active site. The objective of the current work was to basically study three reactions to correlate structure and catalytic activity.

i) Gas phase cumene cracking reaction at 300 $^{0}$C will be studied to test the acidic properties of the aluminosilicate species formed during preparation of Al-MSU-G catalysts. The cracking of pure hydrocarbons and, in particular, cracking of cumene, can provide an important method for investigating the nature of catalytic cracking. Some primary reactions occurring in the cumene cracking are thought to be catalyzed by Lewis acid sites while others occur on Brönsted sites.

ii) Improved framework access can be especially important for catalytic applications in condensed phase reaction systems where diffusion may limit the reaction rate. In order to assess the catalytic reactivity of various MSU-G, we have prepared aluminated forms of mesostructures from different surfactants for the acid-catalyzed conversion of DTBP (2,4 di *tert* butyl phenol) to a flavan using cinnamyl alcohol as an alkylating agent.[31]

iii) Highly loaded sulfonic acid catalysts ($SO_3H$-HMS) prepared by Mori and Pinnavaia[78] will be tested for their catalytic performance as acid catalysts for large molecule acid catalyzed esterification reactions. The preparation of monolauroyl glycerol by reaction of glycerol with lauric acid was carried out in presence of acid catalysts. Jacobs did a considerable amount of work in evaluating the performance of sulfonic

1.

F

of

me

sy

of

an

for

wat

The

Sec

obta

mes

Paul

contr

ratio

comp

demo

acid supported mesoporous silica.[95,96] The object of the current work was to study the effect of a higher amount of acid functionality on the conversion and selectivity of this test reaction.

### 1.4.3 Control of cell size and window size in microemulsion templated MSU-F materials

The final objective of this thesis was to develop a detailed understanding of microemulsion templating in mesoporous silicate chemistry. Ultra large pore mesoporous materials having cell sizes in the range of 20-80 nm can be synthesized using microemulsion templates. Stucky *et al* reported the formation of Mesporous Cellular Foams (MCF) using triblock PLURONIC$^{TM}$ 123, TEOS, and trimethyl benzene (TMB) as an emulsifier.[43,97-99] Kim *et al* reported the formation of MSU-F materials using triblock PLURONIC$^{TM}$ 123 and low cost water soluble Sodium silicate as the source of silica and TMB as an emulsifier.[42] The ratio of the triblock surfactant to TMB has a critical effect on the morphology. Secondly, the swelling effect of a co-solvent such as ethanol will be studied to obtain macroporous materials. A co-solvent, such as ethanol, in the synthesis of mesoporous materials has been used to modify the particle shape and size. Pauly *et al* reported that the textural mesoporosity of HMS mesoporous silicas is controlled by the polarity of the solvent system such water-to-ethanol volume ratio.[91] The ability to control the cell sizes and window sizes without altering the composition of the reaction mixtures using simple hydrothermal restructuring is demonstrated in the present work.

## 1.5 References


(1) *IUPAC Manual of Symbols and Terminology, Colloid and Surface Chemistry, Pure Appl. Chem* **1972**, *31*, 579-638.

(2) Davis, M. E.; Saldarriaga, C.; Montes, C.; Hanson, B. E. *J.Phys.Chem* **1988**, *92*, 2557-2560.

(3) Davis, M. E.; Saldarriaga, C.; Montes, C.; Garces, J.; Crowder, C. *Nature* **1988**, *331*, 698-699.

(4) Barr, T. L.; Klinowski, J.; He, H.; Alberti, K.; Mueller, G.; Lercher, J. A. *Nature* **1993**, *365*, 429-431.

(5) Bedard, R. L.; Bowes, C. L.; Coombs, N.; Holmes, A. J.; Jiang, T.; Kirkby, S. J.; Macdonald, P. M.; Malek, A. M.; Ozin, G. A.; et al. *J. Am. Chem. Soc.* **1993**, *115*, 2300-2313.

(6) Huo, Q.; Xu, R. *J.Chem. Soc., Chem. Commun.* **1992**, 1391-1392.

(7) Merrouche, A.; Patarin, J.; Kessler, H.; Soulard, M.; Delmotte, L.; Guth, J. L.; Joly, J. F. *Zeolites* **1992**, *12*, 226-232.

(8) Moore, P. B.; Shen, J. *Nature* **1983**, *306*, 356-358.

(9) Corma, A.; Fornes, V.; Martinez, A.; Melo, F.; Pallota, O. *Stud. Surf. Sci. Catal* **1988**, *37*, 495-503.

(10) Cartlidge, S.; Nissen, H. U.; Shatlock, M. P.; Wessicken, R. *Zeolites* **1992**, *12*, 889-897.

(11) Cartlidge, S.; Nissen, H. U.; Wessicken, R. *Zeolites* **1989**, *9*, 346-349.

(12) Pinnavaia, T. J.; Kim, H. *NATO ASI Ser., Ser. C* **1992**, *352*, 79-90.

(13) Pinnavaia, T. J.; Kwon, T.; Yun, S. K. *NATO ASI Ser., Ser. C* **1992**, *352*, 91-104.

(14) Barrer, R. M.; MacLeod, D. M. *Trans. Faraday Soc.* **1954**, *50*, 980-989.

(15) Beck, J. S.; Vartuli, J. C.; Roth, W. J.; Leonowicz, M. E.; Kresge, C. T.; Schmitt, K. D.; Chu, C. T. W.; Olson, D. H.; Sheppard, E. W.; McCullen, S. B.; Higgins, J. B.; Schlenker, J. L. *J. Am. Chem. Soc.* **1992**, *114*, 10834-10843.

(16) Kresge, C. T.; Leonowicz, M. E.; Roth, W. J.; Vartuli, J. C.; Beck, J. S. *Nature* **1992**, *359*, 710-712.

(17) Corma, A.; Corell, C.; Martinez, A.; Perez-Pariente, J. *Stud. Surf. Sci. Catal***1994**, *84*, 859-866.

(18) Schreyeck, L.; Caullet, P.; Mougenel, J.-C.; Guth, J.-L.; Marler, B. *J. Chem. Soc., Chem. Commun.* **1995**, 2187-2188.

(19) Heuer, A. H.; Fink, D. J.; Laraia, V. J.; Arias, J. L.; Calvert, P. D.; Kendall, K.; Messing, G. L.; Blackwell, J.; Rieke, P. C.; Thompson, D. H. *Science* **1992** *255*, 1098-1105.

(20) Horvath, G.; Kawazoe, K. *J. Chem. Eng. Jpn.* **1983**, *16*, 470-475.

(21) Arafat, A.; Jansen, J. C.; Ebaid, A. R.; Van Bekkum, H. *Zeolites* **1993**, *13*, 162-165.

(22) Monnier, A.; Schuth, F.; Huo, Q.; Kumar, D.; Margolese, D.; Maxwell, R. S.; Stucky, G. D.; Krishnamurty, M.; Petroff, P.; Firouzi, A.; Janicke, M.; Chmelka, B. F. *Science* **1993**, *261*, 1299-1303.

(23) Hue, Q. S.; Margolese, D. I.; Ciesla, U.; Feng, P. Y.; Gier, T. E.; Sieger, P.; Leon, R.; Petroff, P. M.; Schuth, F.; Stucky, G. D. *Nature* **1994**, *368*, 317-321.

(24) Firouzi, A.; Kumar, D.; Bull, L. M.; Besier, T.; Sieger, P.; Huo, Q.; Walker, S. A.; Zasadzinski, J. A.; Glinka, C.; Nicol, J.; Margolese, D.; Stucky, G. D.; Chmelka, B. F. *Science* **1995**, *267*, 1138-1143.

(25) Hue, Q.; Leon, R.; Petroff, P. M.; Stucky, G. D. *Science* **1995**, *268*, 1324-1327.

(26) Tanev, P. T.; Pinnavaia, T. J. *Science* **1995**, *267*, 865-867.

(27) Tanev, P. T.; Pinnavaia, T. J. *Science* **1996**, *271*, 1267-1269.

(28) Tanev, P. T.; Liang, Y.; Pinnavaia, T. J. *J. Am. Chem. Soc.* **1997**, *119*, 8616-8624.

(29) Pauly, T. Ph.D. Thesis *Chemistry*; Michigan State University: East Lansing, 2000, p 217.

(30) Kim, S. S.; Zhang, W. Z.; Pinnavaia, T. J. *Science* **1998**, *282*, 1302-1305.

(31) Kim, S. S.; Liu, Y.; Pinnavaia, T. J. *Microporous Mesoporous Mater.* **2001**, *44*, 489-498.

(32) Zhao, D.; Feng, J.; Huo, Q.; Melosh, N.; Frederickson, G. H.; Chmelka, B. F.; Stucky, G. D. *Science* **1998**, *279*, 548-552.

(33) Ryoo, R.; Kim, M. J.; Kim, J. M.; Jun, S. *Chem. Commun.* **1997**, 2225-2226.

(34) Huo, Q.; Margolese, D. I.; Stucky, G. D. *Chem. Mater.* **1996**, *8*, 1147-1160.

(35) Bagshaw, S. A.; Prouzet, E.; Pinnavaia, T. J. *Science* **1995**, *269*, 1242-1244.

(36) Bagshaw, S. A.; Pinnavaia, T. J. *Angew. Chem., Int.Ed.* **1996**, *35*, 1102-1105.

(37) Attard, G. S.; Glyde, J. C.; Goltner, C. G. *Nature* **1995**, *378*, 366-368.

(38) Behrens, P. *Angew. Chem., Int. Ed.***1996**, *35*, 515-518.

(39) Huo, Q. S.; Margolese, D. I.; Ciesla, U.; Feng, P. Y.; Gier, T. E.; Sieger, P.; Leon, R.; Petroff, P. M.; Schuth, F.; Stucky, G. D. *Nature* **1994**, *368*, 317-321.

(40) Bagshaw, S. A.; DiRenzo, F.; Fajula, F. *Chem. Commun.* **1996**, 2209-2210.

(41) Zhao, D.; Huo, Q.; Feng, J.; Chmelka, B. F.; Stucky, G. D. *J. Am. Chem. Soc.* **1998**, *120*, 6024-6036.

(42) Kim, S.-S.; Pauly, T. R.; Pinnavaia, T. J. *Chem. Commun.* **2000**, 1661-1662.

(43) Schmidt-Winkel, P.; Lukens, W. W., Jr.; Zhao, D.; Yang, P.; Chmelka, B. F.; Stucky, G. D. *J. Am. Chem. Soc.* **1999**, *121*, 254-255.

(44) Liu, Y.; Pinnavaia, T. J. *Chem. Mater.* **2002**, *14*, 3-5.

(45) Corma, A.; Grande, M. S.; Gonzalez-Alfaro, V.; Orchilles, A. V. *J. Catal.* **1996**, *159*, 375-382.

(46) Zhu, H. Y.; Lu, G. Q.; Zhao, X. S. *J.Phys.Chem B* **1998**, *102*, 7371-7376.

(47) Zhao, X. S.; Lu, G. Q. *J.Phys.Chem B* **1998**, *102*, 1556-1561.

(48) Mokaya, R.; Jones, W. *Chem. Commun.* **1997**, 2185-2186.

(49) Mokaya, R. *J.Phys.Chem B* **1999**, *103*, 10204-10208.

(50) Mokaya, R. *Angew. Chem., Int. Ed.* **1999**, *38*, 2930-2934.

(51) Kim, J. M.; Jun, S.; Ryoo, R. *J. Phys. Chem. B* **1999**, *103*, 6200-6205.

(52) On, D. T.; Reinert, P.; Bonneviot, L.; Kaliaguine, S. *Stud. Surf. Sci. Catal* **2001**, *135*, 929-937.

(53) On, D. T.; Kaliaguine, S. *Angew. Chem., Int. Ed.* **2001**, *40*, 3248-3251.

(54) Kloetstra, K. R.; Zandbergen, H. W.; Jansen, J. C.; Van Bekkum, H. *Chemical Industries (Dekker)* **1998**, *74*, 159-174.

(55) Huang, L.; Guo, W.; Deng, P.; Xue, Z.; Li, Q. *J.Phys.Chem B* **2000**, *104*, 2817-2823.

(56) Richard Kloetstra, K.; Jansen, J. C. *Chem.Commun* **1997**, 2281-2282.

(57) Verhoef, M. J.; Kooyman, P. J.; van der Waal, J. C.; Rigutto, M. S.; Peters, J. A.; van Bekkum, H. *Chem. Mater.* **2001**, *13*, 683-687.

(58) Liu, Y.; Zhang, W.; Pinnavaia, T. J. *Angew. Chem., Int. Ed.* **2001**, *40*, 1255-1258.

(59) Zhang, Z. T.; Han, Y.; Zhu, L.; Wang, R. W.; Yu, Y.; Qiu, S. L.; Zhao, D. Y.; Xiao, F. S. *Angew. Chem., Int. Ed.* **2001**, *40*, 1258-1260

(60) Zhang, Z. T.; Han, Y.; Xiao, F. S.; Qiu, S. L.; Zhu, L.; Wang, R. W.; Yu, Y.; Zhang, Z.; Zou, B. S.; Wang, Y. Q.; Sun, H. P.; Zhao, D. Y.; Wei, Y. *J. Am. Chem. Soc.* **2001**, *123*, 5014-5021.

(61) Liu, Y.; Pinnavaia, T. J. *Stud. Surf. Sci. Catal* **2002**, *142B*, 1075-1082.

(62) Wight, A. P.; Davis, M. E. *Chem. Rev.* **2002**, *102*, 3589-3613.

(63) Brunel, D. *Microporous Mesoporous Mater.* **1999**, *27*, 329-344.

(64) Brunel, D.; Fajula, F.; Nagy, J. B.; Deroide, B.; Verhoef, M. J.; Veum, L.; Peters, J. A.; van Bekkum, H. *Appl.Catal., A: Gen.* **2001**, *213*, 73-82.

(65) Harmer, M. A.; Sun, Q.; Michalczyk, M. J.; Yang, Z. *Chem.Commun* **1997**, 1803-1804.

(66) Harmer, M. A.; Farneth, W. E.; Sun, Q. *J. Am. Chem. Soc.* **1996**, *118*, 7708-7715.

(67) Kim, H.-C.; Volksen, W.; Miller, R. D.; Huang, E.; Yang, G.; Briber, R. M.; Shin, K.; Satija, S. K. *Chem. Mater.* **2003**, *15*, 609-611.

(68) Kim, H.-C.; Wilds, J. B.; Kreller, C. R.; Volksen, W.; Brock, P. J.; Lee, V. Y.; Magbitang, T.; Hedrick, J. L.; Hawker, C. J.; Miller, R. D. *Adv. Mater.* **2002**, *14*, 1637-1639.

(69) Kim, H.-C.; Wilds, J. B.; Hinsberg, W. D.; Johnson, L. R.; Volksen, W.; Magbitang, T.; Lee, V. Y.; Hedrick, J. L.; Hawker, C. J.; Miller, R. D.; Huang, E. *Chem. Mater.* **2002**, *14*, 4628-4632.

(70) Mercier, L.; Pinnavaia, T. J. *Environ. Sci. Technol.* **1998**, *32*, 2749-2754.

(71) Mercier, L.; Pinnavaia, T. J. *Adv. Mater.* **1997**, *9*, 500-&.

(72) Mercier, L.; Pinnavaia, T. J. *Chem. Mater.* **2000**, *12*, 188-196.

(73) Fryxell, G. E.; Liu, J.; Hauser, T. A.; Nie, Z. M.; Ferris, K. F.; Mattigod, S.; Gong, M. L.; Hallen, R. T. *Chem. Mater.* **1999**, *11*, 2148-2154.

(74) Feng, X.; Fryxell, G. E.; Wang, L. Q.; Kim, A. Y.; Liu, J.; Kemner, K. M. *Science* **1997**, *276*, 923-926.

(75) Chen, X. B.; Feng, X. D.; Liu, J.; Fryxell, G. E.; Gong, M. L. *Sep. Sci. Technol.* **1999**, *34*, 1121-1132.

(76) Chen, X.; Feng, X.; Liu, J.; Fryxell, G. E.; Gong, M. *Sep. Sci. Technol.* **1999**, *34*, 1121-1132.

(77) Mercier, L.; Pinnavaia, T. J. *Microporous Mesoporous Mater.* **1998**, *20*, 101-106.

(78) Mori, Y.; Pinnavaia, T. J. *Chem. Mater.* **2001**, *13*, 2173-2178.

(79) Inagaki, S.; Guan, S.; Ohsuna, T.; Terasaki, O. *Nature* **2002**, *416*, 304-307.

(80) Inagaki, S.; Koiwai, A.; Suzuki, N.; Fukushima, Y.; Kuroda, K. *Bull. Chem. Soc. Jpn.* **1996**, *69*, 1449-1457.

(81) Corma, A. *Chem. Rev.* **1997**, *97*, 2373-2419.

(82) Monnier, A.; Schuth, F.; Huo, Q.; Kumar, D.; Margolese, D.; Maxwell, R. S.; Stucky, G. D.; Krishnamurty, M.; Petroff, P.; et al. *Science* **1993**, *261*, 1299-1303.

(83) Antonelli, D. M.; Ying, J. Y. *Angew. Chem., Int. Ed.***1996**, *35*, 426-430.

(84) Lee, J.-S.; Joo, S. H.; Ryoo, R. *J. Am. Chem. Soc.* **2002**, *124*, 1156-1157.

(85) Joo, S. H.; Choi, S. J.; Oh, I.; Kwak, J.; Liu, Z.; Terasaki, O.; Ryoo, R. *Nature* **2001**, *412*, 169-172.

(86) Kruk, M.; Jaroniec, M.; Kim, T.-W.; Ryoo, R. *Chem. Mater.* **2003**, *15*, 2815-2823.

(87) Kaskel, S.; Farrusseng, D.; Schlichte, K. *Chem. Commun.* **2000**, 2481-2482.

(88) Kang, H.; Jun, Y.-w.; Park, J.-I.; Lee, K.-B.; Cheon, J. *Chem. Mater.* **2000**, *12*, 3530-3532.

(89) Trikalitis, P. N.; Rangan, K. K.; Kanatzidis, M. G. *J. Am. Chem. Soc.* **2002**, *124*, 2604-2613.

(90) Trikalitis, P. N.; Rangan, K. K.; Bakas, T.; Kanatzidis, M. G. *Nature*, *410*, 671-675.

(91) Pauly, T. R.; Pinnavaia, T. J. *Chem. Mater.* **2001**, *13*, 987-993.

(92) Pauly, T. R.; Liu, Y.; Pinnavaia, T. J.; Billinge, S. J. L.; Rieker, T. P. *J. Am. Chem. Soc.* **1999**, *121*, 8835-8842.

(93) Polverejan, M.; Pauly, T. R.; Pinnavaia, T. J. *Chem. Mater.* **2000**, *12*, 2698-2704.

(94) Polverejan, M.; Liu, Y.; Pinnavaia, T. J. *Stud. Surf. Sci. Catal.* **2000**, *129*, 401-408.

(95) Bossaert, W. D.; De Vos, D. E.; Van Rhijn, W. M.; Bullen, J.; Grobet, P. J.; Jacobs, P. A. *J. Catal.* **1999**, *182*, 156-164.

(96) Van Rhijn, W. M.; De Vos, D. E.; Sels, B. F.; Bossaert, W. D.; Jacobs, P. A. *Chem.Commun* **1998**, 317-318.

(97) Lettow, J. S.; Han, Y. J.; Schmidt-Winkel, P.; Yang, P.; Zhao, D.; Stucky, G. D.; Ying, J. Y. *Langmuir* **2000**, *16*, 8291-8295.

(98) Schmidt-Winkel, P.; Lukens, W. W., Jr.; Yang, P.; Margolese, D. I.; Lettow, J. S.; Ying, J. Y.; Stucky, G. D. *Chem. Mater.* **2000**, *12*, 686-696.

(99) Schmidt-Winkel, P.; Lukens, W. W., Jr.; Zhao, D.; Yang, P.; Chmelka, B. F.; Stucky, G. D. *Mater. Res. Soc. Symp. Proc.* **1999**, *576*, 241-246.

2.

ele

10

an

fra

nu

hie

the

hyc

der

are

2.

core

strip

com

hiera

rang

surfa

lamel

stripe

# CHAPTER 2

## Assembly of Mesostructures using Gemini Surfactants

### 2.1 Abstract

The hierarchical structures of mesostructured silicas assembled from electrically neutral Gemini surfactants of the type $C_nH_{2n+1}NH(CH_2)_mNH_2$ with n = 10, 12, 14 and m = 3, 4 are described. As expected for Gemini surfactants with an all *anti* chain configuration and a packing parameter near 1.0, lamellar framework walls are formed regardless of the length of the alkyl chain (n) and the number of carbon atoms (m) linking the amino group centers. But different hierarchical structures are observed depending on a delicate balance between the hydrophilic interactions at the surfactant head group - silica interface and the hydrophobic interactions between the surfactant alkyl groups. For Gemini derivatives with n = 12 or 14 and m = 3 or 4, hierarchical vesicles are formed that are analogous to those assembled previously from Gemini surfactants with m = 2. However, for n = 10, a new coiled slab structure (m = 3) and an onionlike core-shell structure (m = 4) are formed. In addition, a previously unobserved stripelike silica structure is obtained from a $C^o_{12+2+0}$ Gemini surfactant in combination with an α, ω-diamine co-surfactant. The relative stability of these hierarchical structures depends on the delicate competition between the long-range elastic forces occurring in the hydrophobic region of the assembled surfactant and the short range chemical forces in the hydrophilic moiety. As with lamellar silicas with hierarchical vesicle structures, the new coiled slab and stripelike phases promise to be chemically significant morphologies, because

they can minimize the framework pore length and provide optimal access to the framework walls under diffusion limiting conditions.

## 2.1. Introduction

### 2.1.1 Vesicular Morphologies

Among the various particle shapes that have been observed for mesostructured silica compositions formed through supramolecular assembly pathways,[1-7] those with sponge-like, tubular and vesicular hierarchical structures have special chemical significance. These latter morphologies are capable of minimizing the *length* of the pores embedded in a mesostructured framework, provided that the pore network is three-dimensional, thereby facilitating access to the internal surface area of the mesostructure. This improvement in framework access is realized without the need for reducing the particle size to intractable colloidal dimensions, because the sponge-like, tubular, and vesicle shapes allow for particle dimensions that are suitable for facile processing and recovery through filtration without compromising rapid diffusion.[8-10] Thus, sponge-like, tubular and vesicular particle shapes are preferred to more monolithic particle geometries, particularly in applications such as condensed phase chemical catalysis, adsorption, and sensing where it is desirable to minimize diffusion in order to achieve optimal performance.

Mesoporous metal oxide molecular sieves with vesicle-like morphologies are of interest as potential catalysts and sorbents in part because the mesostructured shells and intrinsic textural pores of the vesicles should efficiently transport guest species to framework binding sites. However most of the vesicle morphologies reported prior to Kim et al[10] had shells of undesirable thickness. More important, like many molecular sieves with conventional particle

morphologies, the framework structures defining the vesicle shells were lacking in structural stability. A vesicular aluminophosphate with mesoscale d spacing and surface patterns that mimicked radiolarian skeletons collapsed with a complete loss of hierarchical patterns at 300 °C.

Vesicle hierarchical structures are distinguished from hollow sphere structures on the basis of the shell thickness. Ideally, vesicle structures that are well suited for limiting pore length have shells made of a single layer or, at most, a few lamellae. The total thickness of the shell is ~2-10 nanometers with some mesopores oriented orthogonal to the lamellae, so that the minimum framework pore length is approximately the thickness of the shell. Hollow sphere and tubular structures[6,11 12-15], with few exceptions,[16-18]have much thicker walls in the sub-micrometer to micrometer range.

### 2.2.2 MSU-G mesotructures

The first examples of lamellar silicas with predominantly single wall and multi-wall vesicle structures, denoted MSU-G silicas, were formed through an electrically neutral $S^oI^o$ assembly pathway, where $I^o$ was a silicon alkoxide precursor and $S^o$ was a structure-directing Gemini surfactant of the type $C_nH_{2n+1}NH(CH_2)_2NH_2$.[10] Quaternary ammonium ion forms of Gemini surfactants also are capable of assembling mesostructures through electrostatic charge matching pathways, but under these conditions monolithic hierarchical structures are obtained.[19 20]

α, ω-Diamine surfactants have been shown to afford vesicular particles,[21] although the vesicle walls in this case were always multi-lamellar and,

consequently, much thicker (~100 nm) in comparison to vesicular mesostructures formed from $C^{o}_{n+2+0}$ Gemini surfactants.

More recently, vesicular hierarchical structures have been observed through electrostatic assembly pathways using alkyl ammonium ion surfactants as the structure director, but in these cases it was necessary to use high intensity ultrasound[22, 23] or co-surfactants[24] to promote vesicle formation. Although these latter methods offer some processing advantages, the vesicular morphology was accompanied by the formation of a large fraction of other particle morphologies with chemically less significant shapes.

Very recently, vesicular structures with 12-nm thick walls, 4 nm wormhole framework mesopores, and uniform spherical diameters of ~ 1000 nm have been assembled from a non-ionic triblock surfactant and co-surfactant emulsion.[25] Thus, only electrically neutral Gemini surfactants and one specific emulsion composition are known to afford high yields of truly vesicular hierarchical structures with very thin walls on the order of 10 nm or less.

### 2.2.3 Gemini Surfactants

Gemini amine surfactants are represented by a family of versatile compositions of the general type $C_nH_{2n+1}NH(CH_2)_mNHC_kH_{2k+1}$. The surfactants can be in neutral form, as written, or, alternatively in mono- or di-cationic form if one or both nitrogen centers are protonated or in quaternary form. The surfactant compositions can be distinguished according to the number of carbon atoms linked to the amino groups through the use of the notation $C^{o}_{n+m+k}$,[18] where the superscript indicates the surfactant in electrically neutral form. In the present

work we examined the hierarchical properties of related MSU-G lamellar silicas assembled using $C^{o}_{n+m+0}$ Gemini surfactant derivatives with m = 3, 4 and n = 10, 12, 14. Increasing the number of carbon atoms separating the amino groups from m = 2 to m = 3 and 4 also leads to the assembly of hierarchical vesicles, at least when n = 12 and 14. However, for n = 10, a new coiled slab hierarchical structure (m = 3) and an onionlike core-shell structure (m = 4) are formed. In addition, a previously unobserved stripelike silica structure is obtained from a $C^{o}_{12+2+0}$ Gemini surfactant in combination with an α, ω-diamine co-surfactant. As with silicas with hierarchical vesicle structures, the new coiled slab and stripelike phases promise to be chemically significant, because these unique hierarchical forms also limit the lengths of the framework pores.

## 2.3. Experimental Section

**Materials.** The source of silicon was tetraethyl orthosilicate (TEOS) obtained from Aldrich. The Gemini surfactants $C_nH_{2n+1}NHC_mH_{2m}NH_2$, where n=10, 12, 14 and m=3, 4) were synthesized as described in literature[26,27] using ethylenediamine, 1,3-diaminopropane, 1,4-diaminobutane, 1-bromodecane, 1-bromododecane, 1- bromotetradecane, supplied by Aldrich. Absolute ethanol and deionized water were used as solvents for mesoporous molecular sieve synthesis.

### 2.3.1 Synthesis of surfactant

The condensation of diamine and alkyl halide may be effected by refluxing the mixture of the two components or in a solvent such as ethyl alcohol or n-butanol. A large excess of ethylenediamine is used in order to avoid the formation of other than the monoalkyl derivatives. The typical procedure followed for *N*-n-dodecylethylenediamine is as follows. 0.08 mole (9.55 g) of ethylenediamine and 0.02 (4.7 g) mole of n-dodecyl chloride was added to sufficient absolute ethyl alcohol (10 cc.) to dissolve the two immiscible liquids. The solution was refluxed for 3 h in an oil-bath and ethyl alcohol was evaporated, causing the residual liquid to separate into two layers. The upper layer was separated, 30 cc. of water was added, and the precipitated white solid was extracted with ether. The ether extract was dried over anhydrous sodium sulfate, and the solvent was evaporated, which yielded 3 g of product. In order to remove the last traces of unchanged ethylenediamine, the crude product was suspended in 20 cc. of water and the ether extraction was repeated. Analogous reactions

were carried out with 1-3 diaminopropane and 1-4 diaminobutane with decyl chloride, dodecyl chloride, and tetradecyl chloride to obtain the respective monoalkylated diamines.

**Reaction 2.1** Reaction of 1-chlorododecane with ethylene diamine

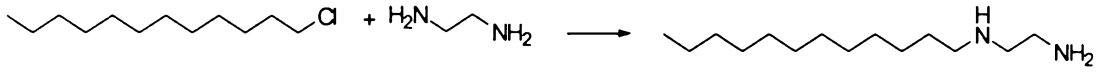


1-Chlorododecane Ethylenediamine N n-dodecyl ethylenediamine

### 2.3.2 Mesostructure Synthesis

**Pure surfactant mesostructure assembly**

The desired Gemini surfactant, prepared and purified according to literature procedures,[26] was stirred in water to obtain a milky white solution. Tetraethyl orthosilicate (TEOS) in ethanol was added gradually at room temperature to form a reaction mixture of the following molar composition:

$$1.0\text{TEOS}: 0.25\ C_nH_{2n+1}NH(CH_2)_mNH_2: 77.7\ H_2O: 3.5\ \text{EtOH}$$

The reaction mixture was allowed to stand for 20 minutes and then stirred for 20 minutes before subjecting it to hydrothermal conditions in a Teflon lined autoclave at 100 $^0$C for 48 h. Subsequently, the material obtained was filtered, washed thoroughly with water than ethanol, and air-dried at room temperature. The surfactant was removed by calcination at 620 $^o$C for 4 h in air.

**Co-surfactant assisted mesostructure assembly**

For the synthesis of the stripelike phases, mixtures of the $C^{o}_{12+2+0}$ Gemini surfactant and the Jeffamine D-400 co-surfactant were stirred in water to obtain a milky white solution. Tetraethylorthosilicate (TEOS) in ethanol was added gradually at room temperature to form a reaction mixture of the following molar composition.

1.0 TEOS: (0.25-x) $C_nH_{2n+1}NHC_mH_{2m}NH_2$: x Jeffamine D-400: 77.7 $H_2O$: 3.5 EtOH

The reaction mixture was allowed to stand for 20 min. and stirred for 20 min. before subjecting it to hydrothermal conditions in a Teflon lined autoclave at 100 $^0$C for 48 h. The product was filtered, washed thoroughly with water than ethanol, and air-dried at room temperature. The surfactant was removed by calcination at 620 $^0$C for 4 h in air.

**2.3.3 Characterization**

The physical properties of MSU-G mesoporous silicas where determined using X-ray diffraction (XRD), nitrogen adsorptometry and transmission electron microscopy (TEM). Powder x-ray diffraction patterns measured on a Rigaku Rotaflex Diffractometer equipped with a rotating anode using Cu K$\alpha$ radiation ($\lambda$ = 0.154 nm). Scan conditions are reflective mode from 1° to 20°- 2$\theta$ continuous at 2° /min and data collection every 0.05 ° 2$\theta$. $N_2$ adsorption-desorption data were obtained at —196 °C on a Micromeritics ASAP 2010. Samples were out

gassed at 150 °C and $10^{-6}$ Torr for a minimum of 6 h prior to analysis. TEM images were obtained on a JEOL 100CX microscope with a $CeB_6$ filament and an accelerating voltage of 120 KV. Samples were prepared either by dusting onto a carbon coated holey film supported on a 300 mesh Cu grid, or by sonicating the powdered sample for 20 minutes in EtOH, then evaporating 2 drops onto the carbon coated holey film.

## 2.4. Results

### 2.4.1 Vesicular, coiled slab and onion-like structures

Figure 2.1 A provides TEM images of the hierarchical silica structures assembled from $C^{o}_{n+m+0}$ Gemini surfactants containing 10 carbon atoms in the hydrophobic group (n = 10) and the spacer groups separating the amino centers in the hydrophilic moiety with carbon atom numbers of m = 3. Figure 2.1 B shows a higher magnification image of 2.1 Å. The 50–100 nm particles assembled from the $C^{o}_{10+3+0}$ Gemini surfactant are unique, consisting of 2-4 concentrically coiled silica slabs with a thickness of 8-10 nm. Figure 2.1 C and D are representative TEM images for the truly vesicular, very thin-walled hollow spheroid structures obtained from Gemini surfactants with the same carbon chain spacers in the hydrophilic group (m = 3), but with a hydrophobic group that has been increased by two carbon atoms to n = 12. Equivalent silica vesicles were obtained upon increasing the hydrophobic group length still further to n = 14, while keeping the length of the hydrophilic spacer at m = 3.

Figure 2.2 shows TEM images obtained from $C^{o}_{n+m+0}$, where m=4 and n=10 or 12. As shown in Figure 2.2A, the particles made from $C^{o}_{10+4+0}$ have a multifold core-shell or onionlike structure made of cross-linked silica shells ~2-3 nm thick. The cross-linking of the concentric shells by silica pillars generates mesopores between the lamellae. Figure 2.2B shows a higher resolution image of 2.2A where the onion-like morphology is clearly evident. Figure 2.2 C and D are representative TEM images for the very thin-walled hollow vesicular

**Figure 2.1** Transmission electron micrographs of calcined mesostructured silicas assembled obtained from $C^{o}_{m+3+0}$ Gemini surfactants. (A) Low magnification predominantly coiled slab structures obtained from $C^{o}_{10+3+0}$. (B) High magnification image of A. (C) and (D) typical vesicular morphologies obtained from $C^{o}_{12+3+0}$ showing thin undulated silica sheets with framework pores orthogonal creating a 3-D pore network

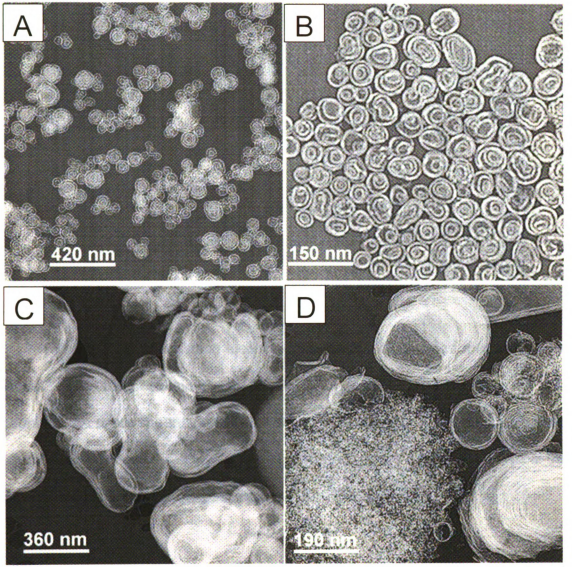
A
420 nm
B
150 nm
C
360 nm
D
190 nm

**Figure 2.2** Transmission electron micrographs of calcined mesostructured silicas assembled obtained from $C^{o}_{m+4+0}$ Gemini surfactants. (A) Low magnification predominantly onion-like structures obtained from $C^{o}_{10+4+0}$. (B) High magnification image of A showing the cross-linked pillars. (C) and (D) typical thin spheroid vesicular morphologies obtained from $C^{o}_{12+4+0}$

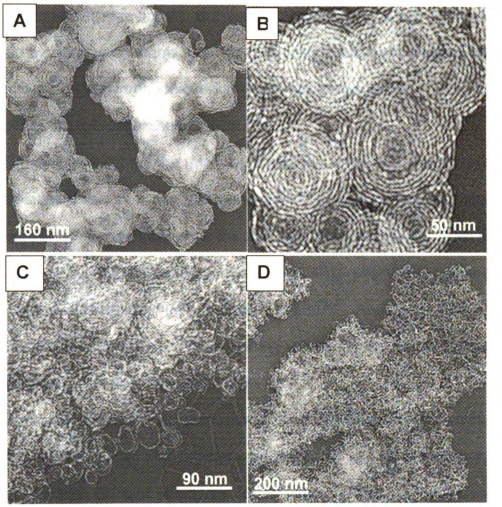
A
160 nm
B
50 nm
C
90 nm
D
200 nm

structures obtained from Gemini surfactants with the same carbon chain spacers in the hydrophilic group (m=4), but with a hydrophobic group that has been increased by two carbon atoms to n=12. Equivalent silica vesicles were obtained upon increasing the hydrophobic group length still further to n=14, while keeping the length of the hydrophilic spacer at m = 4.

Figure 2.3 illustrates the relatively broad low angle XRD reflection for the as-synthesized coiled structure assembled from $C^{o}_{10+3+0}$ in comparison, which the much narrower reflections found for the as-made vesicles obtained from $C^{o}_{12+3+0}$ and $C^{o}_{14+3+0}$. For each mesostructure, the single XRD reflection is retained upon removal of the surfactant through calcination at 620 °C. Analogous XRD patterns were obtained for the $C^{o}_{n+4+0}$. The d-spacing values for the as-synthesized and calcined samples are summarized in Table 2.1.

Representative $N_2$ adsorption – desorption isotherms are shown in Figure 2.4 for the calcined coiled slab structure made from $C^{o}_{10+3+0}$ in comparison to the isotherms for the vesicular structures obtained from $C^{o}_{12+3+0}$ and $C^{o}_{14+3+0}$. The well-expressed adsorption steps at partial pressures between 0.2 and 0.5 signal the presence of uniform framework mesopores for each mesostructure. In addition, all three mesostructures exhibit hysteresis loops above a partial pressure of 0.5, indicating the existence of complimentary inter- or intra-particle textural mesoporosity with a pore size distribution that is much larger and broader than the size distribution of the framework mesopores. Correspondingly Figure 2.5 shows nitrogen isotherms obtained from $C^{o}_{n+4+0}$.

## Table 2.1. Structural Parameters and Textural Properties of Hierarchical Silica Mesostructure Derived from $C^{o}_{n+m+o}$ Gemini Surfactants.

| Surfactant | Primary Hierarchical Structure | XRD Basal Spacing (nm) | | Framework Pore Size (nm) | BET Surface Area ($m^2/g$) | Pore Vol. ($cm^3/g$) |
|---|---|---|---|---|---|---|
| | | As-made | Calcined | | | |
| $C^{o}_{10+3+0}$ | Concentric Coiled Slabs | 4.0 | 3.9 | 3.0 | 631 | 0.82 |
| $C^{o}_{10+4+0}$ | Onionlike | 4.4 | 4.3 | 3.2 | 594 | 0.65 |
| $C^{o}_{12+3+0}$ | Vesicle | 5.7 | 5.4 | 3.8 | 458 | 0.55 |
| $C^{o}_{12+4+0}$ | Vesicle | 6.8 | 5.4 | 3.6 | 557 | 1.06 |
| $C^{o}_{14+3+0}$ | Vesicle | 5.8 | 5.2 | 3.8 | 463 | 0.61 |
| $C^{o}_{14+4+0}$ | Vesicle | 6.9 | 5.6 | 4.6 | 557 | 1.12 |

[a]Products assembled at 100 °C from TEOS at a silicon/surfactant molar ratio of 4.0. [b]Calcination temperature, 620 °C. [c]Pore sizes are based on the Horvath-Kawazoe model. [d]Total mesopore volume determined from the nitrogen adsorption isotherm at $P/P^{o}$ = 0.97

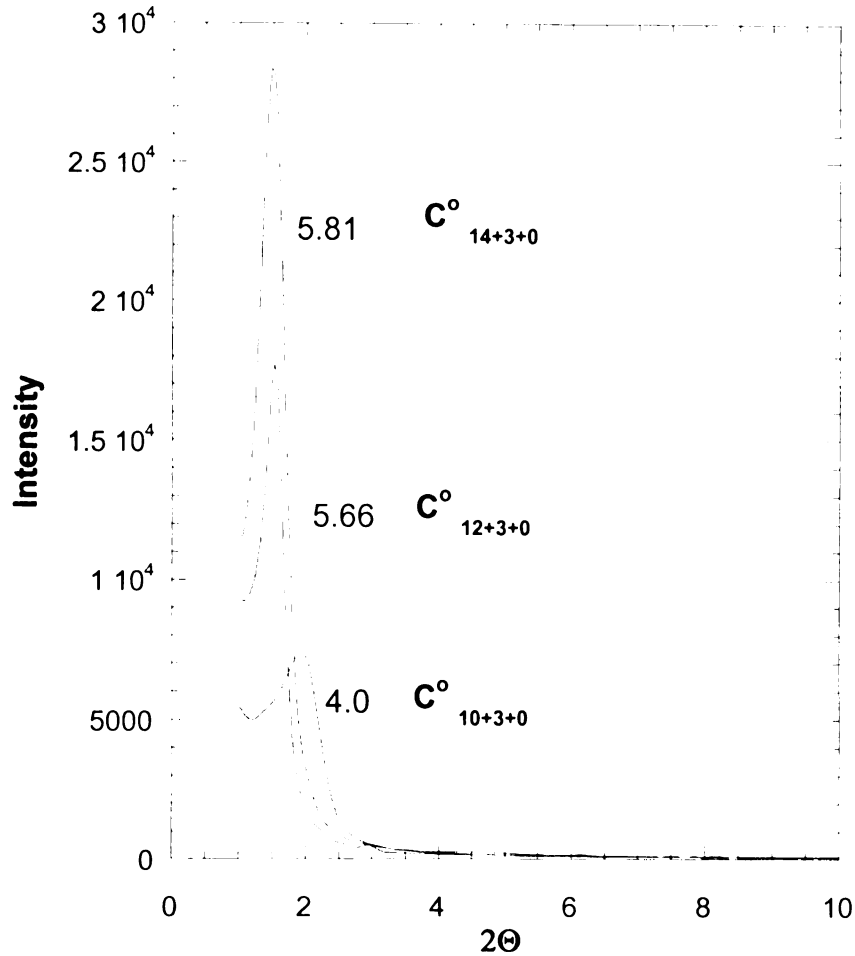


**Figure 2.3** Low angle X-ray diffraction patterns for the as-synthesized silica mesostructures assembled from $C^{o}_{m+n+0}$ Gemini surfactants. The mesostructure made from $C^{o}_{10+3+0}$ has a unique coiled slab structure, whereas those made form $C^{o}_{12+3+0}$ and $C^{o}_{14+3+0}$ are vesicular. The reported values are the d-spacings in nm.

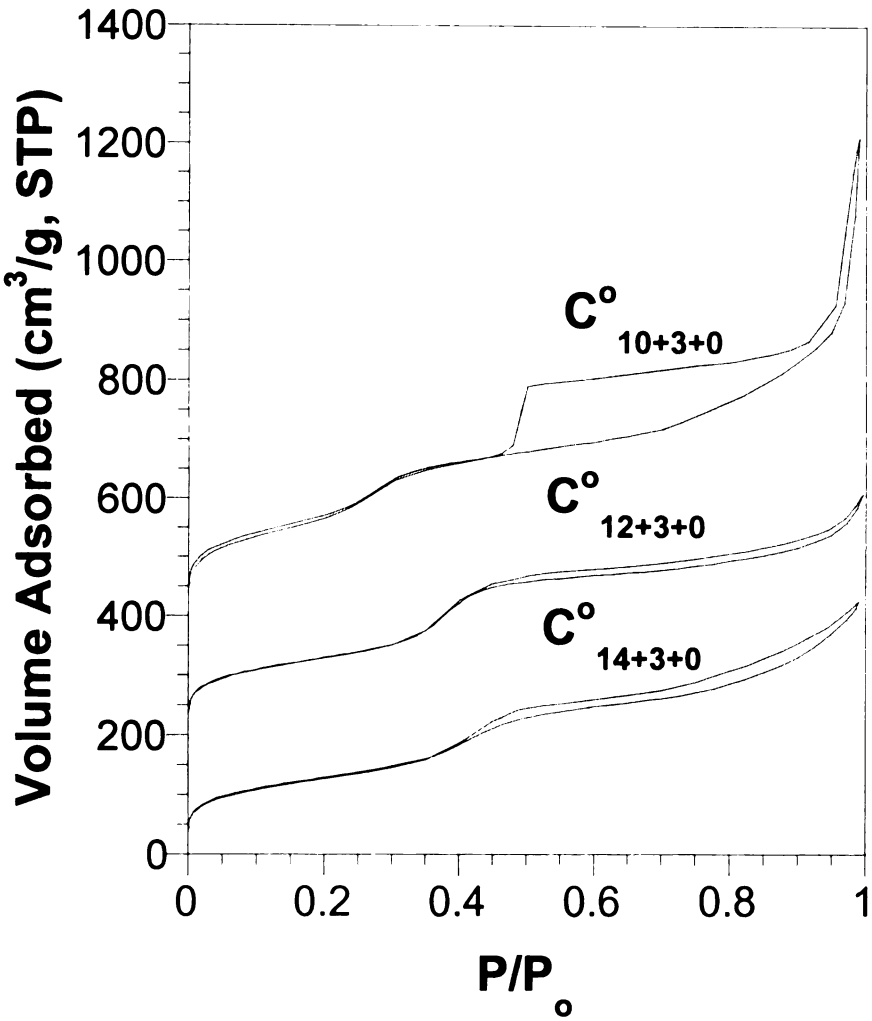


**Figure 2.4** Nitrogen adsorption - desorption isotherms for silica mesostructures assembled from $C^{o}_{n+3+0}$ and calcined at 620 °C for 4 h. The isotherms are offset by a value of 200 for clarity

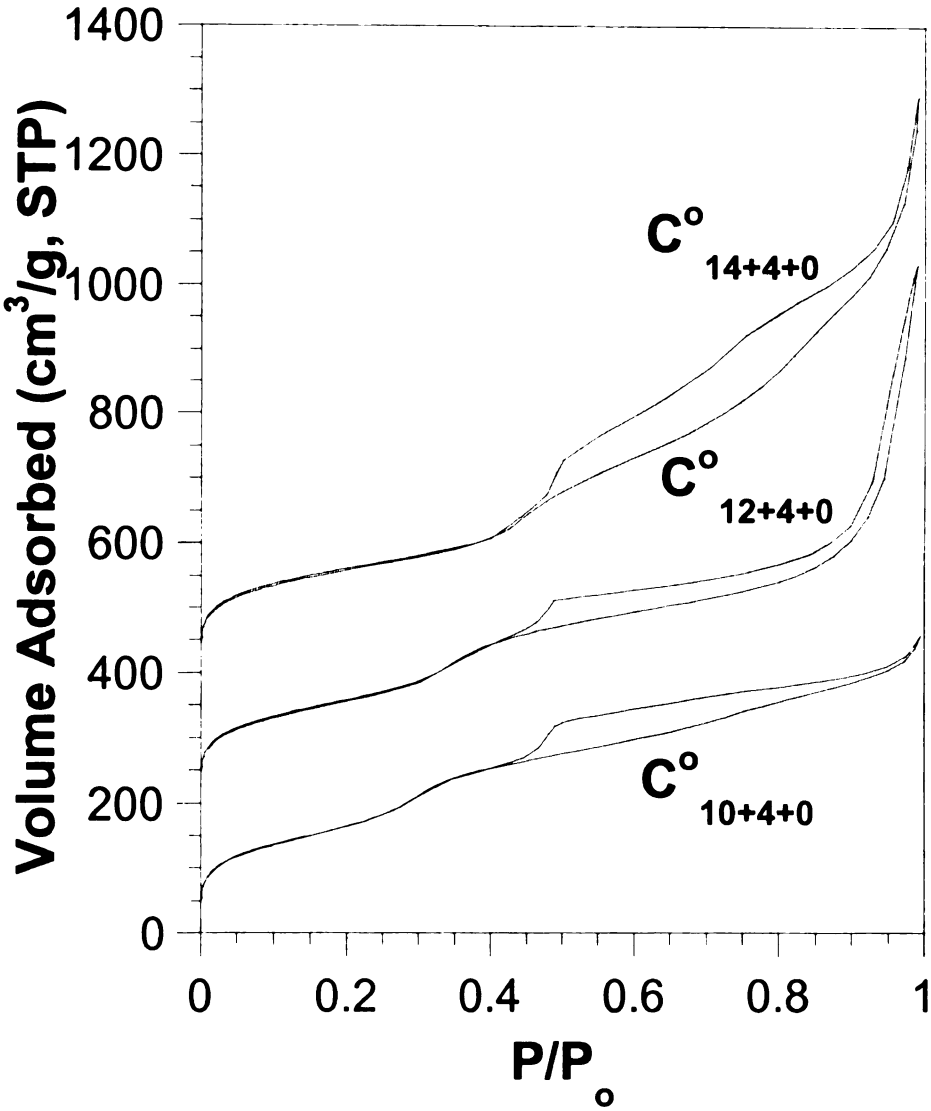


**Figure 2.5** Nitrogen adsorption - desorption isotherms for silica mesostructures assembled from $C^{o}_{n+4+0}$ and calcined at 620 °C for 4 h. The isotherms are offset by a value of 200 for clarity.

Table 2.1 summarizes the hierarchical particle morphologies, basal spacings, surface areas, pore sizes and total pore volumes for the all of the lamellar silicas assembled from the $C_nH_{2n+1}NHC_mH_{2m}NH_2$ Gemini surfactants with n = 10, 12, 14 and m = 3, 4. Regardless of the hierarchical structure type, the framework pore sizes, BET surface areas and total pore volumes are in the approximate ranges 3.0 – 4.6 nm, 460 – 630 $m^2/g$, and 0.55 – 1.1 $cm^3/g$, respectively.

**2.4.2 Co-surfactant assisted formation of stripe-like phase**

In an effort to reduce the amount of Gemini surfactant needed to assemble silica vesicles, we attempted to replace a fraction of a vesicle–directing Gemini with an α,ω-diamine co-surfactant that is approximately the length of a lipid bilayer assembled from the Gemini surfactant. The Gemini surfactant selected was a $C^{o}_{12\ +2\ +\ 0}$ derivative and the co-surfactant was a commercially available Jeffamine D-400 polypropylene oxide diamine of the type $H_2NCH(CH_3)CH_2$-$[OCH_2CH(CH_3)]_x$-$NH_2$, where x ~ 5.5. Indeed, it was possible to replace up to 30 mol% of the Gemini with the co-surfactant with the retention of a vesicular hierarchical structure at an overall silicon to surfactant + co-surfactant ratio of 4:1.

However, for Gemini: D-400 molar ratios between 60:40 and 30:70, an entirely new hierarchical structure dominated. As illustrated by the TEM images in Figure 2.6 (A-E) the new silica structure is comprised of folded silica slabs cross-linked by silica pillars to form framework mesopores. Figure 2.6 Aand B

**Figure 2 .6** Transmission electron micrograph images at (A) low and (B) high magnification for the stripelike mesostructured silica assembled from $C^{o}_{12+2+0}$ and Jeffamine D-400 as a co-surfactant. (C), (D), (E) and (F) are TEM images obtained by tilting the sample stage gradually from $0^{o}$-$60^{o}$

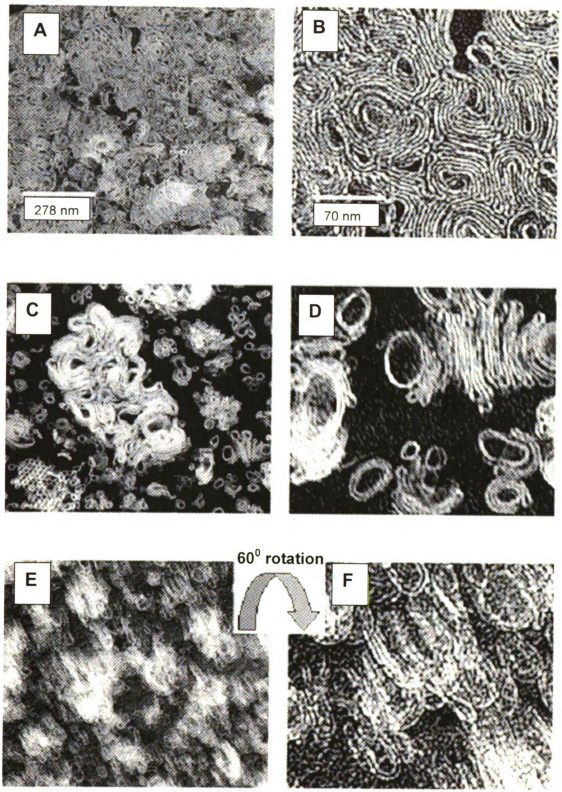
A
278 nm
B
70 nm
C
D
60⁰ rotation
E
F

show low magnification TEM images of the folder lamellar structure. Figures 2.6 C-E show TEM images of the same sample obtained by tilting the sample stage of the TEM instrument. This folded lamellar structure resembles the stripe phases that are often formed through the nanoscale segregation of diblock co-polymers. [28,29] Figure 2.7 shows a digitally magnified TEM image of Figure 2.6 B showing the surface features.

Table 2.2 provides the basal spacings, surface areas, and framework pore sizes for the vesicle and stripe-like hierarchical silica structures assembled from $C^{o}_{12+2+0}$ Gemini surfactant and Jeffamine D-400 co-surfactant mixtures. The stripe-like mesostructures afford framework pore sizes on the order of 2.7–3.4 nm and surface areas of 420–490 $cm^3/g$ that are comparable to those of vesicular mesostructures.

## Table 2.2. Hierarchical Silica Mesostructures Assembled from $C^{o}_{12+2+0}$ Gemini Surfactant and Jeffamine D-400 Co-Surfactant.[a]

| *$C^{o}_{12+2+0}$/D400* (mol/mol) | *Hierarchical Structure* | d *spacing* (nm) | Pore diameter (nm) | Surface area ($m^2/g$) |
|---|---|---|---|---|
| 100/0 | Vesicles | 5.66 | 3.2 | 412 |
| 80/20 | Vesicles | 5.52 | 3.3 | 436 |
| 70/30 | Vesicles | 5.66 | 3.3 | 442 |
| 60/40 | Stripelike | 5.66 | 3.4 | 480 |
| 50/50 | Stripelike | 5.02 | 3.1 | 490 |
| 40/60 | Stripelike | 5.02 | 3.2 | 433 |
| 30/70 | Stripelike | 5.02 | 2.7 | 422 |

[a] Assembled from TEOS as the silica source at 100 °C for 48 h in $H_2O$: ethanol = 9:1(v/v). Overall molar ratio of Si to surfactant and co-surfactant was 4:1.
[b] Pore sizes are based on the Horvath-Kawazoe model.

**Figure 2.7** Digitally magnified transmission electron micrograph of figure 2.7 (B) for clarity

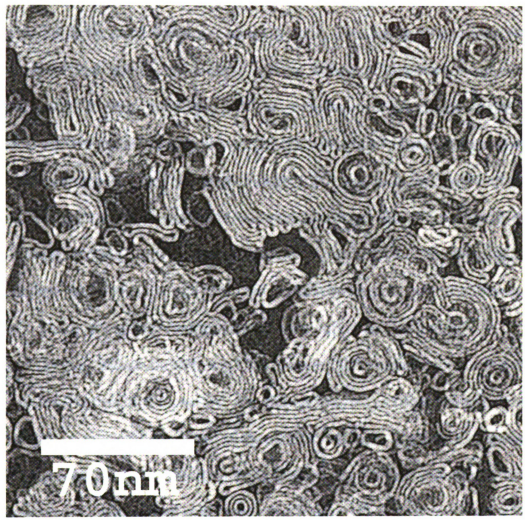
70nm

## 2.5. Discussion

The coiled slab, onion-like, vesicle, and stripe-like hierarchical forms of silica assembled from structure-directing $C^{o}_{n+m+0}$ Gemini surfactants are all derived from a lamellar framework structure. As with lamellar silicas with hierarchical vesicle structures, the new coiled slab and stripe-like phases promise to be chemically significant morphologies, because they can minimize the framework pore length and provide optimal access to the framework walls under diffusion limiting conditions. The lamellar framework geometry is consistent with well-packed Gemini surfactant molecules in an all *anti*-chain configuration and a packing parameter near 1.0[30] that is independent of the length of the alkyl chain (n) and the number of carbon atoms (m) linking the amino group centers. The global curvature leading to the hierarchical morphologies, however, depends on subtle differences in hydrophobic and hydrophilic interactions that are dependent on the values of n and m.

For Gemini derivatives with n = 10, increasing the separation between the amino centers from m = 3 to m = 4, transforms the hierarchical structure from coiled slabs to a multifold core-shell or onion-like structure. The layer curvature for both structures is similar, resulting in particles of similar size (50-100 nm) but of different layer thickness and degree of silica pillar cross-linking (c.f. Figure 2.1 B and 2.2 B). The coiled slab structure formed from $C^{o}_{10+3+0}$ is unique among mesostructured silicas, being formed through the concentric coiling of comparatively few (2-4), but thick (~8-10 nm), lamellae and relatively little cross linking silica between the lamellae. The related onion-like structure assembled

from $C^{o}_{10+4+0}$ exhibits more extensive cross-linking of many more (>4) and much thinner (2-3 nm) lamellae. Related multifold core-shell or onion-like forms of silica, as well as carbon, have been observed previously.[31-34]

Increasing the length of the hydrophobic tail of the Gemini surfactant from n = 10 to n = 12 or 14, results primarily in silica vesicles for both m = 3 and m = 4 (c.f. Figure 2.1 B and 2.2 B). This latter result is consisted with the previous report[10] of vesicle formation for silicas assembled from Gemini surfactants with m=2 and n=12, 14. This earlier study also revealed that the vesicles contained framework mesopores that were orthogonal to the lamellae, as well as between the lamellae in the case of multi-lamellar vesicles. Owing to the orthogonal pore structure, even single-walled vesicles are mesoporous. Figure 2.8 A shows the schematic representation of a surfactant $L_{\alpha}$-$L_3$ phase transition showing an intermediate in which adjacent bi-layers are connected through and elementary passage. The occurrence of both orthogonal and interlayer mesopores was attributable to a framework structure that is intermediate between a $L_3$ lamellar phase and a bicontinuous $L_{\alpha}$ phase.[35,36] Analogous orthogonal framework pores are expected for the vesicles formed in the present work. Figure 2.8 B shows the pathway used for the preparation of mesostructured MSU-G silicas, which involves the initial formation of a lipid-bilayer $L_{\alpha}$ phase followed by transformation of the intermediate phase accompanied by the condensation and hydrolysis of tetraethylorthosilicate species in presence of water.

Replacing up to 30 mol% of a $C^{o}_{12+2+0}$ Gemini surfactant with an α,ω–diamine Jeffamine D-400 co-surfactant of the type $H_2NCH(CH_3)CH_2$-

$[OCH_2CH(CH_3)]_x$-$NH_2$, where x ~ 5.5 does not compromise the formation of vesicle hierarchical structures, as we anticipated on the basis of size matching between the expected diameter of the surfactant micelle and the length of the co-surfactant. The synthesis and purification of Gemini surfactants through the alkylation of ethylene diamine is very process intensive. Being able to substitute a substantial fraction of the Gemini surfactant with a commercially available co-surfactant such as Jeffamine D-400 allows one to extend the yields and thereby lower the cost of producing vesicular silica mesostructures.

At $C^o_{12+2+0}$:co-surfactant molar ratios 60:40 to 30:70 highly undulated layers are formed that segregate into microdomains resembling the domains found in the stripe phases of certain block co-polymers.[28,29] The domain structure of these novel stripelike silicas results from the abrupt and severe folding of the lamellae onto themselves, as shown in the TEM image for the stripelike phase in Figure 2.7. An increase in the co-surfactant content to surfactant:co-surfactant molar ratio to a value of 20:80 and beyond resulted exclusively in the assembly of wormhole framework structures.

The new coiled slab and stripe-like hierarchical structures made from Gemini surfactants are well suited for minimizing the lengths of pores orthogonal to the lamellae and thereby facilitating access to the framework walls of these structures. The presence of orthogonal pores for the coiled slab structure is clearly indicated by the pore size determined by nitrogen adsorption. The observed pore size (~4.0 nm) is much smaller than the free space between the slabs (> 8 nm), as judged by TEM (c.f. Figure 2.1 B and 2.2 B). However, the

observed XRD spacing for the coiled slab structure (3.9 nm) is compatible with the correlation distance expected for orthogonal framework pores separated by walls approximately 1.0 nm thick. Analogous orthogonal pores are also likely for the stripe-like hierarchical structures.

A comparison of the textural properties reported in Tables 1 and 2 shows that the coiled slab and stripe-like structures have surface areas and average framework pore sizes comparable to those observed for Gemini – directed lamellar mesostructures with vesicle shapes. Thus, the coiled slab and stripe-like phases, like vesicle structures, are expected to be chemically significant shapes that limit the framework pore length and thereby optimize access to the framework walls under diffusion controlled conditions.

It is clear that the various hierarchical structures observed in the present work are distinguished by surface curvature that is dependent on a delicate balance between the hydrophilic interactions at the surfactant head group silicic acid interface and the hydrophobic interactions between the surfactant alkyl groups. The hydrophilic interactions involve hydrogen bond formation between the Si-OH moieties and the amino groups at the head group of the surfactant, whereas the hydrophobic interactions involve van der Waals interactions between the alkyl chains. Consequently, the balance been the hydrophilic and hydrophobic interactions for an assembly process involving $C^{o}_{n+m+0}$ Gemini surfactants micelles will depend on the number of carbon atoms (n) in the hydrocarbon tail and the number of carbon atoms (m) that separate the amino centers of the surfactant.

The local and global character of the structure directing hydrophobic and hydrophilic interface are characterized by the mean curvature *H* and Gaussian curvature *K*. [37] These latter parameters are related to the radii of the two principal curvatures $R_1$, $R_2$ by $H = 1/R_1 + 1/R_2$ (I) and $K = 1/R_1 * 1/R_2$. (II) These two curvatures, which can vary from point to point on a surface, are related to the shape of a surfactant through the surfactant packing parameter p, the relationship being $p = 1 + Hl + K l^2/3$ (III), where *l* is the characteristic length of the surfactant chain. Thus, for a given p one can have different morphologies of the interface determined by different compatible values of *H* and *K*. The global geometry, however, is determined not only by p, but also by c, the volume fraction of the hydrophobic region, which is determined by the value of n in $C^o_{n+m+0}$ Gemini surfactants. Figure 2.9 A and B schematically correlates the significance between the packing parameter (p) and the mean curvature *H* and Gaussian curvature *K*, where figure 2.9 A depicts the packing parameter and Figure 2.9 B along with equations (I and II) define the mean curvature *H* and Gaussian curvature *K*. Equation (III) gives the relationship between the terms.

It has been shown[38] for a single interface in the (c, p) plane that for p near 1, which is appropriate for our systems, lamellar mesophases form for small values of c. For larger c values, hyperbolical geometries are formed. In many cases, the aggregate morphology can be visualized as a collection of lamellar structures containing disclinations in the form of catenoidal tunnels. This makes the average Gaussian curvature <*K*> nonzero, but small, consistent with the fact that p is nearly 1. In this case one can also have a coiled slab, onion-like, or

vesicle morphology with a large radius of curvature (small magnitude of *K*). The relative stability of these hierarchical structures depends on the delicate competition between the long-range elastic forces occurring in the hydrophobic region of the assembled surfactant and the short range chemical forces in the hydrophilic moiety. For $C^{o}_{n+m+0}$ Gemini surfactants these respective forces are constrained by the magnitudes of m and n.

It is possible to understand the appearance of the stripe-like mesophase obtained from a mixture of α,ω–diamine co-surfactant and the Gemini surfactant. The addition of the co-surfactant effectively changes the values of p and c, thereby moving along a particular trajectory in the (c,p) phase diagram.[36] Taking the number of carbon atoms belonging to the hydrophobic α,ω–diamine chain to be about a factor of 2 larger than the 12 carbon atom chain of the $C^{0}_{12+2+0}$ Gemini surfactant, we anticipate the hydrophobic volume fraction to increase by about 50% without drastically changing p. This could lead to the formation of stripe-like phases resulting from a coalescence of spherical onion-like structures.

**A**

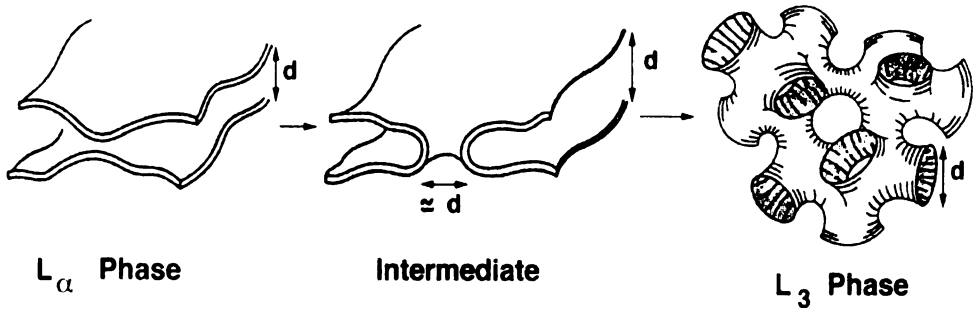


**B**

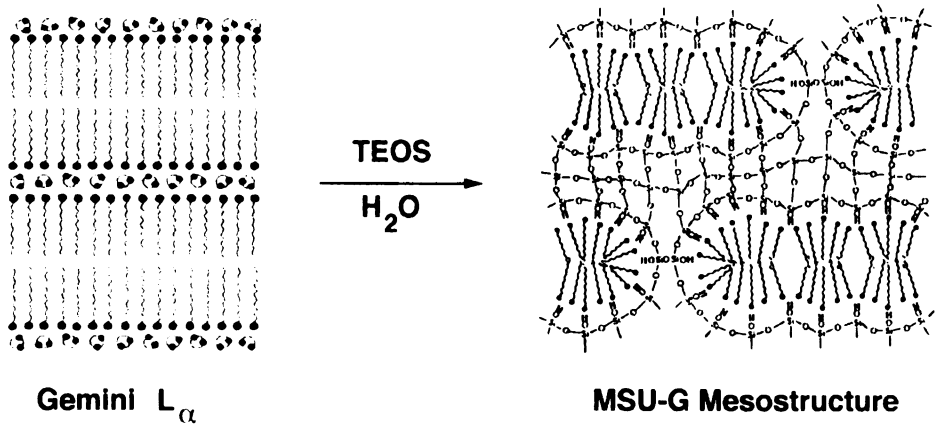


**Figure 2.8 A** shows the schematic representation of a surfactant $L_\alpha$-$L_3$ phase transition showing an intermediate in which adjacent bi-layers are connected through and elementary passage.

**Figure 2.8 B** shows pathway used for the preparation of mesostructured MSU-G silicas, which involves the initial formation of a lipid-bilayer $L_\alpha$ phase followed by transformation to the intermediate phase accompanied by the condensation and hydrolysis of tetraethylorthosilicate species in presence of water.

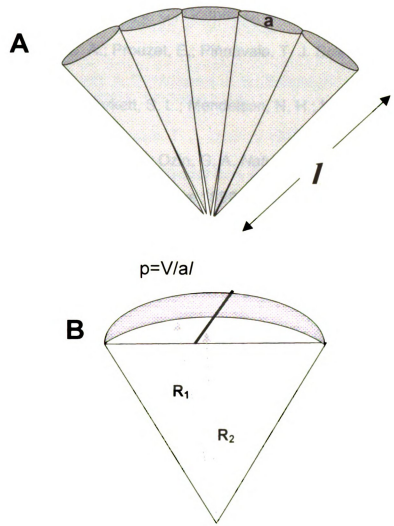


**Figure 2.9 (A and B)** schematically correlate the significance between the packing parameter (p) and the mean curvature *H* and Gaussian curvature *K*, where figure 2.9 A depicts the packing parameter and figure 2.9 B along with equations (I and II) define the mean curvature *H* and Gaussian curvature *K*. Equation (III) gives the relationship between the terms.

## 2.6 References:


(1) Attard, G. S.; Glyde, J. C.; Goltner, C. G. *Nature* **1995**, *378*, 366-368.

(2) Bagshaw, S. A.; Prouzet, E.; Pinnavaia, T. J. *Science* **1995**, *269*, 1242-1244.

(3) Davis, S. A.; Burkett, S. L.; Mendelson, N. H.; Mann, S. *Nature* **1997**, *385*, 420-423.

(4) Yang, H.; Coombs, N.; Ozin, G. A. *Nature* **1997**, *386*, 692-695.

(5) Mann, S.; Ozin, G. A. *Nature* **1996**, *382*, 313-318.

(6) Schacht, S.; Huo, Q.; VoigtMartin, I. G.; Stucky, G. D.; Schuth, F. *Science* **1996**, *273*, 768-771.

(7) Jung, J. H.; Ono, Y.; Shinkai, S. *Angew. Chem., Int. Ed.* **2000**, *39*, 1862-1865.

(8) Pauly, T. R.; Liu, Y.; Pinnavaia, T. J.; Billinge, S. J. L.; Rieker, T. P. *J. Am. Chem. Soc.* **1999**, *121*, 8835-8842.

(9) Zhang, W. Z.; Pauly, T. R.; Pinnavaia, T. J. *Chem. Mater.* **1997**, *9*, 2491-2498.

(10) Kim, S. S.; Zhang, W. Z.; Pinnavaia, T. J. *Science* **1998**, *282*, 1302-1305.

(11) Bruinsma, P. J.; Kim, A. Y.; Liu, J.; Baskaran, S. *Chem. Mater.* **1997**, *9*, 2507-2512.

(12) Lin, H.-P.; Cheng, Y.-R.; Mou, C.-Y. *Chem. Mater.* **1998**, *10*, 3772-3776.

(13) Lin, H.-P.; Mou, C.-Y.; Liu, S.-B. *Adv. Mater.* **2000**, *12*, 103-106.

(14) Li, W.; Sha, X.; Dong, W.; Wang, Z. *Chem. Commun.* **2002**, 2434-2435.

(15) Kosuge, K.; Singh, P. S. *Microporous Mesoporous Mater.* **2001**, *44-45*, 139-145.

(16) Ono, Y.; Nakashima, K.; Sano, M.; Hojo, J.; Shinkai, S. *J. Mater. Chem.* **2001**, *11*, 2412-2419.

(17) Kleitz, F.; Wilczok, U.; Schuth, F.; Marlow, F. *PCCP Phys. Chem. Chem. Phys.* **2001**, *3*, 3486-3489.

(18) Fowler, C. E.; Khushalani, D.; Mann, S. *Chem. Commun.* **2001**, 2028-2029.

(19) Hue, Q.; Leon, R.; Petroff, P. M.; Stucky, G. D. *Science* **1995**, *268*, 1324-1327.

(20) Garcia-Bennett, A. E.; Williamson, S.; Wright, P. A.; Shannon, I. J. *J. Mater. Chem.* **2002**, *12*, 3533-3540.

(21) Tanev, P. T.; Pinnavaia, T. J. *Science* **1996**, *271*, 1267-1269.

(22) Rana, R. K.; Mastai, Y.; Gedanken, A. *Adv. Mater.* **2002**, *14*, 1414-1418.

(23) Prouzet, E.; Cot, F.; Boissiere, C.; Kooyman, P. J.; Larbot, A. *J. Mater. Chem.* **2002**, *12*, 1553-1556.

(24) Lind, A.; Spliethoff, B.; Linden, M. *Chem. Mater.* **2003**, *15*, 813-818.

(25) Sun, Q.; Kooyman, P. J.; Grossman, J. G.; Bomans, P. H. H.; Frederik, P. M.; Magusin, P. C. M. M.; Beelan, T. P. M.; van Santen, R. A.; Sommerdijk, N. A. J. M. *Adv. Mater.* **2003**, *15*, 1097-1100.

(26) Limanov, V. E.; Rapin, S. A.; Ivanov, S. B. *Khimiko-Farmatsevticheskii Zhurnal* **1981**, *15*, 84-86.

(27) Linsker, F.; Evans, R. L. *J. Am. Chem. Soc.* **1945**, *67*, 1581-1582.

(28) Lopes, W. A.; Jaeger, H. M. *Nature* **2001**, *414*, 735-738.

(29) De Rosa, C.; Park, C.; Thomas, E. L.; Lotz, B. *Nature* **2000**, *405*, 433-437.

(30) Israelachvili, J. N. *Intermolecular and Surface Forces*; 2nd ed.; Academic Press, 1992.

(31) Lu, Y. F.; Fan, H. Y.; Stump, A.; Ward, T. L.; Rieker, T.; Brinker, C. J. *Nature* **1999**, *398*, 223-226.

(32) Simon, P.; Huhle, R.; Lehmann, M.; Lichte, H.; Moenter, D.; Bieber, T.; Reschetilowski, W.; Adhikari, R.; Michler, G. H. *Chem. Mater.* **2002**, *14*, 1505-1514.

(33) Abe, M.; Kuroda, J.; Matsumoto, M. *J. Appl. Phys.* **2002**, *91*, 7373-7375.

(34) Cabioc'h, T.; Thune, E.; Riviere, J. P.; Camelio, S.; Girard, J. C.; Guerin, P.; Jaouen, M.; Henrard, L.; Lambin, P. *J. Appl.Phys.* **2002**, *91*, 1560-1567.

(35) Porte, G. *J.Phys. Cond. Matter* **1992**, *4*, 8649.

(36) McGrath, K. M.; Dabbs, D. M.; Yao, N.; Aksay, I. A.; Gruner, S. M. *Science* **1997**, *277*, 552-556.

(37) S. Hyde; S. Andersson; K. Larsson; Z. Blum; T. Landh; S. Lidin; Ninham, B. W. *The Language of shape : the role of curvature in condensed matter--physics, chemistry, and biology Chapter 1*; Elsevier: Amsterdam [Netherlands] ; New York, 1997.

(38) S. Hyde; S. Andersson; K. Larsson; Z. Blum; T. Landh; S. Lidin; Ninham, B. W. *The Language of shape : the role of curvature in condensed matter--physics, chemistry, and biology page no.158*; Elsevier: Amsterdam [Netherlands] ; New York, 1997.

# Chapter 3

# Stability and Activity of MSU-G Catalysts

## 3.1 Abstract

The exceptional thermal and hydrothermal stability of pure silica MSU-G materials was explored. Also alumination of MSU-G mesostructures was carried out using different Al precursors. The effect of the precursor on the mesoporosity was evaluated. Al-MSU-G derivatives prepared through *in situ* alumination reactions with sodium aluminate are far more efficient acid catalysts than 2%Al-MCM-41 for cumene cracking and the conversion of 2,4-di-*tert*-butylphenol and cinnamyl alcohol to a bulky flavan as the primary alkylation product. The exceptional stability of MSU-G mesostructures is consistent with the very high degree of framework cross-linking ($Q^4/Q^3$=6.2) and thick framework walls (~25 Å). The improved catalytic activity of MSU-G mesostructures is attributable to the vesicular particle morphology, which facilitates reagent access to catalytic centers in the lamellar framework.

## 3.2 Introduction

### 3.2.1 Thermal and hydrothermal stability

The MCM-41 mesostructure in as-synthesized and calcined form has limited structural stability under hydrothermal conditions. Although the framework of MCM-41 is stable in air to temperatures of at least 850 °C[1], structural collapse of the surfactant-free form can occur in water is less than 24 h at 100 °C [2,3]. Several approaches to improving the hydrothermal stability of MCM-41 through post-synthesis modification methods have been reported, including the hydrothermal treatment in the presence,[2] and absence of salts,[4,5] the silylation of surface SiOH groups,[6,7] and the incorporation of certain metal ions (e.g., aluminum) in the framework.[8] Kim *et al* reported the direct assembly of ultra-stable mesoporous silicas with lamellar framework structures (denoted MSU-G) through the hydrolysis of silicon alkoxides in the presence of electrically neutral gemini surfactant of the type $C_nH_{2n+1}NH(CH_2)_2NH_2$ as structure directors. In contrast to the dense, monolithic mesostructures that are assembled electrostatically from cationic forms of gemini surfactants,[9] the MSU-G mesostructures obtained through an H-bonding pathway adopt a vesicular particle morphology. Because the vesicle shells are very thin (~3 to 70 nm) in comparison to the particle diameter (20–1400 nm), the framework surfaces are especially accessible for adsorption and catalysis. Another distinguishing feature of MSU-G mesostructures is the high degree of framework cross-linking, which

contributes to their unparalleled thermal and hydrothermal stability in comparison to other silica mesostructures prepared by direct assembly.[10] More recently, mesoporous aluminosilicates obtained by using protozeolitic clusters out-perform all the mesoporous materials obtained by conventional precursors.[11] However, the enhanced thermal and hydrothermal stability of MSU-G silicas involving no post-synthetic modification or sophisticated protozeolitic precursors is noteworthy.

### 3.2.2 Aluminated mesostructures

The identification and development of new heterogeneous solid acid catalysts for fine chemical and petrochemical products is becoming an area of growing interest.[12] In this regard, the discovery of mesoporous materials, designated as MCM-41[13,14] and HMS[15] having regular pore sizes and large surface area have opened new possibilities in the field of adsorption and heterogeneous catalysis

However, with regard to catalysis, purely siliceous mesoporous molecular sieves are of limited use owing to the absence of active sites in their matrices. Active sites may be generated *via* chemical modification involving the introduction of heteroatoms into the silica matrix. Various heteroatoms including transition metals, heterpolyacids, and organometallic complexes have been incorporated in mesoporous materials such MCM-41 and HMS. The incorporation of aluminum (which gives rise to solid acid catalysts with acid sites

associated with the presence of aluminum in framework positions) is the most common example. The introduction of aluminum into mesoporous silicas normally takes place in a homogeneous form and results in uniform incorporation of aluminum with little control of its spatial distribution. Increasing the aluminum content in the synthesis gel generally results in a uniform increase in the amount of incorporated aluminum throughout the entire sample. The incorporation of aluminium in the tetrahedral framework depends strongly on the source of aluminum used for the preparation.[16-19] For example, Janicke et al.,[16] and Reddy and Song[19] have claimed aluminum isopropoxide as the best source in relation to aluminum sulphate and pseudoboehmite. Luan et al.[17] have favored aluminum sulphate over the other aluminum sources like catapal Alumina (75% $Al_2O_3$; Vista Chemicals), aluminum orthophosphate, aluminum acetylacetonate, aluminum isopropoxide and aluminum hydroxide hydrate. Borade and Clearfield,[18] Occelli et al.[20] reported using sodium aluminate as a source incorporates aluminum to a maximum amount in the framework sites.

### 3.2.3 Hydrocarbon cracking

The cracking of hydrocarbons to produce lower molecular weight compounds is an important industrial process that permits the conversion of heavy natural oils to lighter products such as gasoline, thereby increasing the yield of motor fuels obtained from a barrel of petroleum crude. Cracking can be affected by heat alone (thermal cracking) or with the aid of a catalyst (catalytic cracking). Most cracking catalysts are combinations of silica and alumina oxides with acidic

properties. The currently accepted cracking theory supports the initial formation of an adsorbed carbonium ion which can be formed on the surface of the catalyst, either by the abstraction of a hydride ion from a saturated hydrocarbon or by addition of a proton to an olefin or aromatic compound.[21] Once a carbonium ion is formed, various ionic reactions such as isomerization, disproportionation, hydrogen transfer, cyclization, aromatization, coke formation and, also, cracking. The large number of reactions occurring in the industrial catalytic process, coupled with the complexity of an industrial gas oil feed, makes the interpretation of this process very difficult. For this reason, in order to study the activity of cracking catalysts, researchers used a single substrate, which could undergo a typical cracking reaction while yielding a few products. The cracking of cumene was thought to fulfill these requirements adequately yielding benzene and propylene as the major products. (Reaction 3.1)

**Reaction 3.1**

Cumene cracking reactions were performed in a 6 mm i.d. fixed bed quartz reactor containing 200 mg of catalysts. The cumene flow rate was 4.1 μmol $min^{-1}$ in a 20 mL $min^{-1}$ carrier gas of $N_2$. Cumene conversions were reported under steady-state conditions after 30 min on stream at 300 $^0$C.

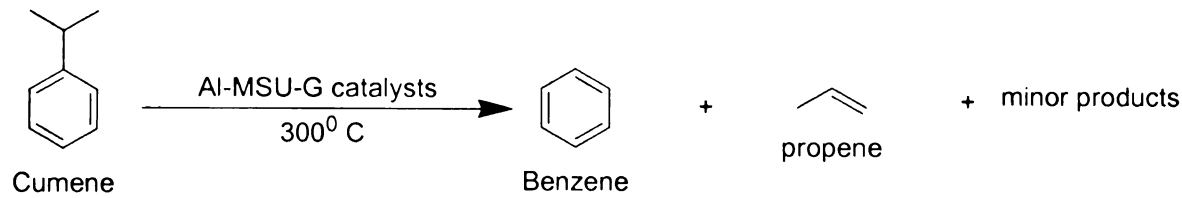


### 3.2.4 Alkylation reactions

Mesoporous aluminosilicates catalysts recently have been shown to be an effective solid acid catalyst for the alkylation of 2,4-di-*tert*-butylphenol by cinnamyl alcohol to yield a flavan.[22] We selected this reaction for evaluating the catalytic significance of shape in Al-MSU-G mesostructures, in part, because it is a sterically demanding condensed phase transformation and potentially susceptible to diffusion limitations arising from restricted access to the active acid sites in the framework. Also, cinnamyl alcohol self-degrades to unwanted side products, such as the corresponding symmetric ether, under strong acid catalytic conditions. Consequently, the selectivity to flavan is an indicator of the effectiveness of the desired reagent pairing and conversion at the moderately acidic sites within the framework mesopores. Previous studies of alkylation of 2,4-DTBP have been either aimed at studying the effect of weak acid sites in framework mesoporous materials or access in mesoporous materials with textural porosity.[22-24] This thesis explores the effect of shape on the product distribution. MSU-G materials can be obtained in vesicular, coiled slab, onion-like

and stripe-like morphology, as described in Chapter 2. In this chapter, we evaluate the performance of Al-MSU-G catalysts with different morphologies. (Reaction 3.2)

## Reaction 3.2

The reaction of 1.0 mmol of each reagent in 50 mL isooctane as solvent was carried out under vigorous stirring in a 100 mL three-neck flask equipped with a condenser and thermometer. When the temperature of the mixture reached 90 °C, a 250 mg portion of catalyst was added and the reaction was allowed to continue for 24 h.

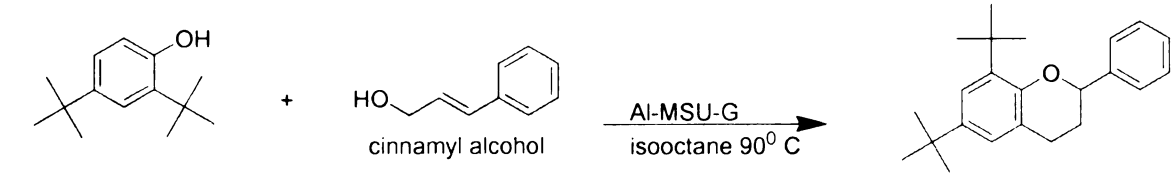


2, 4 di-tert-butylphenol + cinnamyl alcohol → Flavan

## 3.3 Experimental

### Materials

The source of silicon was tetraethyl orthosilicate (TEOS) obtained from Aldrich. The Gemini surfactants $C_nH_{2n+1}NHC_mH_{2m}NH_2$, where n=10, 12, 14 and m=3, 4) were synthesized as described in literature using ethylenediamine, 1,3-diaminopropane, 1,4-diaminobutane, 1-bromodecane, 1-bromododecane, 1-bromotetradecane, supplied by Aldrich. Absolute ethanol and deionized water were used as solvents for the mesoporous molecular sieve synthesis. Sodium aluminate, aluminum tributoxide, aluminum nitrate were obtained from Aldrich and used without purification.

### 3.3.1 Synthesis of Pure silica MSU-G materials

MSU-G was prepared as described previously in Chapter 2 from neutral gemini surfactant under hydrothermal conditions. A gel with the molar composition 1.0TEOS: 0.25 $C_nH_{2n+1}NH(CH_2)_mNH_2$: 77.7 $H_2O$: 3.5 EtOH was prepared by adding the surfactant to the ethanol and water mixed solvent, stirring the solution at room temperature for 20 h, and then adding the TEOS. The gel was transferred into a Teflon-lined autoclave, and the mixture was heated at 100 °C for 48 h under autogenous pressure. After the autoclave was cooled to room temperature, the as-synthesized MSU-G was filtered, washed

with water and ethanol, and air-dried. Finally, the surfactant was removed from the as-synthesized product by calcination in air at 620 °C for 4 h.

For the synthesis of the stripe-like phases, mixtures of the $C^{o}_{12+2+0}$ Gemini surfactant and the Jeffamine D-400 co-surfactant were stirred in water to obtain a milky white solution. Tetraethylorthosilicate (TEOS) in ethanol was added gradually at room temperature to form a reaction mixture of the following molar composition was formed.

1.0 TEOS: (0.25-x) $C_nH_{2n+1}NHC_mH_{2m}NH_2$: x Jeffamine D-400: 77.7 $H_2O$: 3.5 EtOH

The reaction mixture was allowed to stand for 20 minutes and stirred for 20 minutes before subjecting it to hydrothermal conditions in a Teflon lined autoclave at 100 °C for 48 hrs. The product was filtered, washed thoroughly with water and ethanol, and air-dried at room temperature. The surfactant was removed by calcination at 620 °C for 4 h in air.

### 3.2.2 Synthesis of Al-MSU-G

MSU-G silica was prepared in an autoclave by the same procedure as described above, except that the reaction time was 24 h and then the reaction mixture was cooled to room temperature. An alumina source (namely, aluminum nitrate, aluminum iso-butoxide, or sodium aluminate) was added to the as-synthesized silica in its original mother liquor so that the overall Si: Al ratio was 50:1. The resultant mixture was stirred and heated again at 100 °C for another 24 h. Because the original mother liquor is basic, even the cationic aluminum

precursors are expected to form aluminate anions suitable for grafting to the silicate framework under alumination conditions. The resulting products were washed with water and ethanol, air dried, and calcined in air at 620 °C for 4 h to remove the surfactant. Analogous synthesis was carried out for obtaining Si:Al ratios of 20:1 and 10:1 using $C_{10}H_{21}NH(CH_2)_3NH_2$ as a surfactant and tetraethyl orthosilicate (TEOS) as the silica source and sodium aluminate as the Aluminum precursor.

### 3.3.3 Stability studies

The thermal stability of the pure silica MSU-G materials was tested by calcining the as-synthesized sample at 1000 $^{o}$C under static conditions in a furnace for 4 h. The heating rate was kept at 2 $^{o}$C per minute.

The hydrothermal stability of pure silica MSU-G materials was determined in the way described below. MSU-G silica calcined (0.1 g) at 620 $^{0}$C was mixed with 10 mL of deionized water and sealed in a glass vial using Teflon seals. The vial was then placed in an oven at 100 $^{0}$C for 48-60 h under static conditions. Following the hydrothermal treatment the materials were filtered dried and recalcined at 550 $^{0}$C for 4 h.

### 3.3.4 Characterization

The physical properties of MSU-G mesoporous silicas where determined using X-ray diffraction (XRD), nitrogen adsorptometry and transmission electron

microscopy (TEM). Powder x-ray diffraction patterns were measured on a Rigaku Rotaflex Diffractometer equipped with a rotating anode using Cu Kα radiation (λ = 0.154 nm). $N_2$ adsorption-desorption data were obtained at –196 °C on a Micromeritics ASAP 2010. Samples were out gassed at 150 °C and $10^{-6}$ Torr for a minimum of 6 h prior to analysis. TEM images were obtained on a JEOL 100CX microscope with a $CeB_6$ filament and an accelerating voltage of 120 KV. Samples were prepared either by dusting onto a carbon coated holey film supported on a 300 mesh Cu grid, or by sonicating the powdered sample for 20 min in EtOH, then evaporating 2 drops onto the carbon coated holey film. $^{27}Al$ MAS NMR spectra were recorded on a Varian VXR-400S spectrometer with zirconia rotors 4 mm in diameter and spun at 8 KHz. The spectra were measured at 104.3 MHz and corrected by subtracting the residue signal contribution from the empty MAS rotor. External $Al(H_2O)_6^{3+}$ was used as a chemical shift reference.

### 3.3.5 Cumene cracking reaction using Al-MSU-G catalysts (Reaction 3.1)

Cumene cracking reactions were performed in a 6 mm i.d. fixed bed quartz reactor containing 200 mg of catalysts. The cumene flow rate was 4.1 μmol $min^{-1}$ in a 20 mL $min^{-1}$ carrier gas of $N_2$. Cumene conversions were reported under steady-state conditions after 30 min on stream at 300 °C. The products were analyzed by means of a GC equipped with a SPB-1 capillary column and a FID detector. The schematic reactor design is shown in Figure 3.1.

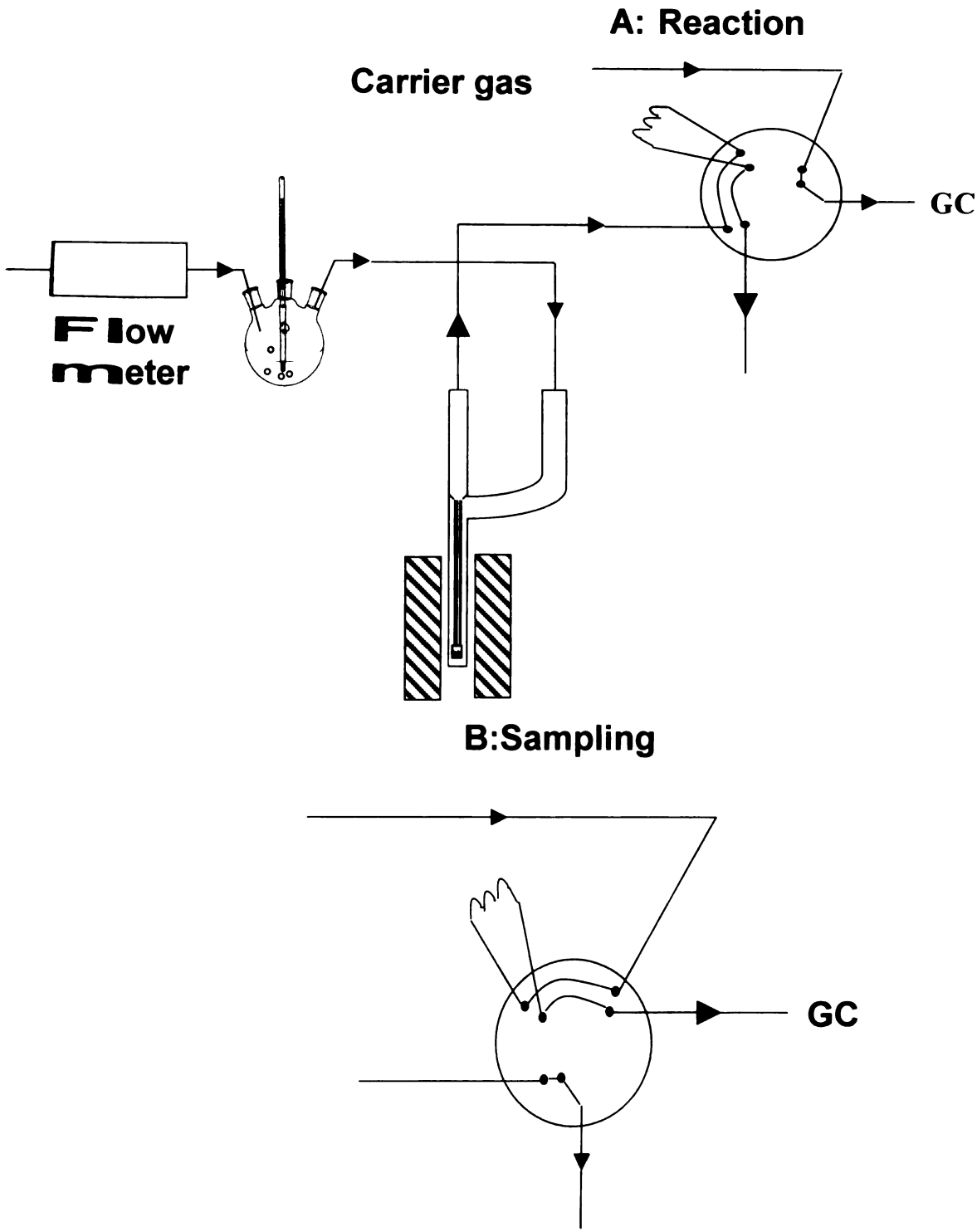


**Figure 3.1** Schematic representation of cumene cracking fixed bed quartz reactor interfaced to a GC equipped with FID detector

### 3.3.6 Alkylation of 2,4-di-*tert*-Butylphenol (DTBP) with Cinnamyl Alcohol (Reaction 3.2)

The acid catalytic activities of 2% Al-MSU-G and 2% Al-MCM-41 mesostructures were tested for the alkylation of 2,4-di-*tert*-butylphenol (DTBP) with cinnamyl alcohol. The reaction of 1.0 mmol of each reagent in 50 mL isooctane as solvent was carried out under vigorous stirring in a 100 mL three-neck flask equipped with a condenser and thermometer. When the temperature of the mixture reached 90 °C, a 250 mg portion of catalyst was added and the reaction was allowed to continue for 24 h. The products were analyzed by means of a GC equipped with a SPB-1 capillary column and a FID detector. The reaction products were confirmed by GC-MS analysis. 1,3-di-*tert*-butylbenzene was used as an internal standard for the quantitative analysis of the products.

## 3.4 Results and discussion

### 3.4.1 Thermal and hydrothermal stability

Table 3.1 summarizes the structural properties of the calcined forms of a MSU-G silica prepared by supramolecular H-bonding interactions between the hydrolysis products of TEOS and the polar head groups of the electrically neutral gemini surfactant $C_{12}H_{25}NH(CH_2)_3NH_2$ ($C^0_{12+3+0}$). Included in the table for comparison purposes are the structural properties of calcined MCM-41silica electrostatically assembled in the presence of an onium ion surfactant (i.e., cetyltrimethylammonium ion), which is comparable in size to the gemini surfactant. Another important distinction between MSU-G and the electrostatically assembled silicas is the very high degree of $SiO_4$ unit cross-linking in the framework. $^{29}Si$ MAS NMR spectroscopy indicates the ratio of $Q^4/Q^3$ sites in as-synthesized MSU-G to be 6.2,[24] while as-synthesized silica mesostructures, whether assembled from ionic or neutral surfactants, exhibit a $Q^4/Q^3$ ratio less than 2.0. Also the calcined derivatives of electrostatically assembled silica have $Q^4/Q^3$ values near 3.0.[14,27] In accord with the high degree of framework cross-linking and the thick framework walls of MSU-G, the stability of this mesostructure under thermal and hydrothermal conditions are far superior to those of MCM-41 silica.

Table 3.1 also provides a more quantitative indication of the structural damage that occurs for MSU-G and MCM-41 upon 1000 °C calcination and

hydrothermal treatment for 56-144 h. The MSU-G silica on calcinations at 1000 $^0$C shows remarkable stability retaining 100% of surface area and only a decrease of 18% in the pore volume. Under identical condition MCM-41 silica shows an 88% decrease in surface area, a92% decrease in pore volume and no HK[28] pore size distribution, indicating a complete collapse of the framework structure. Moreover, MCM-41 loses 79% of its initial surface area and 38% of its pore volume and no HK pore size distribution after only 56 h of hydrothermal treatment in boiling water, as compared to the MSU-G samples which retain good structural integrity. Figure 3.2 shows the $N_2$ isotherms for MSU-G silica ($C^0_{12+3+0}$) calcined at 620 $^0$C for 4 h, 1000 $^0$C for 4 h, and after hydrothermal treatment in water at 100 $^0$C for 72 h and 144 h respectively. However, it is evident that upon hydrothermal treatment for 144 h that MSU-G ($C^0_{12+3+0}$) has degraded considerably, losing 56% of the surface area and 45% pore volume, yet remarkably keeping the HK pore size at about the same value of 3.2 nm.

The post-synthesis modified forms of MCM-41 in the form of KIT-1 appear to be approaching the framework characteristics achieved through the direct assembly of MSU-G silicas at 100 °C, namely, thicker and more fully cross-linked walls. The fact that thicker and more fully cross-linked walls are more readily achieved for MSU-G than for MCM-41 may be related a fundamental difference in assembly mechanisms. In the H bonding pathway used to assemble MSU-G, the evolving silica framework is electrically neutral, and this favors optimal framework cross-linking through condensation reactions of neighboring

**Table 3.1.** Structural properties of MSU-G silica assembled using $C_{12}H_{25}NH(CH_2)_3NH_2$ as a surfactant and TEOS as silica source under hydrothermal conditions at $100^0$ C for 48h compared to MCM-41

| Conditions | $S_{BET}$ ($m^2/g$) | % change | Pore Vol. ($cm^3/g$) | % change | HK Pore size (nm) |
|---|---|---|---|---|---|
| **Properties of Vesicular MSU-G** | | | | | |
| **620° C/4h** | 472 | - | 0.55 | - | 3.8 |
| **1000° C/4h** | 472 | 0 | 0.45 | 18 | 3.0 |
| **100°C $H_2O$, 72 h** | 289 | 38 | 0.32 | 41 | 3.5 |
| **100°C $H_2O$, 144 h** | 206 | 56 | 0.3 | 45 | 3.2 |
| **Properties of hexagonal MCM-41** | | | | | |
| **620° C/4h** | 1169 | - | 0.87 | - | 3.2 |
| **1000° C/4h** | 134 | 88 | 0.07 | 92 | - |
| **100°C $H_2O$, 56 h** | 245 | 79 | 0.54 | 38 | - |

SiOH groups. In contrast, charge balance must be maintained between the surfactant and the silicate framework in the electrostatic assembly of MCM-41 Consequently, some fraction of the $SiO_4$ units in MCM-41 must contain terminal $SiO^-$ units, and these units impede framework cross-linking.

### 3.4.2 Effect of Alumina source and Alumina loading on the hierarchical structure of MSU-G ($C^0_{10+3+0}$)

Table 3.2 shows the textural properties of 2 mol% Al-MSU-G ($C^0_{12+3+0}$) structures obtained using $C_{10}H_{21}NH(CH_2)_3NH_2$ surfactant, TEOS as the silica source and $NaAlO_2$, $Al(NO_3)_3$ and $Al(iOBu)_3$ as the alumina sources respectively. Figure 3.3 shows the $N_2$ adsorption desorption isotherms obtained for the above-mentioned MSU-G ($C^0_{10+3+0}$) materials. $NaAlO_2$ was found to be the best source for alumination under the experimental conditions. Aluminum nitrate and aluminum butoxide also provided analogous mesotructures with 2 mol% Al loading. However, the materials obtained using aluminum nitrate and aluminum butoxide showed 20% and 14 % lower BET surface area values respectively. Figure 3.4 shows the $^{27}Al$ NMR spectra obtained for a calcined MSU-G ($C^0_{10+3+0}$) compositions formed from $Al(NO_3)_3$, $Al(iOBu)_3$ and $NaAlO_2$ as the aluminum source. The peak in the range of 48-54 ppm corresponds to the tetrahedral aluminum centers in the framework, whereas the peak at ~ 0 ppm corresponds to the extraframework octahedral Al.

Table 3.3 summarizes the effect of increasing aluminum loading on the textural properties of MSU-G ($C^0_{10+3+0}$) mesotructures using sodium aluminate as the alumina source. This can be seen from the values of

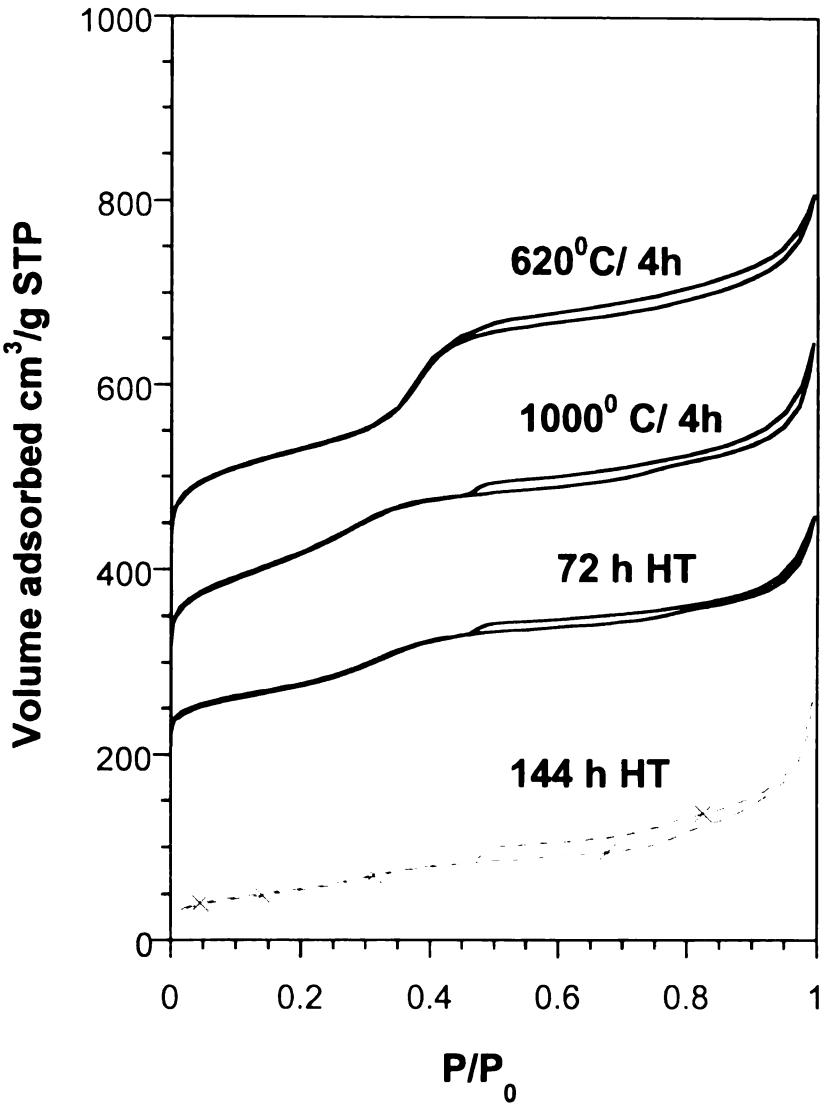


**Figure 3.2** $N_2$ adsorption desorption isotherms for ($C^0_{12+3+0}$) MSU-G mesoporous silica obtained from $C_{12}H_{25}NH(CH_2)_3NH_2$ surfactant and TEOS as the silica source showing effect of thermal and hydrothermal conditions. The isotherms are offset by 200 cc/g STP for the 72 h HT and 100 cc/g STP for the others for clarity.

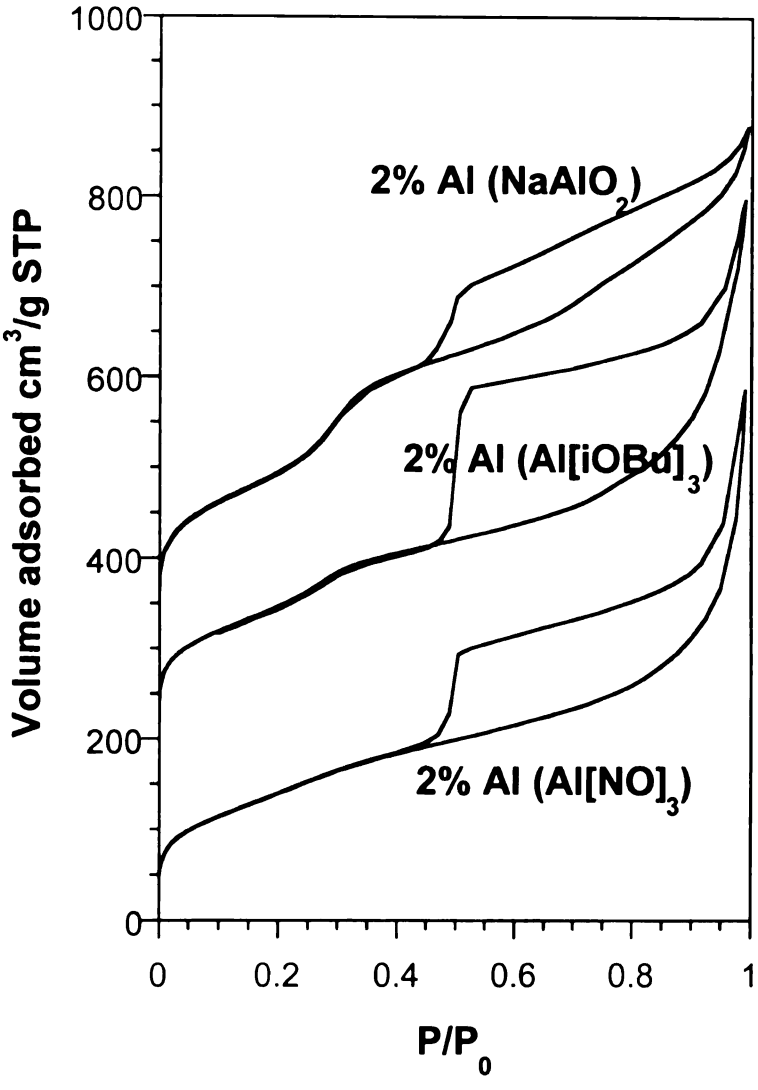


**Figure 3.3** $N_2$ adsorption desorption isotherms for ($C^0_{10+3+0}$) MSU-G mesoporous silica obtained from $C_{10}H_{21}NH(CH_2)_3NH_2$ surfactant and TEOS as the silica source and different Aluminum precursors. The isotherms are offset by 200 cc/g STP and 100 cc/g STP for clarity

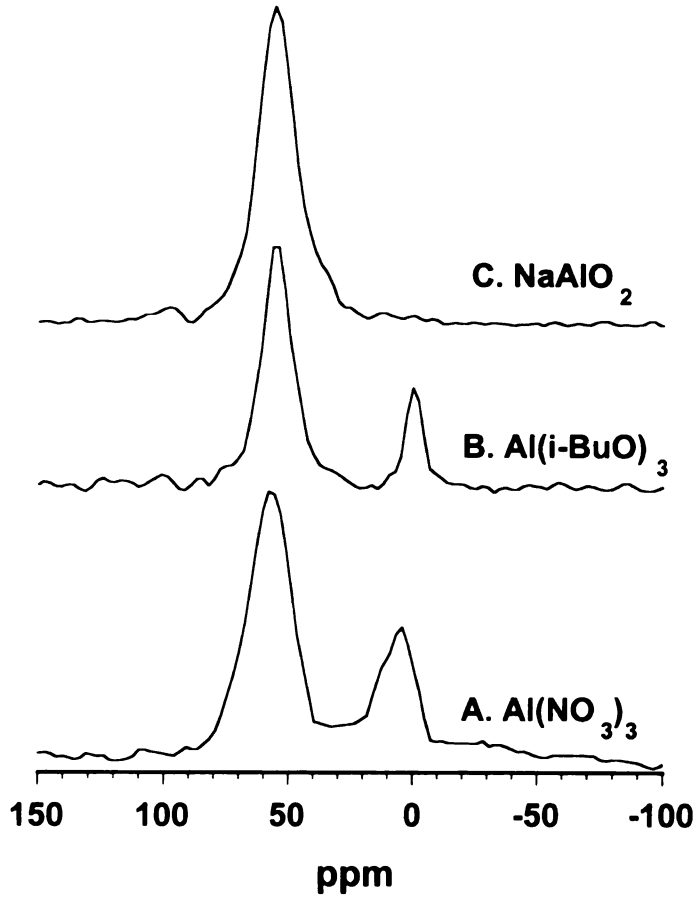


**Figure 3.4** $^{27}$Al MAS NMR of a calcined sample (620 $^{0}$C for 4 h) of 2 mol% Al-MSU-G ($C^{0}_{10+3+0}$) obtained from $C_{10}H_{21}NH(CH2)_2NH_2$ surfactant, TEOS as the silica source and $Al(NO_3)_3$, $Al(iOBu)_3$ and $NaAlO_2$ as the aluminum source showing a tetrahedral Al resonance at ~50 ppm and octahedral Al resonance at ~0 ppm.

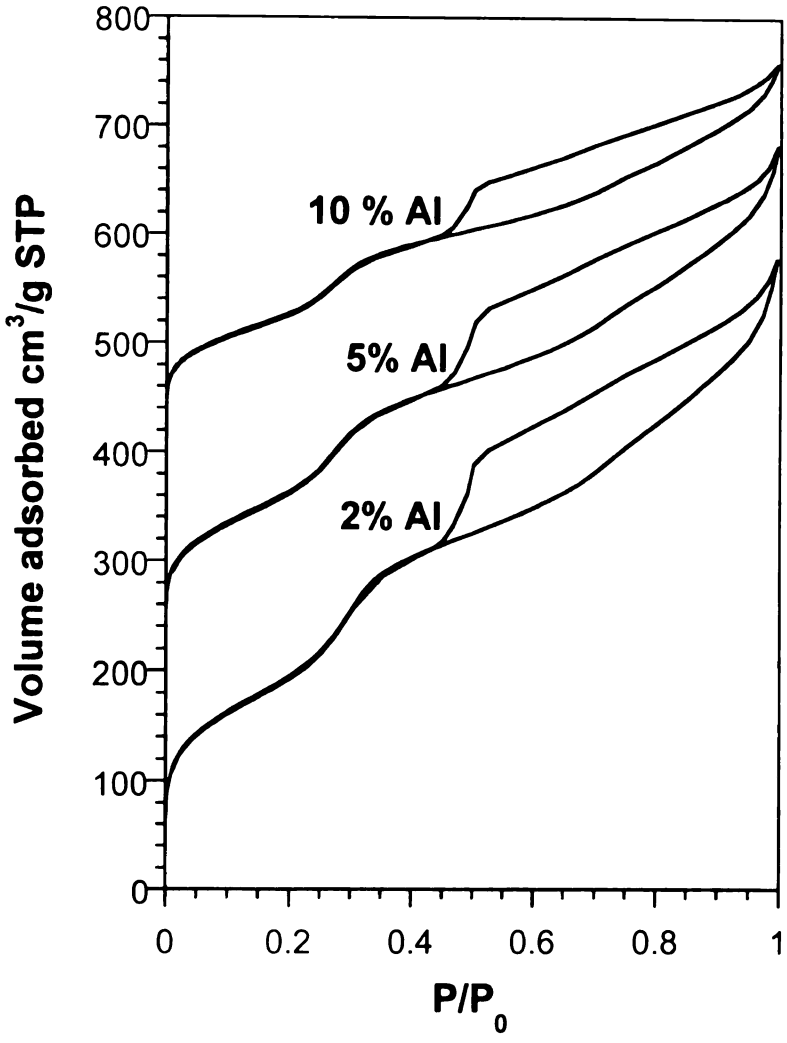


**Figure 3.5** $N_2$ adsorption desorption isotherms for ($C^0_{10+3+0}$) MSU-G mesoporous silica obtained from $C_{10}H_{21}NH(CH_2)_3NH_2$ surfactant, TEOS as the silica source and $NaAlO_2$ as the Alumina source showing the effect of mol% of aluminum The isotherms are offset by 200 cc/g STP for clarity

BET surface areas and HK pore size distribution that up to 5% aluminum can be substituted into the framework without significant loss of surface area. However, upon 10% substitution of the silicon centers by aluminum, there is a 27% decrease in surface area, with retention of HK pore size. It can be concluded from this study that among the various aluminum sources used, the use of sodium aluminate as the aluminum source leads to maximum aluminum loading with minimal effects on the structure. (Figure 3.5)

### 3.4.3 Cumene cracking

Using the cumene conversion reaction as a well-established test of hydrocarbon cracking activity, we compared the acidic reactivity of 2 mol% Al-MSU-G mesostructures with 2 mol% MCM-41 mesostructures and microporous acidic zeolite H-Y. The initial cumene cracking activities after 30 minutes on stream are listed in Table 3.4 in comparison to various other aluminosilicates mesostructures with different Al loadings and assembly pathways. The initial cumene cracking activities were found to be strongly dependant on the amount of Al present in the mesostructures. Al-MSU-G catalysts were found to be active for a longer time on stream, as compared to the Al-MCM-41 catalysts. This was attributed to the fast deactivation of the active sites due to coking and pore clogging in the primarily monolithic MCM-41. The reaction showed significantly higher cumene cracking activity (98%) for microporous zeolite H-Y. The reason for the higher activity for the zeolite is due to the presence of strong brönsted acids sites in a zeolite as a result of its crystalline nature causing all the

aluminum and silicon centers to be completely cross-linked creating negatively charged interstices on the surface where a strongly acidic proton can reside.

**Table 3.2**. Structural properties of 2% Al- MSU-G catalysts synthesized using $C_{10}H_{21}NH(CH_2)_3NH_2$ as a surfactant and TEOS as silica source under hydrothermal conditions at $100^0$ C for 48h using different aluminum precursors.

| **Conditions** | **$S_{BET}$ ($m^2/g$)** | **% change** | **Pore Vol. ($cm^3/g$)** | **% change** | **HK Pore size (nm)** |
|---|---|---|---|---|---|
| MSU-G | 650 | - | 0.82 | - | 3.0 |
| 2% Al $NaAlO_2$ | 725 | +11 | 0.81 | -1 | 3.1 |
| 2% Al $Al(NO)_3$ | 521 | -20 | 0.68 | -17 | 2.6 |
| 2% Al $Al(OiBu)_3$ | 557 | -14 | 0.8 | -2 | 3.0 |

**Table 3.3**. Structural properties of Al- MSU-G catalysts assembled using $C_{10}H_{21}NH(CH_2)_3NH_2$ as a surfactant and TEOS as silica source and $NaAlO_2$ as aluminum source under hydrothermal conditions at $100^0$ C for 48h

| **Conditions** | **$S_{BET}$ ($m^2/g$)** | **% change** | **Pore Vol. ($cm^3/g$)** | **% change** | **HK Pore size (nm)** |
|---|---|---|---|---|---|
| MSU-G | 650 | - | 0.82 | - | 3.0 |
| 2% Al $NaAlO_2$ | 725 | +11 | 0.81 | -1 | 3.1 |
| 5% Al $NaAlO_2$ | 619 | -5 | 0.67 | -18 | 3.0 |
| 10% Al $NaAlO_2$ | 476 | -27 | 0.51 | -37 | 3.0 |

### 3.4.4 Alkylation using Cinnamyl Alcohol

We selected the reaction the alkylation of 2,4-di-*tert*-butylphenol (2,4-DTBP) by cinnamyl alcohol as a probe reaction for studying the effect of particle morphology on catalytic activity, in part, because it is a sterically demanding condensed phase transformation and potentially susceptible to diffusion limitations arising from restricted access to the active acid sites in the framework. Also, cinnamyl alcohol degrades to unwanted side products, such as the corresponding symmetric ether, under strong acid catalytic conditions. Consequently, the selectivity of of flavan is an indicator of the effectiveness of the desired reagent pairing and conversion at the moderately acidic sites within the framework mesopores.

The reactivities of the 2%Al-MSU-G mesostructures as acid catalysts for flavan synthesis are provided in Table 3.5 Included for comparison purposes are the yields of flavan obtained using 2%Al-MCM-41 and sulfuric acid. It was found that the shape of the mesotructure significantly influenced the conversions and product distribution. The truly vesicular MSU-G ($C^0_{12+2+0}$) was found to be the most active catalysts yielding 45% flavan while the onion-like MSU-G ($C^0_{10+4+0}$) was the least active yielding only 8 % flavan. The coiled slab morphology was found to have activity similar to MCM-41 yielding 33% flavan and the stripe-like phase ($C^0_{12+2+0/D400}$) was found to be moderately active yielding 27 % flavan.

However, factors other than shape may contribute to the differences in the catalytic efficiencies of MCM-41 and MSU-G structures. These two structures are assembled by fundamentally different mechanisms (H bonding vs. electrostatic

assembly). Consequently, the acidic centers may differ in intrinsic strength and accessibility, even the though the framework walls are amorphous for both structure types. The lowest activity was observed for onion-like MSU-G($C^0_{10+4+0}$), which may be explained on basis of the morphology. The onion-like structure is a densely packed structure with many pillars (Figure 2.2 B) potentially limiting access of the molecules to the active sites. The effective channel length of the onion-like structure will be significantly larger hence preventing the bulky 2,4-DTBP from accessing acid sites adjacent to acid sites where cinnamyl alcohol has been activated by formation of a carbocation. However, since 100% of cinnamyl alcohol is converted to other products it is of prime importance that 2,4-DTBP access the activated cinnamyl alcohol simultaneously before it self degrades to unwanted side products. But to due to severe diffusional limitations in onion-like MSU-G($C^0_{10+4+0}$) mesostructured the conversion of phenol is significantly low.

The conversion of cinnamyl alcohol in all cases is 100%, but the conversion of phenol is considerably lower. The Al-MSU-G($C^0_{12+2+0}$) having vesicular morphology affords the desirable flavan in a 45.1% yield significantly higher than the yield obtained with Al-MCM-41 (33.9%). On the other hand Al-MSU-G($C^0_{10+3+0}$) having a coiled slab morphology affords a yield of 33.1 comparable to Al-MCM-41 and the stripe-like phase MSU-G($C^0_{12+2+0/D400}$) affords a yield (26.7%) considerably lower than the vesicular, coiled slab and hexagonal morphology. This can be manifested in diffusional limitations arising to larger particle size domains present in the stripe-like material.

**Table 3.4** Initial Cumene cracking activity of 2 mol % Al-MSU-G catalysts and MCM-41

| **Catalyst** | **Morphology (Structure)** | **% Al (mol)** | **Initial Cumene cracking (%)** |
|---|---|---|---|
| Al-($C^0_{12+2+0}$) | Vesicular (MSU-G) | 2 | 27.5 |
| Al-($C^0_{10+3+0}$) | Coiled slab (MSU-G | 2 | 33 |
| Al-($C^0_{10+4+0}$) | Onion-like (MSU-G) | 2 | 37 |
| Al-($C^0_{12+2+0/D400}$) | Stripe-like (MSU-G) | 2 | 36 |
| Al-($C^0_{12+2+0}$) | Vesicular (MSU-G) | 15 | 60.5 |
| Al-MCM-41 | Hexagonal | 2 | 21.5 |
| Al-MCM-41 | Hexagonal | 5 | 34.5 |
| Al-MCM-41 | Hexagonal | 10 | 41.2 |
| H-Y | Y zeolite | 4 | 98.3 |

**Table 3.5** Alkylation of 2,4-di-tert-butylphenol with cinnamyl alcohol in the presence of Al-MSU-G catalysts

| Catalyst (2.0 mol % Al) | Conversion of Phenol (%) | Selectivity of Flavan (%) | Flavan yield (%) |
|---|---|---|---|
| Al-$C^{o}_{12+2+0}$ | 69.1 | 65.3 | 45.1 |
| Al-$C^{o}_{10+3+0}$ | 49.1 | 67.0 | 33.1 |
| Al-$C^{o}_{10+4+0}$ | 9.5 | 84.3 | 8.0 |
| Al-$C^{o}_{12+2+0\ /D400}$ | 45.3 | 58.9 | 26.7 |
| Al-MCM-41 | 47.2 | 71.8 | 33.9 |
| $H_2SO_4$ | 25.5 | 36.9 | 9.4 |

### 3.5 Conclusion

Among all the mesostructures formed by direct supramolecular assembly pathways, lamellar MSU-G molecular sieves are unique in three ways. Firstly, MSU-G is the only known silica mesostructure with a lamellar framework that is stable to surfactant removal. Secondly, owing to the high degree of framework cross-linking and relatively thick framework walls, MSU-G silica is stable under hydrothermal conditions at 100 °C. The vesicle-like morphology is maintained upon grafting of reactive aluminum centers to the framework walls. Owing to the improvement in framework accessibility, functionalized derivatives of MSU-G mesostructures can be substantially more active catalysts for condensed phase chemical conversions than MCM-41 and related mesostructures with two or more times the surface area of MSU-G. We also demonstrated the use of Al-MSU-G catalysts in gas phase cumene cracking reactions.

## 3.6 References


(1) Chen, C. Y.; Li, H. X.; Davis, M. E. *Microporous Mater.* **1993**, *2*, 17-26.

(2) Ryoo, R.; Jun, S. *J.Phys.Chem B* **1997**, *101*, 317-320.

(3) Chen, L. Y.; Jaenicke, S.; Chuah, G. K. *Microporous Mater.* **1997**, *12*, 323-330.

(4) Chen, L.; Horiuchi, T.; Mori, T.; Maeda, K. *J.Phys.Chem B* **1999**, *103*, 1216-1222.

(5) Mokaya, R. *J.Phys.Chem B* **1999**, *103*, 10204-10208.

(6) Koyano, K. A.; Tatsumi, T.; Tanaka, Y.; Nakata, S. *J.Phys.Chem B* **1997**, *101*, 9436-9440.

(7) Zhao, X. S.; Lu, G. Q. *J.Phys.Chem B* **1998**, *102*, 1556-1561.

(8) Mokaya, R. *Angew. Chem.Int. Ed.* **1999**, *38*, 2930-2934.

(9) Huo, Q.; Leon, R.; Petroff, P. M.; Stucky, G. D. *Science* **1995**, *268*, 1324-1327.

(10) Kim, S. S.; Zhang, W. Z.; Pinnavaia, T. J. *Science* **1998**, *282*, 1302-1305.

(11) Liu, Y.; Pinnavaia, T. J. *Chem. Mater.* **2002**, *14*, 3-5.

(12) Venuto, P. B. *Microporous Mater.* **1994**, *2*, 297-411.

(13) Kresge, C. T.; Leonowicz, M. E.; Roth, W. J.; Vartuli, J. C.; Beck, J. S. *Nature* **1992**, *359*, 710-712.

(14) Beck, J. S.; Vartuli, J. C.; Roth, W. J.; Leonowicz, M. E.; Kresge, C. T.; Schmitt, K. D.; Chu, C. T. W.; Olson, D. H.; Sheppard, E. W.; et al. *J. Am. Chem. Soc.* **1992**, *114*, 10834-10843.

(15) Tanev, P. T.; Pinnavaia, T. J. *Science* **1995**, *267*, 865-867.

(16) Janicke, M.; Kumar, D.; Stucky, G. D.; Chmelka, B. F. *Stud. Surf. Sci. Catal.* **1994**, *84*, 243-250.

(17) Luan, Z.; He, H.; Zhou, w.; Cheng, C.-F.; Klinowski, J. *J. Chem. Soc., Faraday Trans.* **1995**, *91*, 2955-2959.

(18) Borade, R. B.; Clearfield, A. *Catal. Lett.* **1995**, *31*, 267-272.

(19) Reddy, K. M.; Song, C. *Catal. Today* **1996**, *31*, 137-144.

(20) Occelli, M. L.; Biz, S.; Auroux, A.; Ray, G. J. *Microporous Mesoporous Mater.* **1998**, *26*, 193-213.

(21) Corma, A.; Wojciechowski, B. W. *Catal. Rev. Sci. Eng.* **1985**, *27*, 29-149.

(22) Armengol, E.; Cano, M. L.; Corma, A.; Garcia, H.; Navarro, M. T. *J. Chem. Soc., Chem. Commun.* **1995**, 519-520.

(23) Pauly, T. R.; Liu, Y.; Pinnavaia, T. J.; Billinge, S. J. L.; Rieker, T. P. *J. Am. Chem. Soc.* **1999**, *121*, 8835-8842.

(24) Kim, S. S.; Liu, Y.; Pinnavaia, T. J. *Microporous Mesoporous Mater.* **2001**, *44*, 489-498.

(25) Tanaka, Y.; Sawamura, N.; Iwamoto, M. *Tet. Lett.* **1998**, *39*, 9457-9460.

(26) Iwamoto, M.; Tanaka, Y.; Sawamura, N.; Namba, S. *J. Am. Chem. Soc.* **2003**, *125*, 13032-13033.

(27) Tanev, P. T.; Pinnavaia, T. J. *Chem. Mater.* **1996**, *8*, 2068-2079.

(28) Horvath, G.; Kawazoe, K. *J. Chem. Eng. Jpn.* **1983**, *16*, 470-475.

# Chapter 4

# Microemulsion Templating of MSU-F Silica

## 4.1 Abstract

A new family of mesostructured cellular foams (MSU-F) with microemulsion-templated structures has been synthesized using triblock copolymer P123 as structure-directing agents, 1,3,5-trimethylbenzene (TMB) as swelling agent and low-cost, water-soluble silicate precursors under near neutral conditions. The MSU-F foams consist of uniform spherical cells measuring 16 – 85 nm in diameter, windows with diameters of 5 – 40 nm and a narrow size distribution interconnecting the cells. The pore size can be controlled by adjusting the amount of the organic swelling agent and co-solvent, and by varying the aging temperature. The unique feature of the present work is the exceptional degree to which the foam dimensions can be expanded *without* altering the composition of the porogen. The cell and window dimensions can be increased by as much as 18 nm merely by controlling the duration of hydrothermal treatment. The cell size can also be controlled in the range of 20-85 and window size in the range 5-40 nm by adjusting the amount of the organic swelling agent and co-solvent, and by varying the aging temperature.

## 4.2 Introduction

### 4.2.1 Synthesis of Mesoporous cellular foams from oil in water emulsions

Considerable effort has been invested in expanding the family of micelle-templated structures by different synthesis pathways.[1,2] One important achievement has focused on expanding the pore size of mesoporous materials by changing the aging temperature or by adding organic reagents as swelling agents. Especially notable are the development of strategies for obtaining well-defined macroporous materials (> 50 nm) using either emulsion particles[3] or polymer latex spheres as templates. Various periodic cubic and hexagonal mesoporous silica phases with uniform large pores have been synthesized by using nonionic triblock and star diblock copolymers as templates.[4,5] In a general method, the large pore hexagonal materials (denoted as SBA-15[6] and MSU-H[7] respectively) synthesized using P123 ($PEO_{20}$-$PPO_{70}$-$PEO_{20}$) as a structure director along with either TEOS or sodium silicate as the silicon source could be considered as precursors to the formation of foam like materials, which are denoted as MSU-F, or MCF materials. Figure 4.1. Illustrates the powder X-ray diffraction patterns of as-synthesized and calcined (600 °C) forms of hexagonal MSU-H silica as prepared from Pluronic P123 ($EO_{20}PO_{70}EO_{20}$) as the surfactant at a synthesis temperature of 60 °C.[7] The as-synthesized and calcined products exhibit resolved *hkl* reflections consistent with two-dimensional hexagonal symmetry and unit cell dimensions of 130 and 119 Å, respectively. Figure 4.2. Illustrates the $N_2$ adsorption–desorption isotherms and BJH pore size distribution

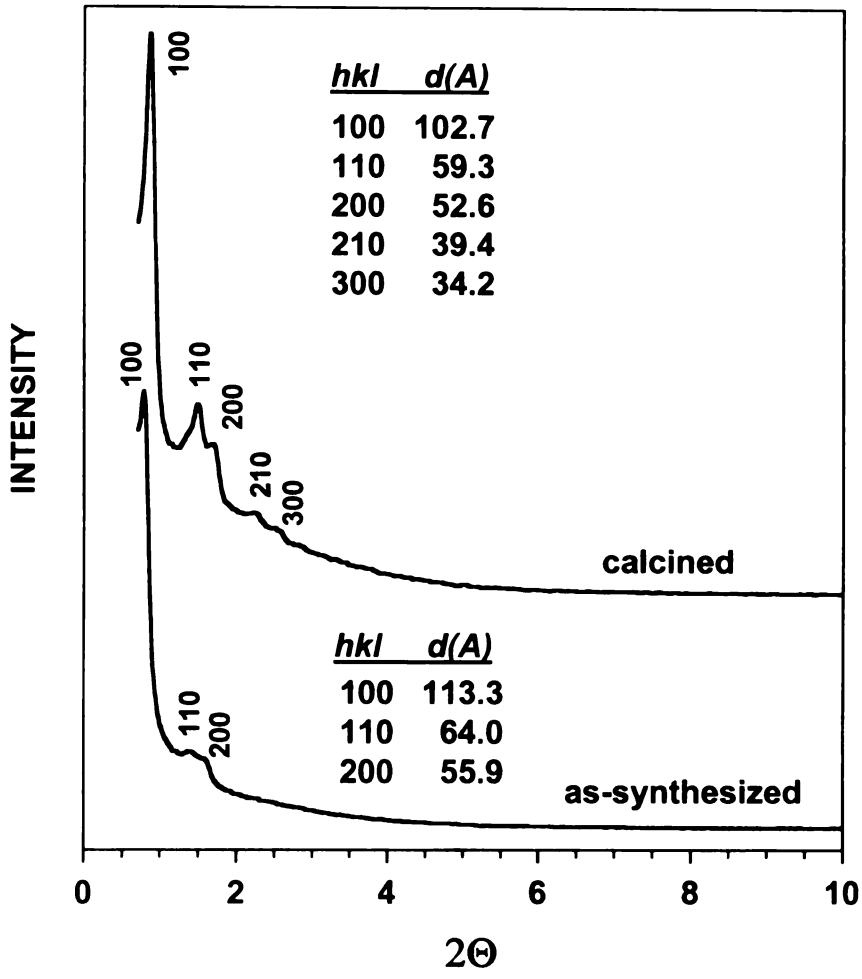


**Figure 4.1**. Powder X-ray diffraction patterns of as-synthesized and calcined (600 °C) forms of hexagonal MSU-H silica as prepared from Pluronic P123 ($EO_{20}PO_{70}EO_{20}$) as the surfactant and at a synthesis temperature of 60 °C

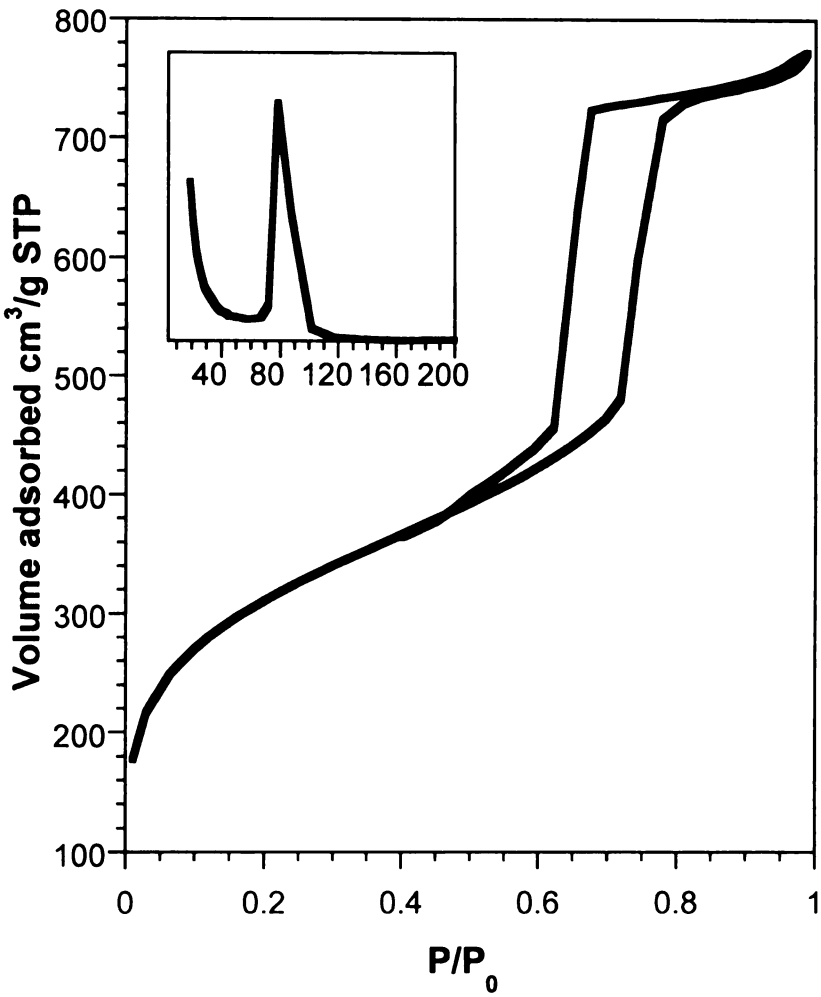


**Figure 4.2.** $N_2$ adsorption–desorption isotherms and BJH pore size distribution plot (insert) calculated from the adsorption branch of the $N_2$ isotherms for calcined MSU-H.

**Figure 4.3** TEM images of the calcined MSU-H silica showing well ordered hexagonal domains

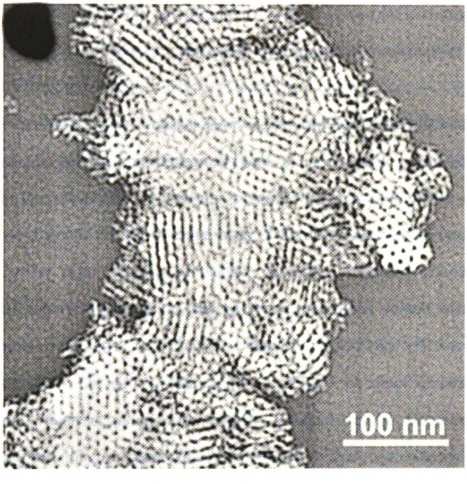
100 nm

plot (insert) calculated from the adsorption branch of the $N_2$ isotherms for calcined MSU-H. A typical, type IV adsorption isotherm with an irreversible H1 hysteresis loop is observed as expected for a large pore material. The step-like uptake of $N_2$ in the range 0.7–0.9 $P/P_0$ corresponds to capillary condensation within framework pores with a BJH diameter of 98 Å. The pore volume is 1.24 $cm^3\ g^{-1}$, the BET surface area is 625 $m^2\ g^{-1}$ for this calcined MSU-H. Control over the pore size is achieved by adjusting the hydrophobic volumes of the self-assembled aggregates.

Figure 4.3 shows a typical TEM image of MSU-H type material showing presence of well-ordered hexagonal pore channels. Stucky and coworkers reported that mesostructured cellular foams (MCF) with well-defined ultra-large pores were synthesized in the presence of non-ionic surfactants and swelling agents under strongly acidic conditions.[8] Also, they prepared closed-cell and open-cell foams templated by polystyrene microspheres coated with cationic surfactants under basic and acidic conditions, respectively.[9] However, these materials share the same synthetic disadvantages as other ultra-large pore materials. These ultra-large pore structures could not be prepared in bulk quantities from low cost reagents. Kim et al reported that mesostructured cellular foams (denoted MSU-F) with large and uniform spherical cell synthesized using triblock copolymer $PEO_{20}$-$PPO_{70}$-$PEO_{20}$ P123 surfactant, 1,3,5-trimethylbenzene (TMB), and low-cost, water-soluble silicate precursors under near neutral conditions.[7] Mesoporous silica molecular sieves with wormhole framework structures, such as the MSU-X family of materials, are also assembled from

neutral surfactants and cost-intensive silicon alkoxides.[10] In an effort to replace the costly alkoxides with sodium silicate, Guth and co-workers reported the preparation of disordered mesostructures from sodium silicate solutions in the presence of a non-ionic surfactant. The complete removal of the surfactant from the products by calcination at 600 °C, however, led to either the extensive restructuring of the silica framework or to the formation of a completely amorphous material.[11] More recently, Kim et al achieved the high-yield synthesis of stable wormhole molecular sieve silicas from low-cost, water-soluble silicate precursors and non-ionic surfactants at near neutral pH.[12] They further demonstrated that it is possible to assemble from sodium silicate *highly ordered* mesoporous silica molecular sieves with very large framework pore structures analogous to both hexagonal SBA-15 and MCF, which are denoted as MSU-H and MSU-F, respectively.[13]

### 4.2.2 Modifications of foam structures

Kaliaguine reported the synthesis of Zeolite-coated mesocellular aluminosilicate foams (zeolite-coated-MCF) synthesized by a two-step procedure. The first step consists of the preparation of the mesocellular alumosilicate foam precursor (MCF) according to the method described earlier and then the desired clear zeolite gel solution containing primary zeolite seeds (NaY and ZSM-5). The second step is a coating of nanozeolite seeds on the MCF surface using the diluted clear zeolite gel. [14] They further conclude that the mesoporous structure of the parent sample had collapsed after this treatment. By contrast, no significant change in the mesopore structure under the same

treatment conditions indicates that the coated samples are much more hydrothermally stable than is the parent MCF sample. This could be attributed to the zeolite seeds coated on the mesopore surface, which create valence bonds with the precursor and heal defect sites, reducing consequently the concentration of silanol groups. It can be concluded that zeolite coated MCF is promising as a new acid catalyst for the conversion of bulky molecules at high temperature. The methodology of coating zeolite seeds into the wall surface of mesoporous aluminosilicates as a means of improving hydrothermal stability and acidity is quite simple, general, and applies to various kinds of zeolite guests and mesoporous materials hosts.

Anderson et al reported the synthesis of macroporous cellular foams using cetyltrimethylammonium bromide (CTAB) and trimethylbenzene (TMB) as a modified oil-water emulsion system.[15] The foams obtained by this method are claimed to be a useful support material for enzyme catalysis and bio-molecular sieving. Imhof and Pine reported the synthesis of titania foams using Pluronic 123 as a template and titaniumtetraisopropoxide as the titania source. These materials could be rendered crystalline by calcining them at higher temperature. The calcined samples showed a mixture of anatase and rutile phases. High temperature calcinations had very little effect on the macroporosity of these materials, but a significant decrease in mesoporosity and surface area was observed. [2]

Recently Tatsumi et al synthesized a new mesoporous carbon consisting of aggregates of uniformly sized spherical particles are aggregated. The

structure is directed by the carbonization of sucrose in the pores of meso-cellular foam silica. The BET specific surface area and the transmission electron micrograph demonstrate that the carbon particles are not solid spheres but hollow ones whose diameter and the thickness of the wall are 30 and 3 nm, respectively.[16]

Liu and Pinnavaia reported the synthesis of steam stable aluminosilicates MSU-S/F structures using protozeolitic clusters as the aluminosilicate source. [17] The materials thus synthesized were reportedly steam stable to 800 °C in up to 20% steam. They further demonstrated using $^{27}Al$ NMR that 85% of the aluminum centers were retained in the mesostructure even after steaming at an overall Si/Al ratio of 50. These materials were shown to have good catalytic activity in the acid catalyzed cracking of cumene at 300 °C.

## 4.3 Experimental Section

**Materials.** The silica source was sodium silicate (27 % $SiO_2$, 14 % NaOH) from Aldrich, and the source of aluminum is sodium aluminate ($NaAlO_2$) from Strem Chemicals Inc. The templating agent was ($PPO_{70}$-$PEO_{20}$-$PPO_{70}$) P123 obtained from BASF. The swelling agent was 1,3,5-trimethylbenzene (TMB) purchased from Aldrich. Acetic acid ($CH_3COOH$; 99%) was from Merck. All these chemicals were used directly without further purification.

**4.3.1 General Procedure for Microemulsion Templating of MSU-F Silicas.** MSU-F silicas are prepared in acidic solutions of P123 and sodium silicate with TMB as the organic swelling agent. In a typical preparation, 1.2 g of P123 was dissolved in 10 mL of water and 10 mL of 1M acetic acid at room temperature. Desired amounts of TMB are added, and the mixture was shaken at room temperature. Following 1 h of shaking, 2.7 g of sodium silicate solution in 30 mL of water was added. After 20 h at 35 °C, the precipitate mixture was aged at 100 °C for upto 24 h under static conditions. The mixture was then allowed to cool to room temperature, and the precipitate was isolated by filtration, washed with water, and allowed to air-dry at room temperature for at least 2 d.

**4.3.2 Characterization**

Nitrogen adsorption-desorption isotherms were obtained at –196 °C on a Micromeritics Tristar 3000 sorptometer using static adsorption procedures. Samples were outgassed at 150 °C and $10^{-6}$ Torr for a minimum of 12 h prior to analysis. BET surface areas were calculated from the linear part of the BET plot

according to IUPAC recommendations. The cell size and the window size were determined by the adsorption branch and the desorption branch of the isotherm, respectively, the BJH and the BdB-FHH method.

TEM images were obtained on a JEOL 100CX microscope with a $CeB_6$ filament and an accelerating voltage of 120 KV, aperture of 20 $\mu$m. Sample grids are prepared via sonication of powdered sample in ethanol for 20 min and evaporating 1 drop of the suspension onto a carbon-coated, holey film supported on a 3 mm, 300 mesh copper grid. Alternatively TEM sample preparation was done by ultramicrotomy. The basic protocol for ultramicrotomy was as follows: The sample was embedded in a polymeric resin LR-White™, which was than cured in a mold so as form a capsule. The capsule was than trimmed to requisite proportions so that it can be cut to ultra-thin sections at places where the sample was located using an ultramicrotome.

## 4.4 Results and Discussion

### 4.4.1 Effect of TMB/P123 ratios

In this study, the amounts of trimethylbenzene (TMB) added to the P123 solutions were systematically varied to control of the pore size in mesoporous silicas with large pore. By using a fixed amount of P123, acetic acid, sodium silicate, and water, it was possible to vary the TMB/P123 mass ratio from 0 to 1.25. Figure. 4.4 A and 4.4 B show the $N_2$ adsorptions isotherms and BJH pore size distributions, respectively, for calcined samples prepared at varied TMB/P123 mass ratio. As the TMB/P123 mass ratio increased, the positions of the adsorption branches for the samples shifted toward higher partial pressures, which indicates the framework pore size enlarges, and the pore volume increases. The physical properties of samples prepared at varied TMB/P123 ratio are listed in Table 4.1.

A higher TMB/P123 mass ratio leads to adifferent framework structure of mesostructured cellular foams MSU-F as compared with the highly ordered hexagonal structure of MSU-H. MSU-H type silicas are formed at TMB/P123 < 0.2, while MSU-F are assembled at TMB/P123 ≥ 0.4. A similar behavior is observed for the formation of SBA-15[18] and MCF[8] silicas. In the absence of TMB, P123 forms cylindrical micelles in aqueous solution, which is in agreement with literature data.[19] It is proposed that MSU-H with a hexagonal framework structure is formed upon addition of sodium silicate to the P123 micelles. The presence of small amounts of TMB (TMB/P123 < 0.2) may lead to periodic undulation in the cylindrical micelle of P123 surfactants and give rise to MSU-H

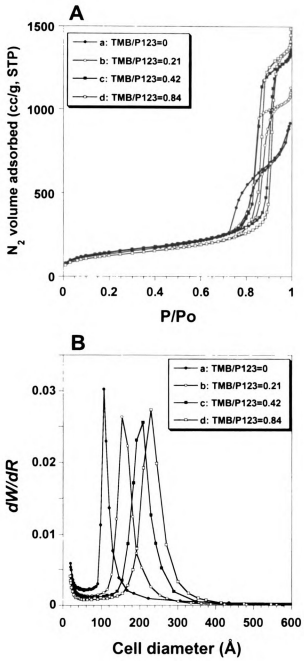


**Figure 4.4**. (A) Nitrogen adsorption-desorption isotherms and (B) BJH pore size distribution plots for calcined mesoporous silicas synthesized at TMB/P123 mass ratios of (a) 0.00, (b) 0.21, (c) 0.42 and (d) 0.84. The samples were first assembled at 35 °C for 20 h and subsequently aged at 100 °C for 20 h.

**Table 4.1**. Physicochemical properties of mesoporous silicas assembled at different TMB/P123 mass ratios (w/w)[a].

| sample | TMB/P123 (w/w) | Cell diameter (nm) | Window diameter (w/w) | $S_{BET}$ ($m^2/g$) | Pore volume ($cm^3/g$) |
|---|---|---|---|---|---|
| 1 | 0 | 10.6 | b | 488 | 1.42 |
| 2 | 0.21 | 15.2 | b | 525 | 1.75 |
| 3 | 0.42 | 20.8 | 12.7 | 514 | 2.17 |
| 4 | 0.63 | 22.6 | 14.7 | 448 | 2.18 |
| 5 | 0.83 | 22.9 | 14.4 | 444 | 2.31 |
| 6 | 1.25 | 22.6 | 14.5 | 543 | 2.46 |

a) Cell diameter and window diameter determined according BJH method. The initial assembly was carried out at 35 °C for 20 h and then aging at 100 °C for 20 h at $P123/SiO_2 = 0.16$

b) These reactions products had a hexagonal (MSU-H) structure

type material, hexagonal silicas with pore sizes of < 15 nm. At TMB/P123 ≥ 0.4, microemulsion templating takes over, and spherical, TMB-swollen P123 template the formation of MSU-F. The amount of TMB plays a major role in determining the structures of the mesoporous silicas assembled by TMB/P123 templates.[20]

Further evidence for changes in the framework structure of mesoporous silicas at varying TMB/P123 mass ratios is provided by the typical transmission electron micrograph (TEM) image shown in Figure 4.5. Figure 4.5 A clearly exhibits the ordered hexagonal framework structure of MSU-H prepared without addition of TMB. In comparison to conventional SBA-15, which has a particle size in the micrometer range, MSU-H shows smaller particle sizes in the range of 300 –500 nm.[5,13] The synthesis temperature provides a means to control the particle size of MSU-H.[21] In general, smaller particle sizes provided textural mesoporosity, evidenced by nitrogen adsorption isotherms, which improved catalytic reactivity in some liquid phase reactions.[22] Accordingly, owing to the textural mesoporosity of MSU-H, MSU-H should be a more promising catalyst than SBA-15.

At a TMB/P123 mass ratio of 0.21, TEM images of the sample shows a change in the morphology of the framework structure. The walls of cylindrical pores began to buckle forming spherical nodes. Figure 4.5 C and D show images of bulk and an ultra thin section of mesostructured cellular foams formed at a TMB/P123 mass ratio of 0.84. Large mesopores with uniform and regular sizes are visible in the TEM images in Figure 4.5 D. The large pores appear to be

**Figure 4.5**. TEM images of calcined mesoporous silicas synthesized at TMB/P123 mass ratios of (A) 0.00, (B) 0.21, and (C) 0.84. Image of (D) represent an ultra thin section of (C) sample. No ethanol was present in the reaction mixture.

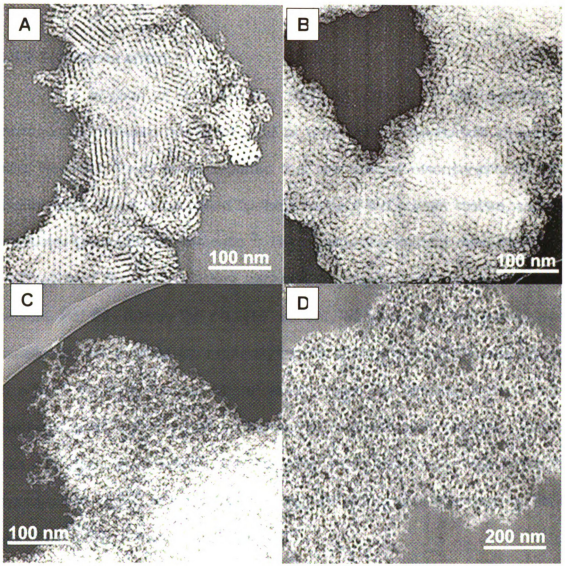
A
100 nm
B
100 nm
C
100 nm
D
200 nm

separated by thin silica walls, and the overall structure consists of roughly spherical cells separated by thin silica walls.

### 4.4.2 Co-solvent effect

The addition of a co-solvent, such as ethanol, in the synthesis of mesoporous materials has been used as a modifier of the particle shape and size. Recently, Pauly et al. reported that the textural mesoporosity of HMS mesoporous silicas is controlled by the polarity of the solvent system, such as the water-to-ethanol volume ratio.[22] The sponge-like textural mesoporosity of HMS allowed the more efficient transport of reagents to framework reaction centers. For this reason the catalytic reactivity of sponge-like HMS particles is usually superior to MCM-41, especially for conversions involving large substrates in a liquid reaction medium where reaction rates are diffusion limited. In the synthesis of MCF from TEOS by the method of Stucky and coworkers, ethanol was also used as co-solvent, but the ethanol was essentially released by the hydrolysis of TEOS. At the same time, they did not provide adequate results to reveal the effect of ethanol as co-solvent.[8]

One of objectives of this study was to investigate the possibilities of tailoring both the framework structure and size of MSU-F silicas by varying the ethanol volume% over the range from 0 to 20. Figure 4.6 provides the nitrogen adsorption isotherms and BJH pore size distributions, respectively, for calcined MSU-F silicas prepared at varying ethanol volume% while keeping the TMB/P123 mass ratio constant at 0.84. The shift to higher relative pressures

**Figure 4.6.** Nitrogen adsorption-desorption isotherms for MSU-F silicas prepared at varying ethanol volume % (A) 0, (B) 5, (C) 10, (D) 15, and (E) 20. The samples were assembled at 35 °C for 20 h and subsequent at 100 °C for 20 h with TMB/P123 mass ratio of 0.84. Insert: The BJH cell and window size distributions from the adsorption and desorption isotherm branches, respectively.

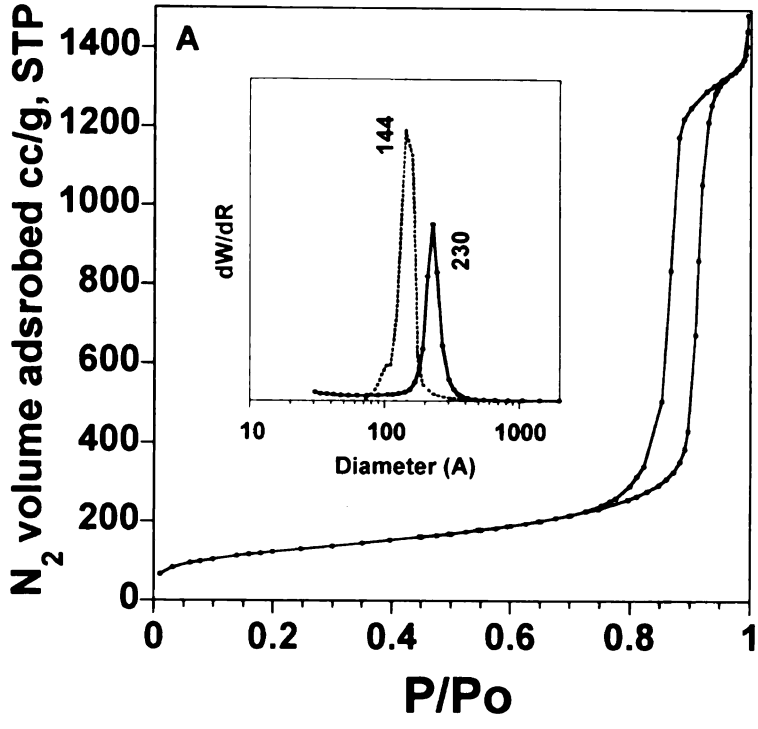
A
$N_2$ volume adsrobed cc/g, STP
1400
1200
1000
800
600
400
200
0
0
0.2
0.4
0.6
0.8
1
P/Po
dW/dR
144
230
10
100
1000
Diameter (A)

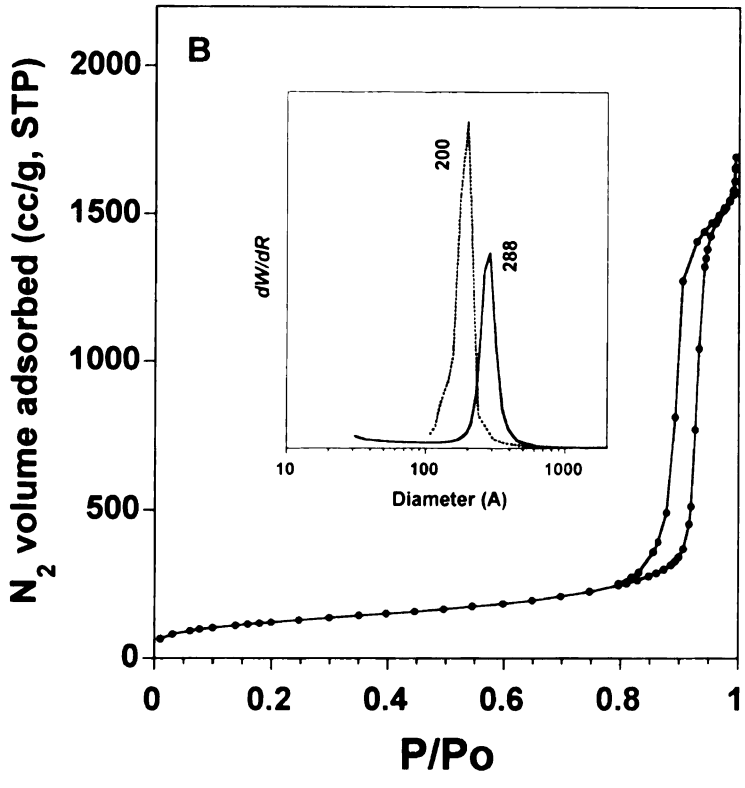
B
$N_2$ volume adsorbed (cc/g, STP)
2000
1500
1000
500
0
0
0.2
0.4
0.6
0.8
1
P/Po
dW/dR
200
288
10
100
1000
Diameter (A)

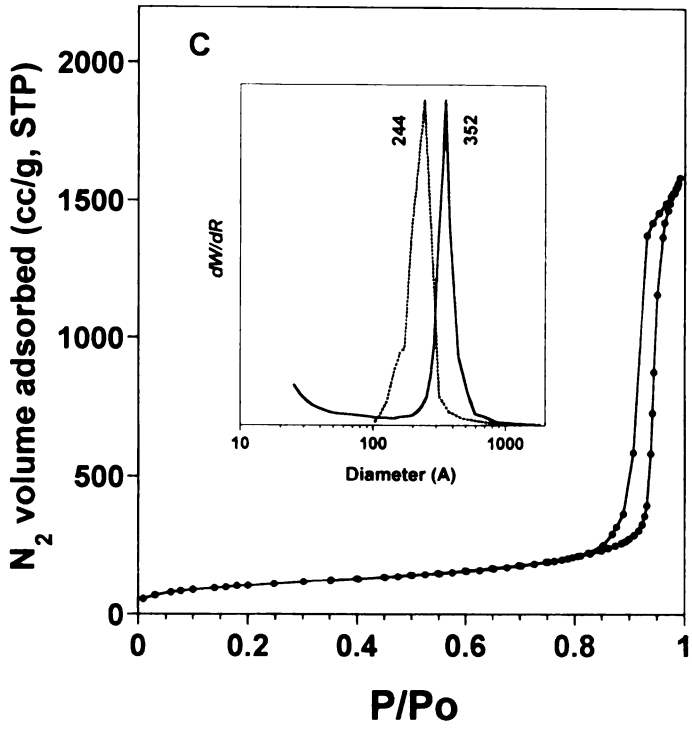
C
2000
1500
1000
500
0
0
0.2
0.4
0.6
0.8
1
N2 volume adsorbed (cc/g, STP)
P/Po
dW/dR
244
352
10
100
1000
Diameter (A)

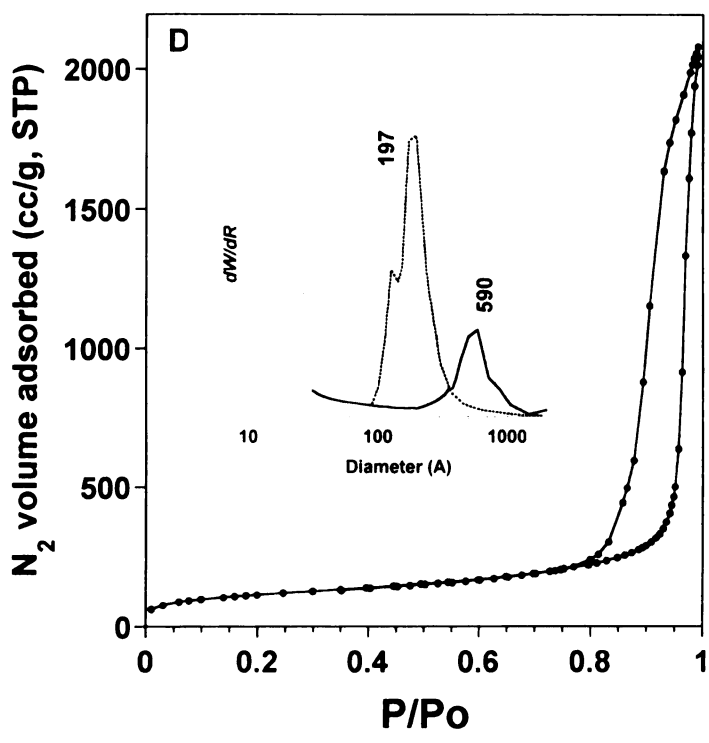
D
2000
1500
1000
500
0
0
0.2
0.4
0.6
0.8
1
N2 volume adsorbed (cc/g, STP)
P/Po
dW/dR
197
590
10
100
1000
Diameter (A)

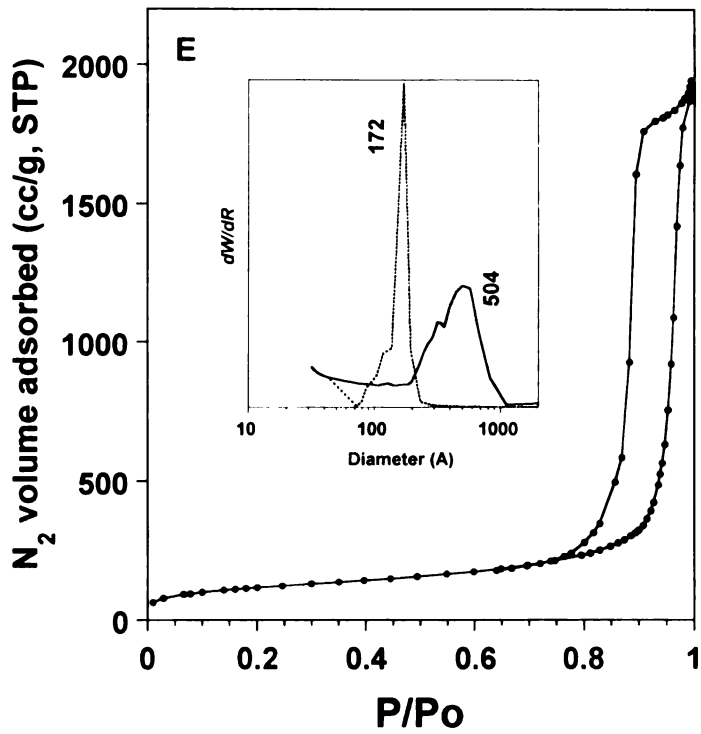
E
2000
1500
1000
500
0
0
0.2
0.4
0.6
0.8
1
P/Po
N2 volume adsorbed (cc/g, STP)
dW/dR
172
504
10
100
1000
Diameter (A)

**Table 4.2**. Physicochemical properties of MSU-F silicas assembled at different ethanol concentration [a]

| Sample | EtOH (vol %) | Cell diameter (nm) | Window diameter (w/w) | $S_{BET}$ ($m^2/g$) | Pore volume ($cm^3/g$) |
|---|---|---|---|---|---|
| 7 | 0 | 22.9 | 14.4 | 444 | 2.31 |
| 8 | 5 | 28.8 | 20.0 | 440 | 2.63 |
| 9 | 10 | 35.2 | 24.4 | 374 | 2.46 |
| 10 | 15 | 59.0 | 19.7 | 408 | 3.23 |
| 11 | 20 | 50.4 | 17.2 | 451 | 3.01 |

a) The initial assembly was carried out at 35 °C for 20 h and then the reaction mixture was aged at 100° C for 20h, at TMB/P123=0.83 (w/w) and P123/$SiO_2$= 0.16

b) Cell diameter and window diameter determined according BJH method.

indicates an increase in cell size with increasing ethanol volume %. The MSU-F silicas prepared at ethanol vol % ≥ 15 shows a widening of the hysteresis loop between adsorption and desorption branches in comparison to the MSU-F silicas prepared at lower ethanol concentraion of 0, 5, and 10 %. The higher hysteresis loop indicates an increasing difference between the size of the cells and the size of the window. The cell size distribution determined from the adsorption branch of the isotherm for the calcined MSU-F silicas, are shown in Figure 4.6 and listed in Table 4.2. Varying the ethanol content has a remarkable influence on the cell size of MSU-F silica. The cell size increased with increasing amount of ethanol from 22.9 nm at 0 vol% ethanol to 59 nm at 15%, a relative 158% increase. At higher ethanol volume% ≥ 15, the cell size distributions were broader than those of MSU-F prepared at ethanol vol% ≤ 10. On the other hand, the window size remains in the range of 14-24 nm over the entire ethanol concentration range.

In order to understand further the relation between the characterizations of $N_2$ adsorptions isotherms, and pore structure and pore size of MSU-F the transmission electron micrograph (TEM) technique was used to image the cells. In the TEM images on ultra thin sections of the foams (Figure 4.5 D and 4.7 B), we can see clearly the characteristic mesostructured cellular foams structure. The cell size of MSU-F prepared in pure water is very uniform and their shapes are also very regular (Figure 4.5 D). Figure 4.7 A and Figure 4.7 B shows a TEM image of a bulk sample (Figure 4.7 A) and an ultra thin section (Figure 4.7 B) of calcined MSU-F prepared at an ethanol vol% of 15. The material exhibits larger cell size (from 33 to 55 nm) and regular cell size distribution.

**Figure 4.7**. TEM image of (A) calcined MSU-F silicas synthesized at ethanol 15 vol %. The sample was assembled at TMB/P123 mass ratio of 0.84

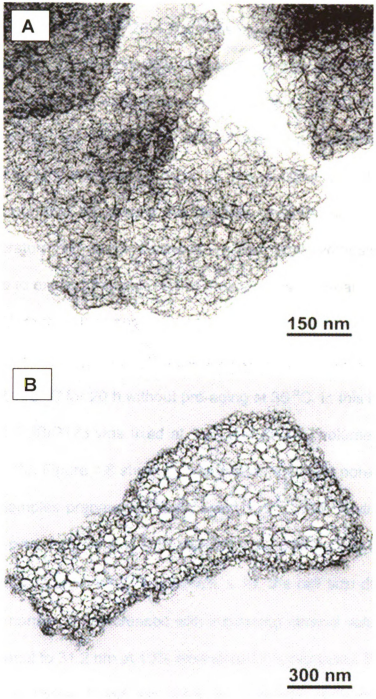
A
150 nm
B
300 nm

### 4.4.3 MSU-F silica with a cell size of 84.4 nm

In the previous section MSU-F silicas were prepared in the presence of TMB and ethanol at 35 °C for 20 h and subsequently aged at 100 °C for 20 h. In this way, we have found it possible to selectively assemble MSU-F silicas with desired the cell sizes and window sizes in the range of 20–60 nm and 12–40 nm, respectively. When the assembly of MSU-F was first performed at 35 °C and followed at 100 °C in ethanol volume% 15, the resulting MSU-F has the largest cell size of around 60 nm among the samples observed so far. In general, the aging temperature in direct synthesis or/and post-synthesis plays a very important role to expand the pore size of mesoporous materials.

To explore the other possibility of controlling the cell size and the window size of MSU-F through aging temperature, MSU-F silicas were directly assembled at 100 °C for 20 h without pre-aging at 35 °C. In this investigation, the mass ratio of TMB/P123 was fixed at 0.83 and ethanol volume% as co-solvent varied from 0–20. Figure 4.8 show $N_2$ adsorptions and BJH pore size distribution for calcined samples prepared at direct aging 100 °C and varying ethanol vol%, and the total pore volume and BET surface area of the calcined samples are listed in Table 4.3. At an ethanol volume% ≤ 10, the cell size distributions were very uniform, narrow, and increased with increasing ethanol volume% from 24.5 nm at 0% ethanol to 31.2 nm at 10% ethanol (a 27% increase). These results are very similar to those found for products prepared through post-synthesis treatment in co-solvent effect section. However, an MSU-F silica with the cell size of 84.4 nm and the window size of 39.7 nm was prepared

**Table 4.3**. Physicochemical properties of MSU-F silica's prepared by directly heating the reaction mixture at 100 °C for 20 h.[a]

| Sample | EtOH (vol %) | Cell diameter (nm) | Window diameter (w/w) | $S_{BET}$ ($m^2/g$) | Pore volume ($cm^3/g$) |
|---|---|---|---|---|---|
| 12 | 0 | 24.5 | 16.0 | 458 | 2.38 |
| 13 | 5 | 28.4 | 20.0 | 448 | 2.59 |
| 14 | 10 | 31.2 | 20.2 | 451 | 2.91 |
| 15 | 15 | 84.4 | 39.7 | 200 | 2.27 |
| 16 | 20 | 58.9 | 38.7 | 307 | 2.92 |

a) Initial synthesis carried out at TMB/P123=0.83 (w/w); P123/$SiO_2$ =0.16

b) Cell diameter and window diameter determined according BJH method.

**Figure 4.8**. Nitrogen adsorption-desorption isotherms for MSU-F silicas prepared at aging 100 °C and at varying ethanol volume% (A) 0, (B) 5, (C) 10, (D) 15, and (E) 20. The samples were assembled with TMB/P123 mass ratio of 0.84. Insert: The BJH cell and window size distribution from adsorption and desorbtion isotherms branches respectively.

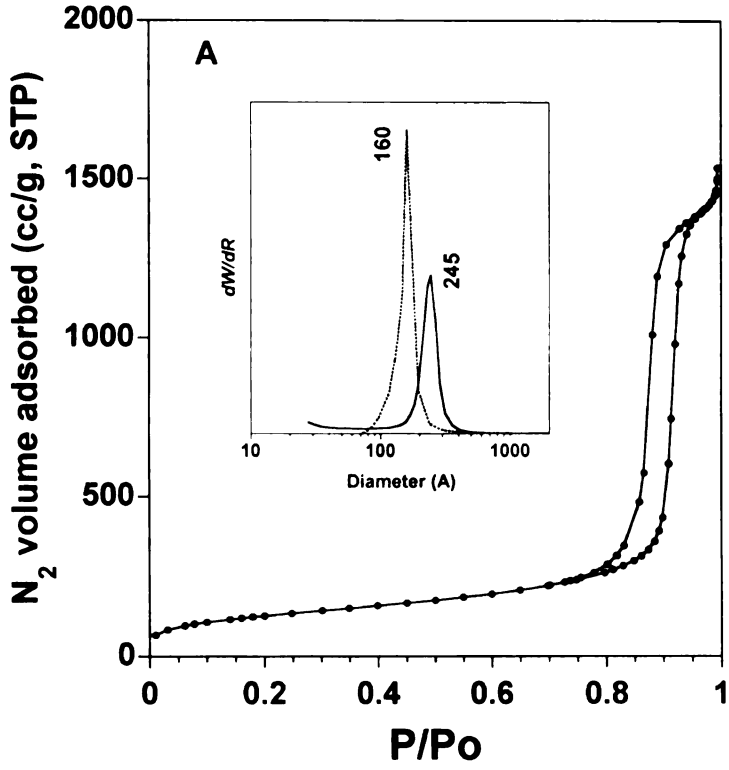
A
2000
1500
1000
500
0
0
0.2
0.4
0.6
0.8
1
P/Po
N2 volume adsorbed (cc/g, STP)
dW/dR
160
245
10
100
1000
Diameter (A)

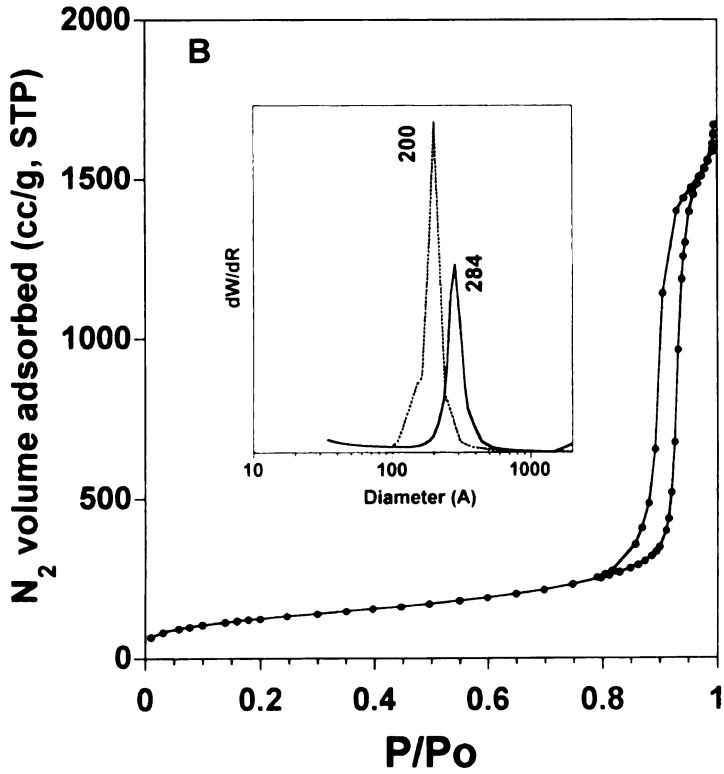
B
2000
1500
1000
500
0
0
0.2
0.4
0.6
0.8
1
P/Po
N2 volume adsorbed (cc/g, STP)
dW/dR
200
284
10
100
1000
Diameter (A)

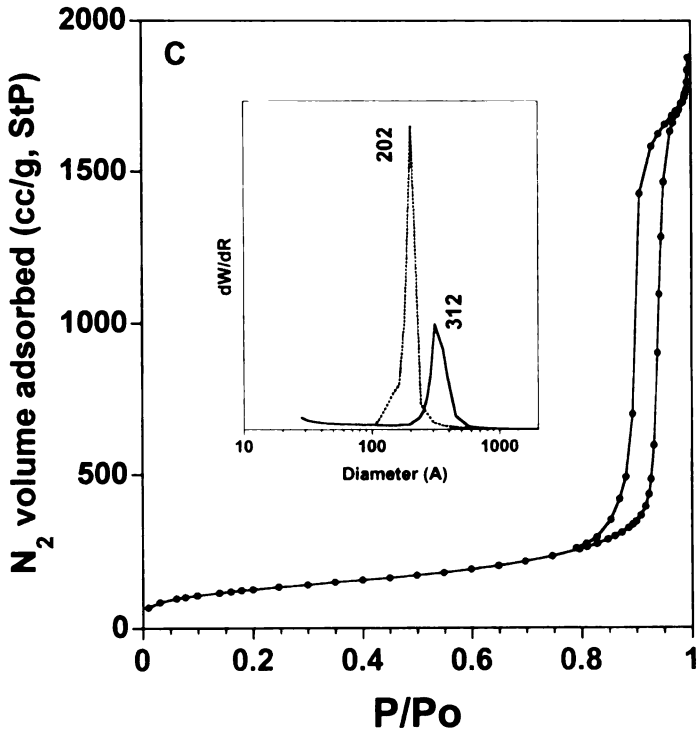
C
2000
1500
1000
500
0
0
0.2
0.4
0.6
0.8
1
P/Po
N2 volume adsorbed (cc/g, StP)
dW/dR
202
312
10
100
1000
Diameter (A)

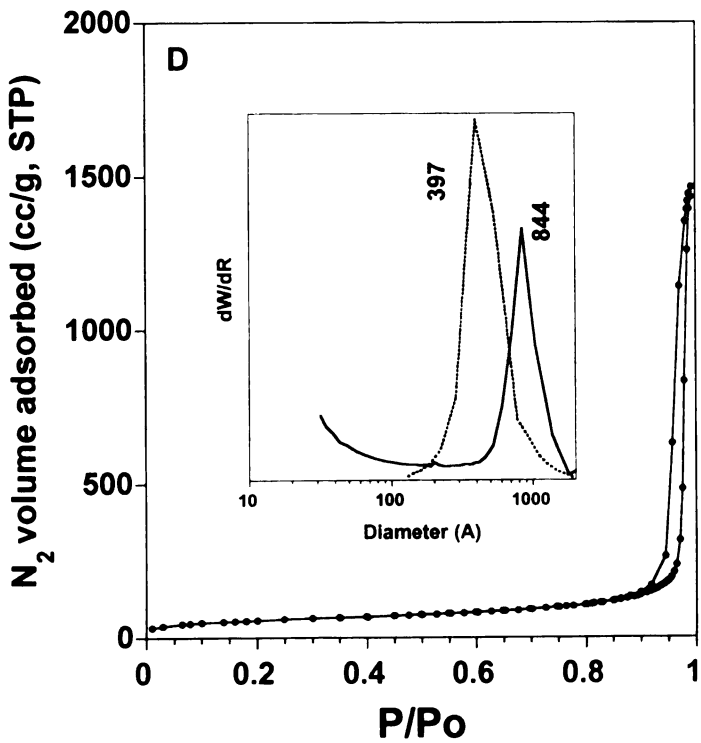
D
2000
1500
1000
500
0
0
0.2
0.4
0.6
0.8
1
P/Po
N2 volume adsorbed (cc/g, STP)
dW/dR
397
844
10
100
1000
Diameter (A)

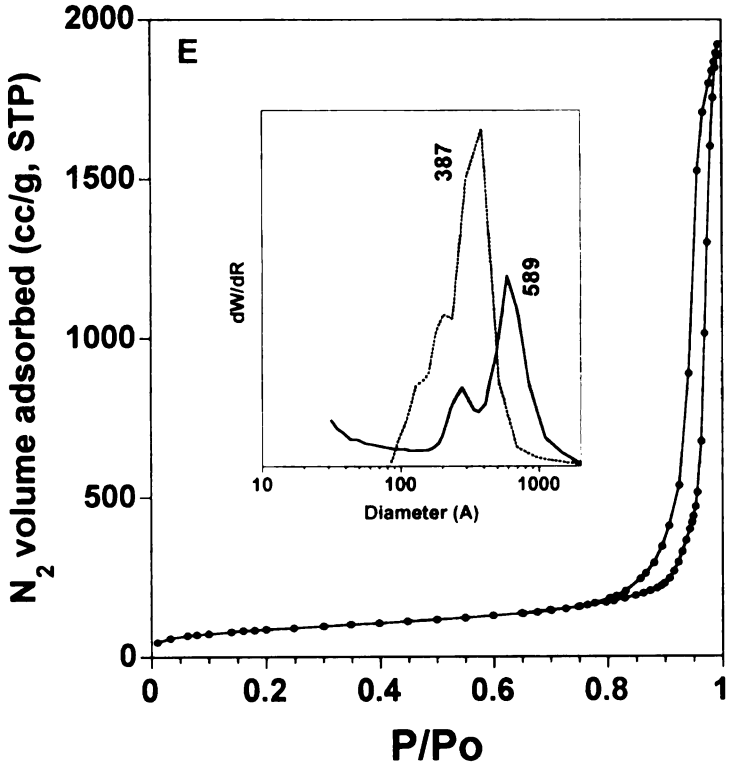
E
2000
1500
1000
500
0
0
0.2
0.4
0.6
0.8
1
P/Po
N2 volume adsorbed (cc/g, STP)
dW/dR
387
589
10
100
1000
Diameter (A)

in 15 volume% ethanol at 100 °C for 20 h. The latter cell size is out of mesopore range, but in the macropore range. The cell size and the window size are 1.4 and 2.0 times larger than those prepared at post-synthesis treatment, respectively. TEM image (not shown) of the sample with the cell size of 84.4 nm is very similar to that of sample in Figure. 4.7. The sample exhibits the largest cell sizes of 84.4 nm in the series of MSU-F silicas in this study.

### 4.4.4 Effect of hydrothermal aging time

Figure 4.9 provides the nitrogen isotherms for calcined MSU-F silica foams that have been assembled at room temperature for 24 h and then subjected to post-assembly hydrothermal treatment at 100 °C. The corresponding cell size distributions are illustrated in Figure 4.10. Table 4.4 reports the BET surface areas, pore volumes and the cell and the window sizes of the reaction products, as determined by applying the BdB-FHH[23] model to the adsorption and desorption isotherms, respectively.

The foam assembled under ambient reaction conditions without post-synthesis hydrothermal treatment exhibited a broad hysteresis in the nitrogen adsorption - desorption isotherms (Figure. 4.9, curve 0h). This behavior is typical of a "closed cell" foam, wherein comparatively narrow 5.6 nm windows connect cells of diameter 16.3 nm. In addition to exhibiting an average cell-to-window size ratio of 2.91, this initial silica foam is characterized by a BET surface area of 743 $m^2g^{-1}$ and a mesopore volume of 1.02 $cm^3g^{-1}$.

Hydrothermal treatment of the as-made foam for a period of 1 h at 100 $^0$C produced a product (denoted MSU-F-P1) that exhibits $N_2$ adsorption - desorption isotherms that are very similar in shape to those of the as-made sample (c.f., curves a and b in Figure 4.9). This indicates that little or no change in cell or window size occurs after a one-hour hydrothermal treatment, as verified by the data in Table 4.4 (compare samples MSU-F-P0 and MSU-F-P1). However, the surface area is increased substantially by ~ 125 $m^2g^{-1}$, along with an increase in pore volume, after a one-hour post-assembly hydrothermal treatment. This suggests that the foam framework is not fully formed under ambient conditions and that subsequent hydrothermal treatment facilitates framework ordering.

Increasing the post-synthesis treatment time to 2 h shifts the step in the adsorption branch toward higher pressure and causes the hysteresis loop to become narrower (see curve 2h, Figure 4.9), signifying an increase in both the cell size and window size (c.f., Table 4.4). At this point in the hydrothermal treatment the cell to window size ratio is 2.14, and the foam can still be classified as a "closed cell" structure. However, after 4 h of hydrothermal treatment the cells and windows grow even larger to values of 25.3 and 16.9 nm, respectively, and the cell to window ratio decreases to 1.49, which is consistent with an open cell foam structure. After 8 h of treatment still greater increases in cell and window sizes are realized. After 24 h, the cell and window sizes approach near-equilibrium values of 34.7 and 22.9 nm, respectively, and a cell to window size ratio of 1.51. The surface areas decrease, and the total pore volumes increase as the cell and window sizes become larger with increasing hydrothermal

treatment, as expected. The observed behavior confirms that the cell size of MSU-F can be tailored through post-assembly hydrothermal treatment and that closed cell foams can be readily transformed into open cell structures through this process.

Further evidence for mesostructured cellular foams of MSU-F silica is provided by the transmission electron micrographs in Figure 4.11. Images A and B for the closed cell product assembled at room temperature are typical of a mesostructured cellular foam structure. Images C and D for the product after being hydrothermally treated for 24 h are similar, except that the cell size is larger, in accord with the nitrogen adsorption results.

**Table 4.4**. Textural Properties of MSU-F Silica Foams After Post –Synthesis Hydrothermal Treatment at 100° C for 0 – 24 h.

| Sample | Time of post-treat (Hrs) | Cell Size (nm) | Window Size (nm) | CellSize/ Window Size | Surface Area ($m^2/g$) | Pore Volume ($cm^3/g$) |
|---|---|---|---|---|---|---|
| MSU-F-P0 | 0 | 16.3 | 5.6 | 2.91 | 608 | 1.02 |
| MSU-F-P1 | 1 | 16.4 | 5.6 | 2.92 | 743 | 1.14 |
| MSU-F-P2 | 2 | 19.5 | 9.1 | 2.14 | 745 | 1.91 |
| MSU-F-P4 | 4 | 25.3 | 16.9 | 1.49 | 573 | 2.18 |
| MSU-F-P8 | 8 | 28.1 | 20.5 | 1.37 | 492 | 2.33 |
| MSU-F-P24 | 24 | 34.7 | 22.9 | 1.51 | 468 | 2.39 |

* Each sample was assembled at ambient temperature at aTMB/P123 mass ratio of 0.83 prior to hydrothermal treatment and subsequently calcined at 600 °C for 4h to remove the surfactant and co-surfactant.

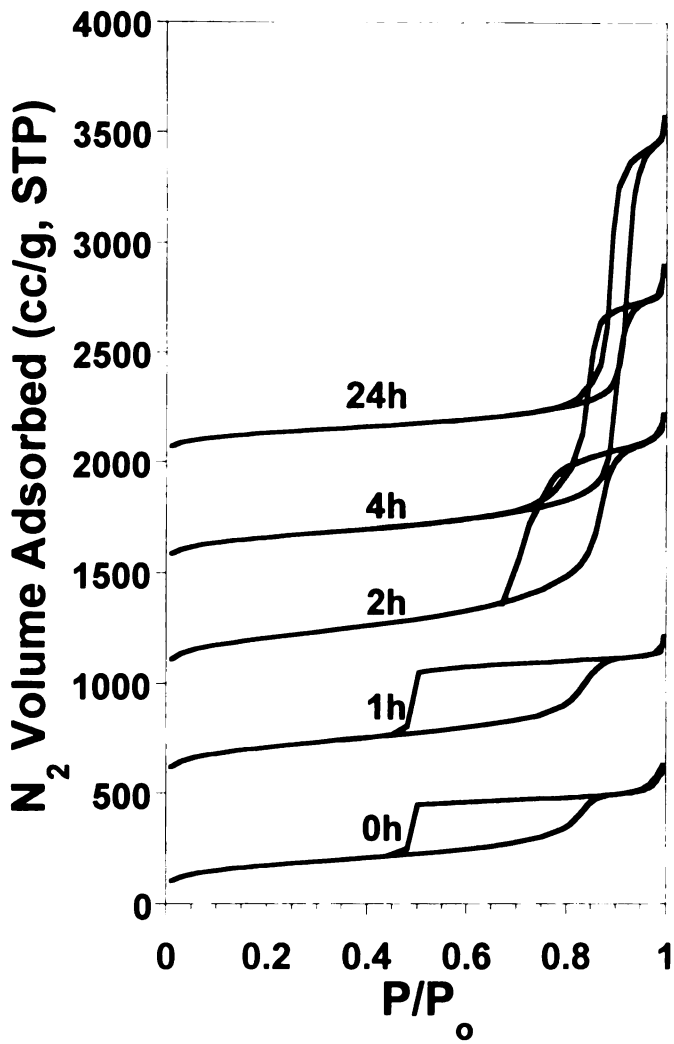


**Figure 4.9.** Nitrogen adsorption/desorption isotherms for calcined MSU-F silicas prepared through post-synthesis hydrothermal treatment of the as-made mesostructure for periods of 0 – 24 h at 100 °C.

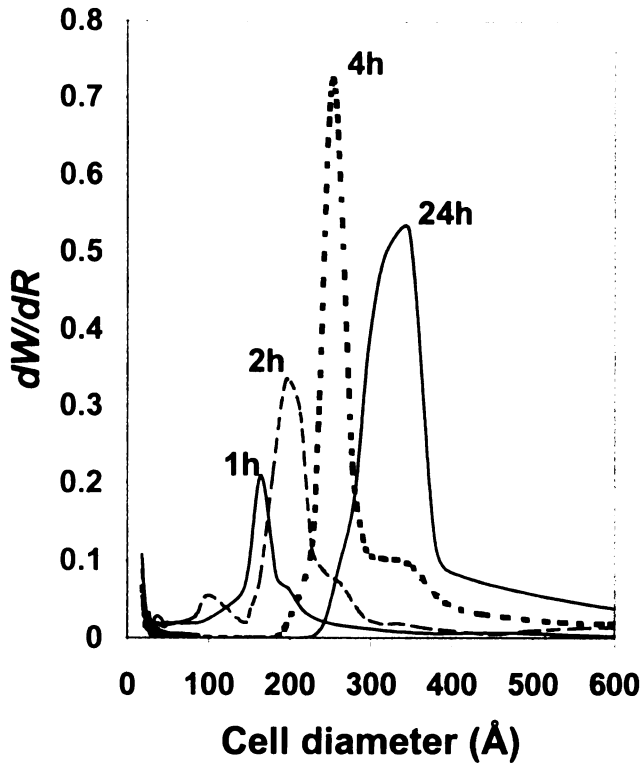


**Figure 4.10.** Cell size distributions for calcined MSU-F silicas prepared trough post-synthesis hydrothermal treatment of the as-made mesostructure for periods of 0 – 24 h at 100 °C. The cell sizes were determined by applying the BdB-FHH model to the adsorption isotherms shown in Figure 4.9.

**Figure 4.11**. TEM images of calcined MSU-F silica foams. Images (A) and (B) are for a whole particle and thin-sectioned samples, respectively, of the closed cell foam assembled at ambient temperature. Images (C) and (D) are whole particle and thin-sectioned samples, respectively, of the open cell structure obtained after 24hours of post-assembly hydrothermal treatment at 100 °C.

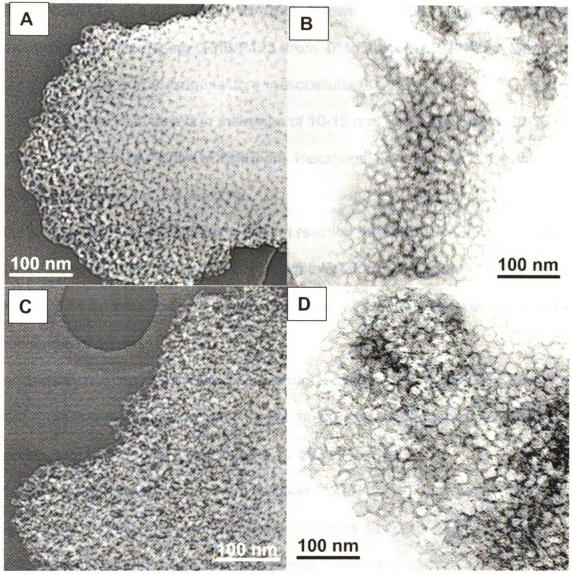
A
100 nm
B
100 nm
C
100 nm
D
100 nm

## 4.5 Summary

Assembly of silica mesotructures from sodium silicate and P123 at pH = 5.6, P123/$SiO_2$ = 0.016, 35 $^0$C for 20 h followed by 100 $^0$C; and TMB as an emulsifier. (a) Increasing TMB/P123 from 0 to beyond 0.21 transforms the mesostructures from hexagonal to a mesocellular foam.

The hexagonal pore size is in the range of 10-15 nm. Foam cell size is 20-33 nm, window size is in the range of 13-15 nm. Hexagonal pore volume is 1.4 cc/g; Foam pore volume is 2.2-2.5 cc/g.

(b) Adding 0-20 vol. % ethanol to a foam reaction mixture at TMB/P123= 0.83 (w/w) increases the cell size from ~ 23 nm to 50-60 nm. Window size is in the range of 14-24 nm. That is the cell expands by > 20-30 nm, window expands by maximum of 10 nm.

(c) Directly heating a foam reaction mixture TMB/P123= 0.83 to 100$^o$ C (w/o the 35$^o$ C digestion step) tends to increase both the cell size and the window size, particularly if ethanol is present at the 15-20 vol. % level.

(d) Post synthesis aging of a foam reaction TMB/P123= 0.83 (w/w) at 100$^o$ C in absence of ethanol increase both cell and window sizes while keeping the difference between the cell and window size constant at ~10 nm

## 4.6 References


(1) Corma, A. *Chem. Rev.* **1997**, *97*, 2373-2419.

(2) Imhof, A.; Pine, D. J. *Adv. Mater.* **1998**, *10*, 697-700.

(3) Lukens, W. W.; Yang, P. D.; Stucky, G. D. *Chem. Mater.* **2001**, *13*, 28-34.

(4) Zhao, D.; Feng, J.; Huo, Q.; Melosh, N.; Frederickson, G. H.; Chmelka, B. F.; Stucky, G. D. *Science* **1998**, *279*, 548-552.

(5) Zhao, D.; Huo, Q.; Feng, J.; Chmelka, B. F.; Stucky, G. D. *J. Am. Chem. Soc.* **1998**, *120*, 6024-6036.

(6) Zhao, D. Y.; Feng, J. L.; Huo, Q. S.; Melosh, N.; Fredrickson, G. H.; Chmelka, B. F.; Stucky, G. D. *Science* **1998**, *279*, 548-552.

(7) Kim, S.S.; Pauly, T. R.; Pinnavaia, T. J. *Chem. Commun.* **2000**, 1661-1662.

(8) Schmidt-Winkel, P.; Lukens, W. W., Jr.; Zhao, D.; Yang, P.; Chmelka, B. F.; Stucky, G. D. *J. Am. Chem. Soc.* **1999**, *121*, 254-255.

(9) Schmidt-Winkel, P.; Lukens, W. W., Jr.; Yang, P.; Margolese, D. I.; Lettow, J. S.; Ying, J. Y.; Stucky, G. D. *Chem. Mater.* **2000**, *12*, 686-696.

(10) Boissiere, C.; van der Lee, A.; El Mansouri, A.; Larbot, A.; Prouzet, E. *Chem. Commun.* **1999**, 2047-2048.

(11) Sierra, L.; Lopez, B.; Gil, H.; Guth, J.-L. *Adv. Mater.* **1999**, *11*, 307-311.

(12) Kim, S. S.; Pauly, T. R.; Pinnavaia, T. J. *Chem. Commun.* **2000**, 835-836.

(13) Kim, S. S.; Pauly, T. R.; Pinnavaia, T. J. *Chem. Commun.* **2000**, 1661-1662.

(14) On, D. T.; Kaliaguine, S. *J. Am. Chem. Soc.* **2003**, *125*, 618-619.

(15) Sen, T.; Tiddy, G. J. T.; Casci, J. L.; Anderson, M. W. *Chem. Commun.* **2003**, 2182-2183.

(16) Oda, Y.; Namba, S.; Yoshitake, H.; Tatsumi, T. *Electrochem.* **2002**, *70*, 953-955.

(17) Liu, Y.; Pinnavaia, T. J. *Stud. Surf. Sci. Catal.* **2002**, *142B*, 1075-1082.

(18) Zhao, D. Y.; Huo, Q. S.; Feng, J. L.; Chmelka, B. F.; Stucky, G. D. *J. Am. Chem. Soc.* **1998**, *120*, 6024-6036.

(19) Mitchell, D. J.; Ninham, B. W. *J. Chem. Soc., Faraday Trans. 2: Molecular and Chemical Physics* **1981**, *77*, 601-629.

(20) Lettow, J. S.; Han, Y. J.; Schmidt-Winkel, P.; Yang, P.; Zhao, D.; Stucky, G. D.; Ying, J. Y. *Langmuir* **2000**, *16*, 8291-8295.

(21) Kim, S. S.; Karkamkar, A.; Pinnavaia, T. J.; Kruk, M.; Jaroniec, M. *J.Phys.Che,m.B* **2001**, *105*, 7663-7670.

(22) Pauly, T. R.; Liu, Y.; Pinnavaia, T. J.; Billinge, S. J. L.; Rieker, T. P. *J. Am. Chem. Soc.* **1999**, *121*, 8835-8842.

(23) Lukens, W. W.; Schmidt-Winkel, P.; Zhao, D. Y.; Feng, J. L.; Stucky, G. D. *Langmuir* **1999**, *15*, 5403-5409.

# Chapter 5

# Esterification of Lauric acid with Glycerol using Mesoporous Sulfonic Acids Catalysts

## 5.1 Abstract

Mercaptopropyl-functionalized wormhole mesostructures, denoted MP-HMS, were prepared through the $S^oI^o$ assembly of alkylamine surfactants ($S^o$) and mixtures of 3-mercaptopropyltrimethoxysilane and tetraethyl orthosilicate as framework precursors ($I^o$). Unprecedented levels of organo functionalization, corresponding to at least 50% of the silicon sites, were achieved while retaining well-expressed mesostructures with pore sizes, pore volumes, and surface areas of 2.8 nm, 0.71 $cm^3/g$, and 1220 $m^2/g$, respectively. Also, up to ~ 90% of the framework silicon sites could be fully cross-linked, lending exceptional hydrothermal stability to the mesostructures. The key to highly functionalized MP-HMS derivatives lies in the use of long-chain alkylamine surfactants as structure directors (e.g. octadecylamine) in combination with a relatively high assembly temperature (e.g. 65 °C) and a high-polarity $H_2O$-EtOH solvent. Highly functionalized MP-HMS derivatives are promising materials for use as heavy-metal ion-trapping agents and as precursors for sulfonic-acid-functionalized mesostructured catalysts. These materials were tested for acid catalyzed esterification of glycerol with lauric acid. Conversions as high as 100% in terms of lauric acid were observed with 66% selectivity for the monoester.

## 5.2 Introduction

### 5.2.1 Organofunctional Mesoporous Silica

The discovery of mesoporous materials has raised the general expectation that the catalytic efficiency of microporous zeolites can be expanded to mesoporous dimensions.[1] It is necessary to introduce functionality into MCM or HMS silica structures, so surface modification techniques are receiving considerable attention. It is clear that the pore walls of mesoporous materials are easily modified with organic functional groups. Along with surface modification direct incorporation of organic and inorganic functionality is receiving a lot of attention.[2] In general, direct assembly pathways are preferred over grafting methods, in part, because direct assembly pathways afford a more uniform distribution of organo groups on the framework walls. Also, direct assembly allows for better cross-linking of the silane moiety to the silica framework. For instance, 20-30% of the framework silicon centers in hexagonal SBA-15[3] and MCM-41[4] mesostructures have been functionalized with mercaptopropyl groups through the direct assembly of MPTMS and tetraethyl orthosilicate (TEOS).

Numerous methods have been utilized to attach organic groups to silica surfaces via the formation of covalent bonds.[5] Chlorination of the silica surface followed by subsequent reaction with Grignard reagents can be used to form silicon-carbon bonds. The use of Grignard reagents limits the variety of functional groups that can be tethered to the surface. However, the formation of a silicon-carbon bond between the organic moiety and the surface is desirable because of the stability of the Si-C bond.[6]

Another well-studied technique of silica surface functionalization is the grafting of organic groups onto a silanol-containing surface using a trichloro- or trialkoxy-organosilane.[7,8] Numerous organosilanes are commercially available. Additionally, techniques for synthesizing organosilanes are documented in the literature.[7-9] The availability of the silanol groups can determine whether the grafted silicon atom is tethered via one, two, or three silicon-oxygen bonds. These types of silicon atoms are denoted as $T^1$ ($LSi(OSi)(OR')_2$), $T^2$ ($LSi(OSi)_2(OR')$), and $T^3$ ($LSi(OSi)_3$) sites, respectively, and where L is the desired organofunctional group. Depending on the organosilane and the available number of surface silanol groups, organic loadings of 0.3-2 mmol/g of solid can be obtained. The covalently attached organic groups can be sufficiently stable for recycling and reuse, and can easily be modified to create a variety of catalytic sites.

Grafting of organosilanes onto surfaces through hydroxyl groups is a well-studied and an often used method of forming organic-inorganic hybrid materials. The tethering is done by covalently attaching the organosilane to a surface silicon atom through the silicon (surface)-oxygen-silicon (external)-carbon bond in the organosilane.[5] The silicon-oxygen bond is then external to the surface and can be cleaved under conditions encountered in some catalytic reactions. Obviously, if this occurs, the solids will not function as a recyclable catalyst. It would be desirable to have the carbon bound directly to a silicon atom incorporated within the framework walls. By incorporation of the organosilane into the synthesis mixture during the formation of the solid, the functional group

presents itself on the surface of the framework walls. In this case the organosilane is on the surface of the framework walls. This forms a more uniform dispersion throughout the solid. In this "one-pot" method of assembly, the organosilanes are co-hydrolyzed and condensed with other silica reagents, (e. g., tetraalkoxysilanes,) in the presence of the structure-directing porogen. Issues of importance when selecting the preparation conditions include the solubility of the organosilane in the mixture, the stability of the organic functional group under reaction conditions (pH, temperature), the ease of extracting the structure directing porogen, and the stability of the organic functional group during the porogen extraction process. High loadings of functional groups can be obtained by co-condensation.[2,6] Mann and co-workers reported the first incorporation of organic groups into mesoporous materials by co-condensation methods.[10] Phenyl and *n*-octyl functionalities were incorporated into MCM-41 silica by the "one-pot" method using TEOS as the silica source and hexadecyltrimethylammonium bromide ($C_{16}$TMABr) as the porogen. The porogen was extracted in acidified ethanol at 75 °C for 24 h.

Mercapto-functional mesoporous molecular sieve silicas have received considerable attention as heavy metal ion trapping agents.[4,11-17] The anchored thiol groups also can be easily oxidized to provide sulfonic acid functionality for applications in solid acid catalysis.[3,4,18-21] The potential use of these derivatives as well as other organofunctional derivatives depends critically on the loading of accessible functional groups into the framework. Open framework mesostructures have been obtained for compositions in which fewer than 30% of

the silicon centers have been functionalized. Therefore, there was a need to devise methods for increasing the loading of mercapto and other functional groups while maintaining the mesoporous framework structure. Yutaka and Pinnavaia elucidated the factors that mediate the framework pore sizes and pore volumes of MP-HMS silicas prepared through a direct assembly pathway.[2] Their results show that highly accessible mesoporous wormhole framework structures can be assembled at MP loadings of at least 50%, and even up to 60 mol % in some cases, through favorable choices of the structure-directing surfactant and assembly conditions. These results hold important implications for use of these MP-HMS derivatives as metal ion trapping agents and as supported sulfonic acid reagents.

### 5.2.2 Esterification of Glycerol

Monoglycerides (MG) consist of a hydrophilic head and a hydrophobic tail, which give them detergency characteristics. Therefore monoglycerides and their derivatives have a wide application as emulsifiers in food, pharmaceutical, and cosmetic industries.[22,23] They increase skin permeability and thus facilitate percutaneous drug absorption. At the moment they are also being considered for use in low-calorie margarines. There are two major industrial routes to monoglycerides.[24,25] First, they are manufactured by glycerolysis, i.e., a base-catalyzed transesterification of triglycerides with glycerol at elevated temperature (e.g., 528 K). Second, monoglycerides can be produced by a direct, single esterification of glycerol with a fatty acid.

In order to lower the temperature of the latter process, an acid catalyst is required, e.g., sulfuric acid, phosphoric acid, or organic sulfonic acids. However, as the three hydroxyl groups in glycerol do not strongly differ in reactivity, mixtures of mono-, di-, and even triglycerides are obtained with acid and base catalysis. Techniques for purification of monoglycerides, e.g., distillation, are limited to food applications since such process steps are expensive. Therefore, it is highly desirable to improve the monoester yield by choosing favorable reaction conditions and designing an appropriate solid catalyst.

In this chapter, mesostructured sulfonic acid catalysts derived from methods reported by Mori and Pinnavaia[2] for the assembly of MP-HMS were used in the acid catalyzed esterification of lauric acid with glyercol. The object of the current work was to study the effect of a higher amount of acid functionality on the conversion and selectivity of this test reaction.

## 5.3 Experimental

### Materials.

Tetraethyl orthosilicate (TEOS), 3-mercaptopropyltrimethoxysilane (MPTMS), and all alkylamine surfactants were purchased from Aldrich Chemical Co. These reagents were used as received without further purification. Deionized water and absolute ethanol were used in the synthesis and surfactant extraction processes, respectively. Lauric acid and glycerol were obtained from Aldrich and used without further purification. Monolauroyl glycerol, used as a calibration standard, was obtained from Sigma.

### 5.3.1 Mesostructure Synthesis

The synthesis of mercapto-functionalized HMS silicas was carried out by first dissolving 2.2 mmol of the octadecylamine surfactant in 2.3 g of ethanol at 65 °C and then diluting the surfactant solution with 29 mL of water preheated at 65 °C. The surfactant solution was then shaken in a reciprocating water bath at the desired assembly temperature for a period of 30 min. A 10-mmol quantity of a *x*MPTS and (1 - *x*)TEOS mixture where *x* equals the molar fraction of total silicon present as mercaptopropyl silane was then added to the surfactant solution. The reaction vessel was sealed, and the mixture was allowed to age with stirring for 72 h. The resulting product was filtered and air-dried for 24 h. Surfactant removal from the as-made mesostructure was accomplished by Soxhlet extraction for a period of 24 h using ethanol as the solvent. The ethanol-extracted product was then allowed to dry in air before use. The product thus obtained was denoted as MP-HMS having dangling mercaptopropyl groups

attached covalently to the mesoporous silica surface. This material was further subjected to oxidation using 30% $H_2O_2$ in MeOH under ambient conditions for 24 h. The product was then filtered and washed with 0.1M $H_2SO_4$ followed by air-drying to obtain sulfonic acid funcationalized HMS material henceforth denoted as x $SO_3H$-HMS where x indicated the extent of functionalization of the silica centers by the sulfonic acid group.

### 5.3.2 Catalytic reaction of glycerol with lauric acid

First, 2.52 g glycerol and 5.48 g lauric acid (molar ratio 1: 1) were added to a 25-mL round bottom flask. After 1 h heating to 385 K, the catalyst (typically 0.1 g, or 5 wt% with respect to glycerol) was added. The reaction mixture was stirred magnetically at ~ 200 rpm. The temperature was held at 385 K with a controller. Samples were taken every hour from the top fat layer and diluted into tetrahydrofuran (THF, 5 wt%) for chromatographic analysis. Samples were analyzed on a HP 5890 GC equipped with a Mass detector on a DB-5 column. The product samples were derivatized using trimethylsilylchloride by conventional methods.

**Reaction 5.1**: Acid catalyzed esterification of lauric acid with glycerol

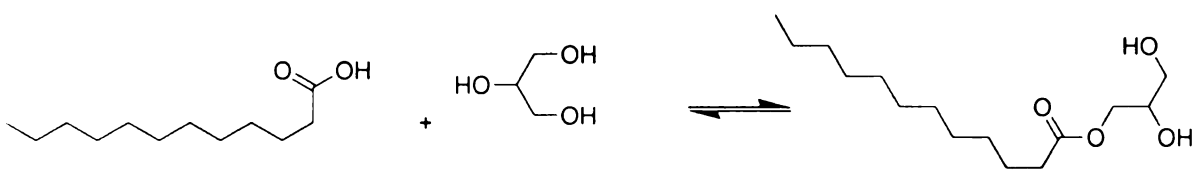


Lauric acid + Glycerol ⇌ 1-Monolauroyl glycerol

### 5.3.3 Characterization.

The physical properties of the mercaptopropyl functionalized silicas were determined using X-ray diffraction (XRD), nitrogen adsorptometry, $^{29}Si$ MAS NMR spectroscopy, and transmission electron microscopy (TEM). Powder XRD patterns were recorded on Rigaku rotaflex diffractometer using Cu $K_\alpha$ radiation. Nitrogen adsorption-desorptioin isotherms were measured at -196 °C on a Micrometrics ASAP 2010 sorptometer, the samples being outgassed for 12 h at 120 °C and $10^{-6}$ Torr prior to measurement. The $^{29}Si$ MAS NMR spectra were recorded on a Varian VRX 400-MHz spectrometer at 79.5 MHz using 7-mm zirconia rotors and a magic-angle spinning speed of at least 4.0 kHz. A pulse delay of 400 s was used to ensure full relaxation of the nuclei prior to each scan.

## 5.4 Results and discussion

### 5.4.1 Catalyst characterization

Figure 5.1. shows the nitrogen isotherms obtained for MP-HMS synthesized using octadecylamine as the structure director and MPTMS and TEOS as the silica source at a 1:1 molar ratio. In this derivative, 50% of the framework silicon centers contain organofunctional mercaptan groups. Included in the figure is the isotherm for $SO_3H$-HMS formed by post-synthetic oxidation of 50% MP-HMS with $H_2O_2$. Both isotherms show a modified Type IV behavior, and show the presence of mesoporous pore filling step, which is relatively broad, indicating a wider pore size distribution as compared to a non-functionalized HMS material.[26,27] The products also lack textural mesoporosity, as indicated by the absence of any uptake in the higher partial pressure regions. However, both the materials BET surface areas in the range of 1000-1700 $m^2/g$ and Horvath-Kawazoe[28] pore size distribution in the range of 2.0-2.8 nm.

Figure 5.2 shows the isotherms for MP-HMS and $SO_3H$-HMS in which 30% of the framework silicon sites are functionalized (x = 0.3). The surface areas and pore size distributions correlate very well with those reported by Yutaka and Pinnavaia.[2]

Figure 5.3 shows the DRIFTS spectrum obtained for MP-HMS and SO3H-HMS samples having x value of 0.50. The weak band at 2600 $cm^{-1}$ present in MPHMS corresponds to S-H stretching frequency indicating presence of thiol groups in the parent material. However, upon oxidation using $H_2O_2$ the band at 2600 disappears indicating essentially complete oxidation of SH groups to $SO_3H$

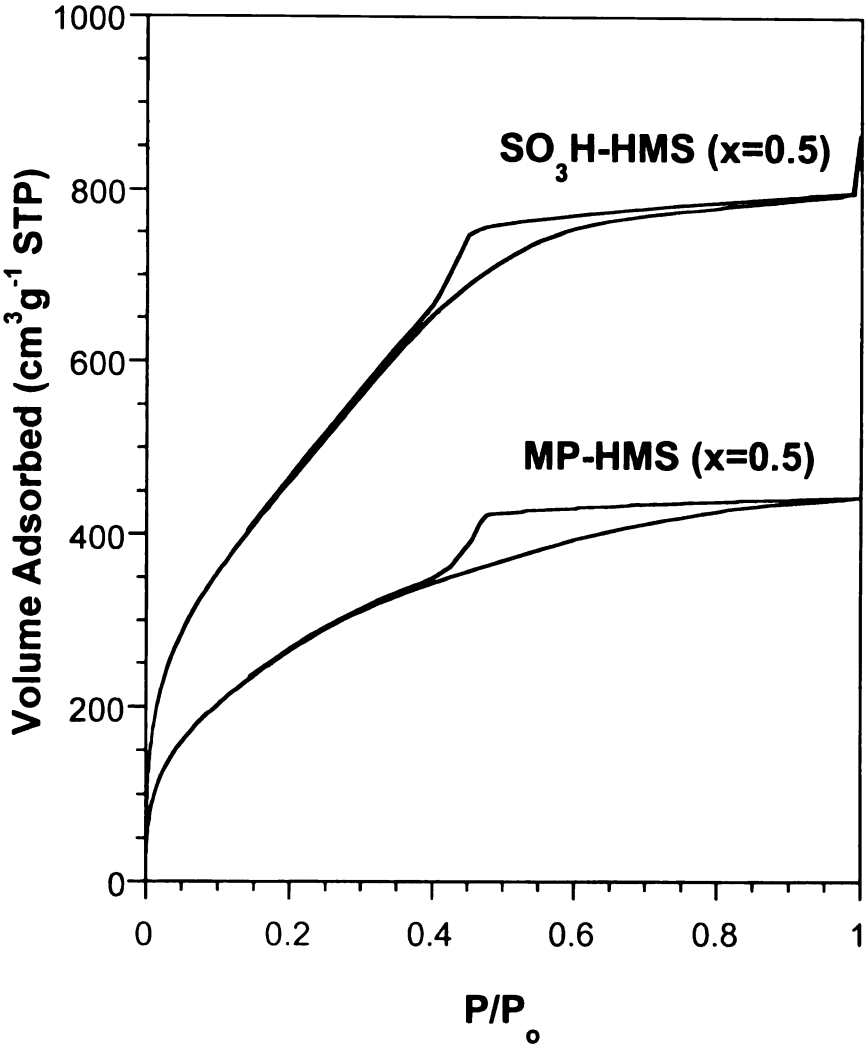


**Figure 5.1** $N_2$ adsorption-desorption isotherms for mercaptopropyl functionalized silicas (MPHMS) formed at 65 °C in the presence of octadecylamine as the surfactant and its corresponding sulfonic acid derivative ($SO_3H$-HMS). The x values indicate the fraction of framework silicon center that have been functionalized by thiol or sulfonic acid groups. The isotherms are offset vertically by 100 $cm^3/g$, STP for clarity.

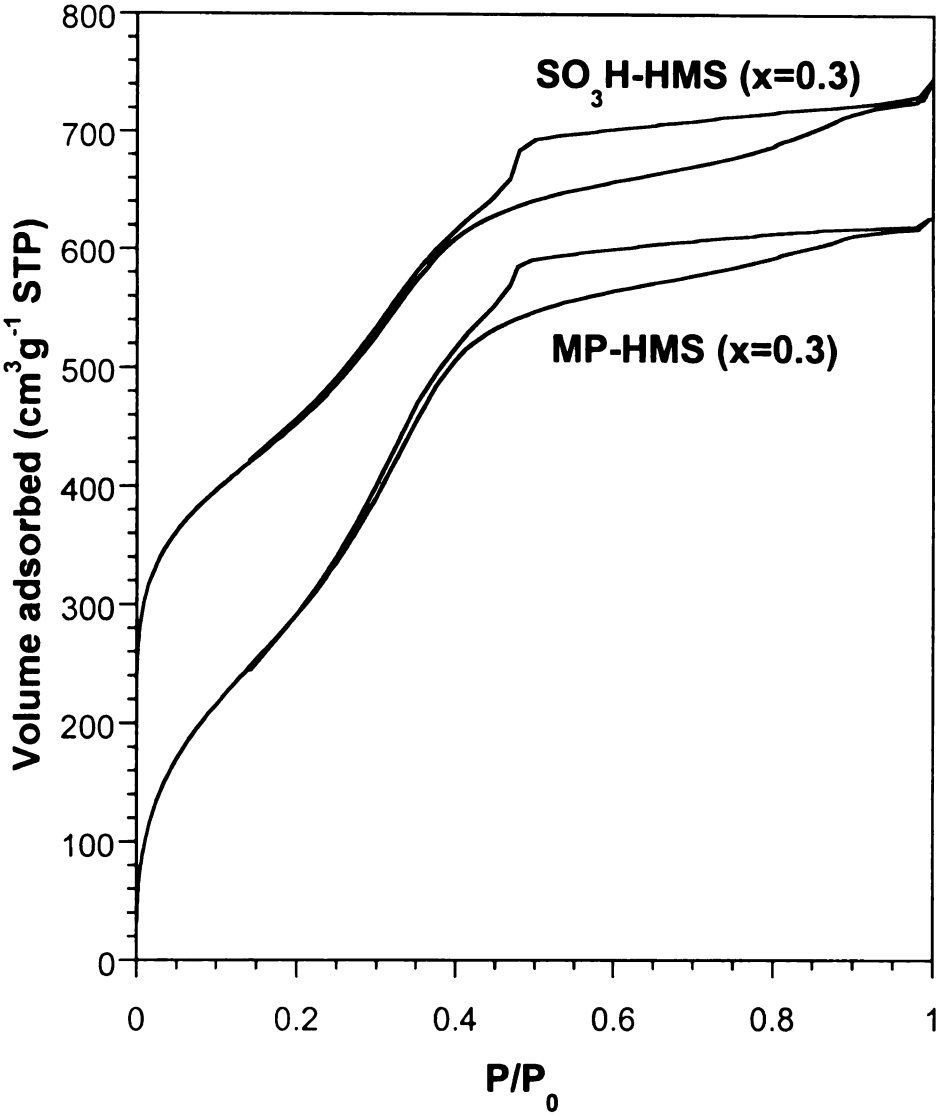


**Figure 5.2** $N_2$ adsorption-desorption isotherms for mercaptopropyl functionalized silicas (MPHMS) formed at 65 °C in the presence of octadecylamine as the surfactant and its corresponging sulfonic acid derivative ($SO_3H$-HMS). The x values indicate the fraction of framework silicon center that have been functionalized by thiol or sulfonic acid groups. The isotherms are offset vertically by 200 $cm^3/g$, STP for clarity.

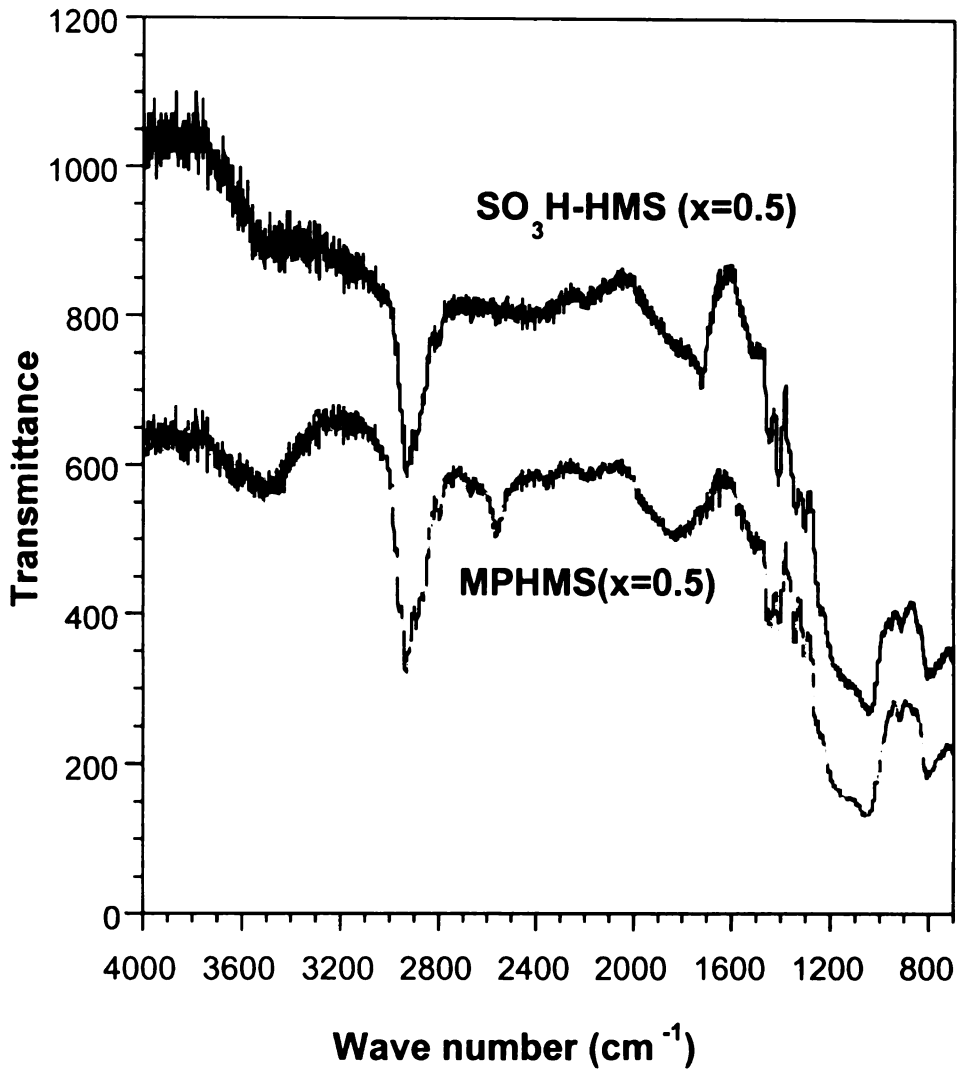


**Figure 5.3** DRIFTS spectrum for mercaptopropyl-functionalized silicas MP-HMS and $SO_3H$-HMS silica (x=0.50). The weak band at 2600 $cm^{-1}$ is assigned to the S-H stretching frequency of the thiol group in MPHMS. The band is absent in the sulfonic acid derivative.

**Table 5.1** Structural parameters for organofunctional silica synthesized by direct assembly method using octadecyl amine as the structure director.

| Sample | Amount of x (mol)[a] | d spacing (nm)[b] | H-K Pore size (nm)[c] | Pore volume ($cm^3/g$)[d] | BET Surface area ($m^2/g$)[e] |
|---|---|---|---|---|---|
| 0.3 x MPHMS | 0.3 | 4.4 | 3.3 | 0.97 | 1148 |
| 0.3x$SO_3H$-HMS | 0.3 | 4.4 | 3.5 | 0.81 | 961 |
| 0.5 x MPHMS | 0.5 | 4.3 | 2.8 | 0.71 | 1220 |
| 0.5x$SO_3H$-HMS | 0.5 | 4.3 | 2.8 | 0.65 | 1200 |

a) Each mesostructure was assembled from *x*:(1 - *x*) MPTS: TEOS mixtures in 90:10 (v/v) $H_2O$/ethanol at 65 °C.
b) Determined by powder X-ray diffraction
c) Determined by the Horvath-Kawazoe model.
d) Total pore volumedetermined at $P/P_0$ = 0.98.
e) Calculated by the Brunauer-Emmett-Teller (BET) method

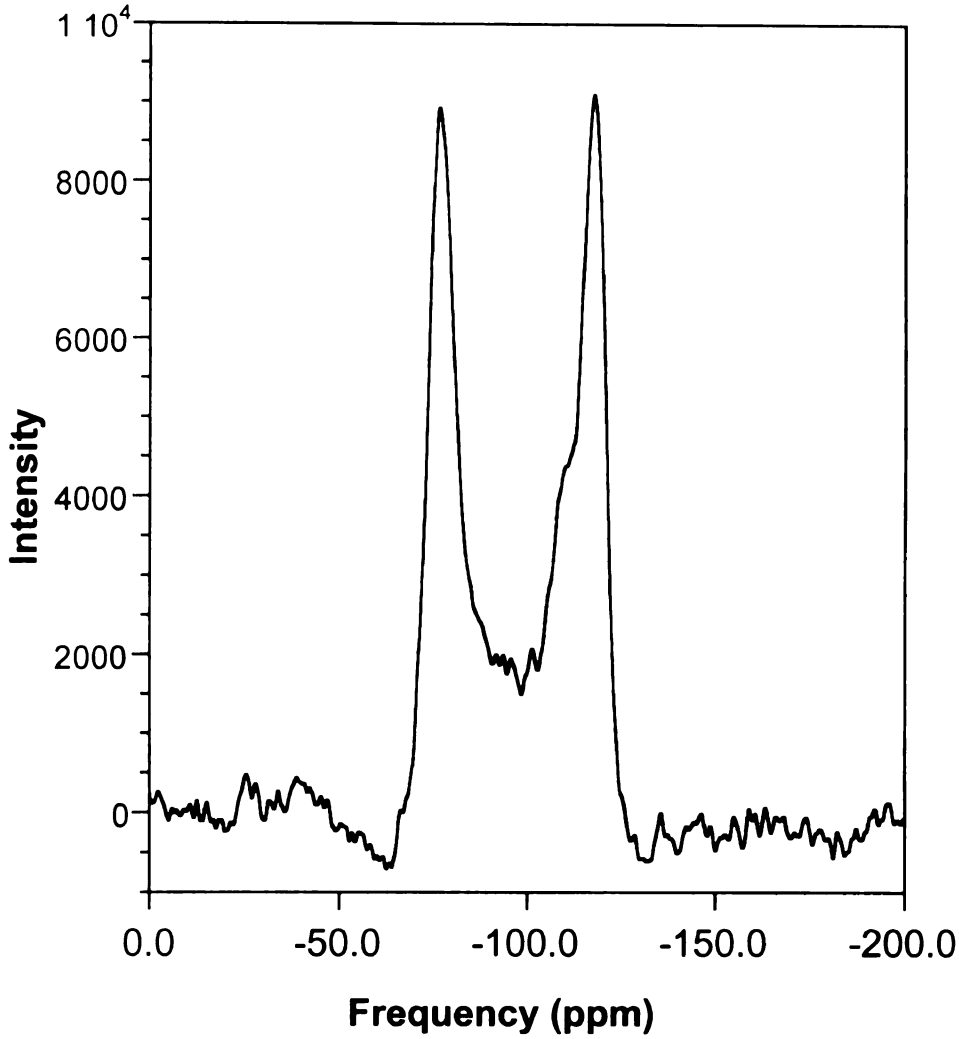


**Figure 5.4.** Representative $^{29}Si$ MAS NMR spectra for a MPHMS (x=0.50) mesostructure assembled at 65 °C from octadecylamine structure director. The spectrum shows the presence of two bands of almost equal intensity. The resonance at -111 ppm is the $Q^4$ peak corresponding to completely cross-linked silica, which is attached to four oxygen atoms, which in turn are attached to silicon atoms. The other resonance at –68 ppm indicates the presence of completely cross-linked organofunctional silicon centers having three O-Si groups and one alkyl group attached to the organofunctional silicon site.

groups. The possibility of oxidation to di-sulfide linkages has not been ignored. However, other investigators[29] have used XPS techniques to prove that oxidation using hydrogen peroxide results in negligible amounts of di-sulfide linkages.

Figure. 5.4 shows the $^{29}Si$ NMR of MPHMS (x=0.50) material obtained from octadecylamine template. The spectrum shows the presence of two bands of almost equal intensity. The resonance at -111 ppm is the $Q^4$ peak corresponding to completely cross-linked silica, which is attached to four oxygen atoms, which in turn are attached to silicon atoms. The other resonance at –68 ppm indicates the presence of completely cross-linked organofunctional silicon centers having three O-Si groups and one attached alkyl group. Negligible (less than 5%) amounts of $Q^3$+$Q^2$+$T^2$ sites are observed in the NMR, indicating a very high degree of cross-linking in these materials. An analogous spectrum is obtained for the sulfonic acid derivative of MP-HMS indicating the presence of a similar silicon environment on oxidation.

Table 5.1 summarizes the textural properties of mercaptopropyl functionalized MP-HMS silicas and the sulfonic acid $SO_3H$-HMS derivative with x = 0.3 and 0.5

### 5.4.2 Esterification of lauric acid using glycerol

Various factors affect the yield and rate of the esterification reactions. The blank reaction (no catalyst added) is significant because of the autocatalysis of lauric acid.[19] The contribution of this spontaneous reaction is known to increase with temperature. Other significant factors include reaction temperature, the ratio of lauric acid: glycerol and the catalyst concentration. Temperatures above

100 °C have been shown to significantly increase conversions due to removal of water from the reaction medium, hence shifting the equilibrium more towards the product. Doubling the initial amount of lauric acid (1: 2 ratio) does not have a major effect on the acid conversion percentage as a function of time, implying that ultimately twice as many moles of fatty acid are converted. However, a marked decrease in monoglyceride selectivity is observed. On the contrary, when the alcohol: acid ratios are raised, there is a larger chance that a fatty acid reacts with glycerol than with a monoglyceride, and this should increase the monoglyceride selectivity

Direct esterification of glycerol with higher fatty acids is usually conducted at high temperatures, in order to increase the mutual solubilities of the immiscible reactant phases. The resulting gain in conversion, however, is counterbalanced by a selectivity loss. This problem can be circumvented by working at relatively low temperature and with an active catalyst, under the condition that the catalytic activity resides in the glycerol phase. Thus, in order to maximize the monoglyceride yield, it is essential to keep the catalyst out of the fatty acid phase before and after micellization.

Table 5.2 summarizes the catalytic activity of various materials reported in this chapter as well other materials reported in literature.[18,19,30] The highest yields are obtained by the catalyst listed in Table 5.1 (entry 4). However, it is clear that the concentration of sulfonic acid groups is remarkably higher in these materials. Entries 1 and 2 (table 5.2) have sulfonic acid concentrations of 0.7 mmol and 1.8 mmol, inspite of having more than twice the active sites 0. 2 HMS-

**Table 5.2** Experimental parameters, yields and selectivity's for various sulfonic acid catalysts obtained from literature.[18,19,30] The entries listed in bold are the catalysts tested experimentally from materials listed in Table 5.1 (entry 4) which show the highest yield for monoglyceride.

| Catalyst | Temp (°C) | Time (h) | Conv % | Selectivity | Yield of monoester | Sulfonic acid conc. (mmol) | Surface area ($m^2/g$) |
|---|---|---|---|---|---|---|---|
| Coated silica gel-$SO_3H$ | 112 | 8 | - | | 51 | 0. 7 | 240 |
| HMS-$SO_3H$ (0. 2) | 112 | 10. 2 | | | 52 | 1. 8 | 943 |
| Silylated MCM-41-$SO_3H$ | 112 | 24 | | | 53 | 0. 7 | 650 |
| Coated MCM-41-$SO_3H$ | 112 | 24 | | | 47 | 1. 7 | 398 |
| Amberlyst-15 | 112 | 11. 8 | | | 44 | 4. 6 | - |
| H-USY | 112 | 23. 5 | | | 36 | - | 757 |
| *p*TSA | 112 | 4 | | | 44 | - | - |
| Blank | 112 | 24 | 20 | 65 | 13 | - | - |
| MCM-41-$SO_3H$-2 | 100 | 8 | 45 | 84 | 38 | 1. 46 | 730 |
| MCM-41-$SO_3H$-3 | 100 | 8 | 35 | 85 | 30 | 1. 33 | 579 |
| MCM-41-$SO_3H$-4 | 100 | 8 | 65 | 80 | 52 | 1. 37 | 693 |
| MCM-41-$SO_3H$-5 | 100 | 24 | 38 | 83 | 32 | 1. 42 | 681 |
| MCM-41-$SO_3H$-2 | 100 | 24 | 90 | 60 | 54 | 1. 46 | 730 |
| MCM-41-$SO_3H$-3 | 100 | 24 | 75 | 78 | 58 | 1. 33 | 579 |
| MCM-41-$SO_3H$-4 | 100 | 24 | 99+ | 40 | 40 | 1. 37 | 693 |
| MCM-41-$SO_3H$-5 | 100 | 24 | 90 | 50 | 45 | 1. 42 | 681 |
| **HMS-$SO_3H$ (0. 5)** | **110** | **12** | **76** | **67** | **51** | **5. 8** | **1225** |
| **HMS-$SO_3H$ (0. 5)** | **110** | **24** | **99+** | **66** | **66** | **5. 8** | **1225** |

$SO_3H$ has similar yields of monoglyceride leading to the belief that other factors such as accessibility of active sites in the solids plays a key role.

Regarding the relation between activity and structure of the mesoporous material, higher concentrations of surface groups do not necessarily lead to the highest conversions; in fact, the most active catalyst (coated silica gel-SO3H) has only 0.7 mmol $SO_3H$ groups (Table 5.2 entry 1). Rather, a good accessibility of the active sites seems important. Even if the average pore diameter decreases gradually upon going from an amorphous structure to a silylated or a coated ordered mesoporous material, we have not been able to observe effects of product shape selectivity, mainly because the less selective background reaction becomes more important as the catalysts' activity decreases.

In conclusion, sulfonic mesoporous materials catalyze biphasic glycerol esterification, coupling large conversion rates to high monoglyceride yields. With the same catalysts, a wide range of esters can be synthesized starting from various polyols and acids.

## 5.5 References


(1) Wight, A. P.; Davis, M. E. *Chem. Rev.* **2002**, *102*, 3589-3613.

(2) Mori, Y.; Pinnavaia, T. J. *Chem. Mater.* **2001**, *13*, 2173-2178.

(3) Margolese, D.; Melero, J. A.; Christiansen, S. C.; Chmelka, B. F.; Stucky, G. D. *Chem. Mater.* **2000**, *12*, 2448-2459.

(4) Lim, M. H.; Blanford, C. F.; Stein, A. *Chem. Mater.* **1998**, *10*, 467-+.

(5) Price, P. M.; Clark, J. H.; Macquarrie, D. J. *Dalton* **2000**, 101-110.

(6) Clark, J. H.; Macquarrie, D. J. *Chem.Commun.***1998**, 853-860.

(7) Pirkle, W. H.; Pochapsky, T. C.; Mahler, G. S.; Corey, D. E.; Reno, D. S.; Alessi, D. M. *J.Org. Chem.* **1986**, *51*, 4991-5000.

(8) Bols, M.; Skrydstrup, T. *Chem.Rev.***1995**, *95*, 1253-1277.

(9) Moller, K.; Bein, T. *Chem. Mater.* **1998**, *10*, 2950-2963.

(10) Burkett, S. L.; Sims, S. D.; Mann, S. *Chem. Commun.* **1996**, 1367-1368.

(11) Feng, X.; Fryxell, G. E.; Wang, L. Q.; Kim, A. Y.; Liu, J.; Kemner, K. M. *Science* **1997**, *276*, 923-926.

(12) Chen, X. B.; Feng, X. D.; Liu, J.; Fryxell, G. E.; Gong, M. L. *Sep. Sci. Technol.* **1999**, *34*, 1121-1132.

(13) Mercier, L.; Pinnavaia, T. J. *Adv. Mater.* **1997**, *9*, 500-&.

(14) Mercier, L.; Pinnavaia, T. J. *Environ. Sci. Technol.* **1998**, *32*, 2749-2754.

(15) Mercier, L.; Pinnavaia, T. J. *Microporous Mesoporous Mater.* **1998**, *20*, 101-106.

(16) Brown, J.; Mercier, L.; Pinnavaia, T. J. *Chem. Commun.* **1999**, 69-70.

(17) Brown, J.; Richer, R.; Mercier, L. *Microporous Mesoporous Mater.* **2000**, *37*, 41-48.

(18) Van Rhijn, W. M.; De Vos, D. E.; Sels, B. F.; Bossaert, W. D.; Jacobs, P. A. *Chem.Commun.***1998**, 317-318.

(19) Bossaert, W. D.; De Vos, D. E.; Van Rhijn, W. M.; Bullen, J.; Grobet, P. J.; Jacobs, P. A. *J. Catal.* **1999**, *182*, 156-164.

(20) Harmer, M. A.; Sun, Q.; Michalczyk, M. J.; Yang, Z. *Chem.Commun.* **1997**, 1803-1804.

(21) Harmer, M. A.; Farneth, W. E.; Sun, Q. *J. Am. Chem. Soc.* **1996**, *118*, 7708-7715.

(22) Baumann, H.; Buehler, M.; Fochem, H.; Hirsinger, F.; Zoebelein, H.; Falbe, J. *Angew.Chem.,Int.Ed.* **1988**, *100*, 41-62.

(23) Jungermann, E. *Cosmetic Science and Technology Series* **1991**, *11*, 97-112.

(24) Corma, A.; Iborra, S.; Miquel, S.; Primo, J. *J.Catal.* **1998**, *173*, 315-321.

(25) Sonntag, N. O. V. *JAOCS, J. Am. Oil Chem. Soc.* **1982**, *59*, 795A-802A.

(26) Tanev, P. T.; Pinnavaia, T. J. *Science* **1995**, *267*, 865-867.

(27) Pauly, T. Ph.D. Thesis *Chemistry*; Michigan State University: East Lansing, 2000, p 217.

(28) Horvath, G.; Kawazoe, K. *J. Chem. Eng. Jpn.* **1983**, *16*, 470-475.

(29) Das, D.; Lee, J.-F.; Cheng, S. *Chem.Commun.* **2001**, 2178-2179.

(30) Wilson, K.; Lee, A. F.; Macquarrie, D. J.; Clark, J. H. *Appl. Catal., A: Gen.* **2002**, *228*, 127-133.